



UNIVERSITAT ROVIRA I VIRGILI

AMBIENT CARBON DIOXIDE CAPTURE AND CONVERSION VIA MEMBRANES

Adrianna Nogalska

ADVERTIMENT. L'accés als continguts d'aquesta tesi doctoral i la seva utilització ha de respectar els drets de la persona autora. Pot ser utilitzada per a consulta o estudi personal, així com en activitats o materials d'investigació i docència en els termes establerts a l'art. 32 del Text Refós de la Llei de Propietat Intel·lectual (RDL 1/1996). Per altres utilitzacions es requereix l'autorització prèvia i expressa de la persona autora. En qualsevol cas, en la utilització dels seus continguts caldrà indicar de forma clara el nom i cognoms de la persona autora i el títol de la tesi doctoral. No s'autoritza la seva reproducció o altres formes d'explotació efectuades amb finalitats de lucre ni la seva comunicació pública des d'un lloc aliè al servei TDX. Tampoc s'autoritza la presentació del seu contingut en una finestra o marc aliè a TDX (framing). Aquesta reserva de drets afecta tant als continguts de la tesi com als seus resums i índexs.

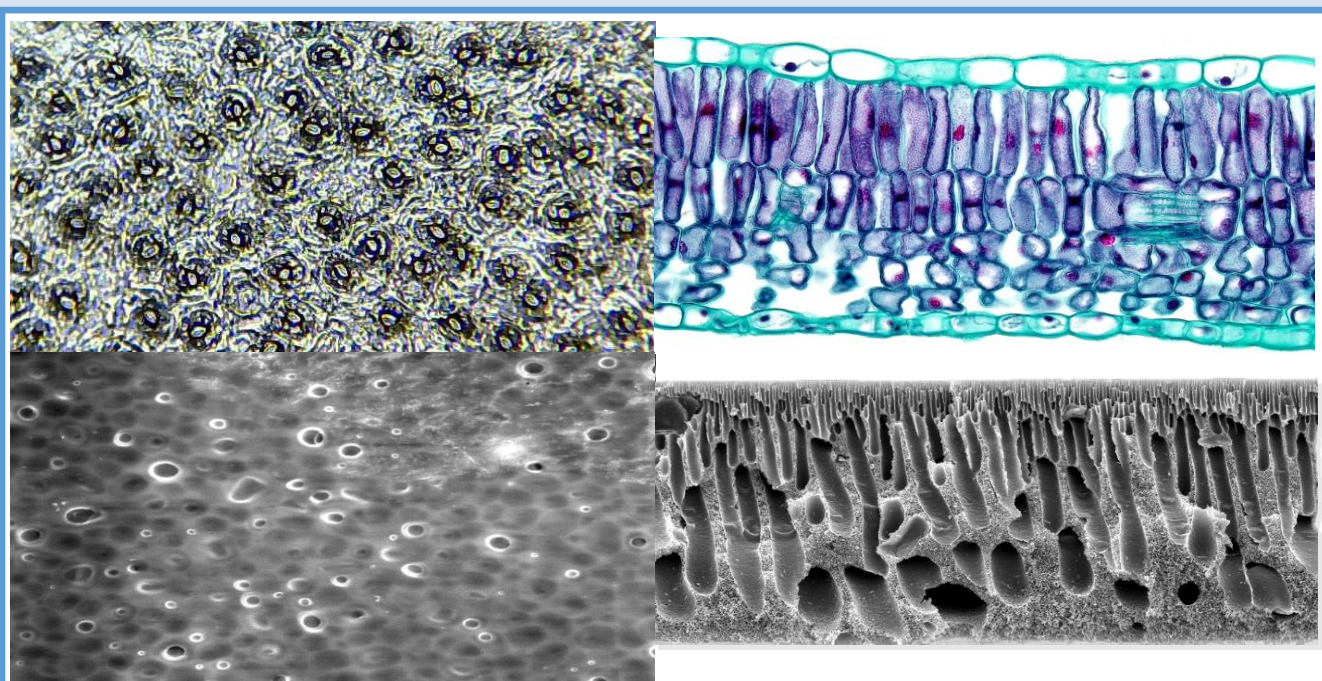
ADVERTENCIA. El acceso a los contenidos de esta tesis doctoral y su utilización debe respetar los derechos de la persona autora. Puede ser utilizada para consulta o estudio personal, así como en actividades o materiales de investigación y docencia en los términos establecidos en el art. 32 del Texto Refundido de la Ley de Propiedad Intelectual (RDL 1/1996). Para otros usos se requiere la autorización previa y expresa de la persona autora. En cualquier caso, en la utilización de sus contenidos se deberá indicar de forma clara el nombre y apellidos de la persona autora y el título de la tesis doctoral. No se autoriza su reproducción u otras formas de explotación efectuadas con fines lucrativos ni su comunicación pública desde un sitio ajeno al servicio TDR. Tampoco se autoriza la presentación de su contenido en una ventana o marco ajeno a TDR (framing). Esta reserva de derechos afecta tanto al contenido de la tesis como a sus resúmenes e índices.

WARNING. Access to the contents of this doctoral thesis and its use must respect the rights of the author. It can be used for reference or private study, as well as research and learning activities or materials in the terms established by the 32nd article of the Spanish Consolidated Copyright Act (RDL 1/1996). Express and previous authorization of the author is required for any other uses. In any case, when using its content, full name of the author and title of the thesis must be clearly indicated. Reproduction or other forms of for profit use or public communication from outside TDX service is not allowed. Presentation of its content in a window or frame external to TDX (framing) is not authorized either. These rights affect both the content of the thesis and its abstracts and indexes.



Ambient carbon dioxide capture and conversion via membranes

Adrianna Nogalska



DOCTORAL THESIS
2018

Adrianna Nogalska

AMBIENT CARBON DIOXIDE CAPTURE
AND CONVERSION VIA MEMBRANES

DOCTORAL THESIS

Supervised by Dr. Ricard Garcia - Valls

Chemical Engineering Department



UNIVERSITAT
ROVIRA i VIRGILI

Tarragona

2018



UNIVERSITAT ROVIRA i VIRGILI

Departament d'Enginyeria Química
Avinguda dels Països Catalans, 26,
43007 Tarragona
977 55 97 00

I STATE that the present study, entitled “Ambient carbon dioxide capture and conversion via membranes”, presented by Adrianna Nogalska for the award of the degree of Doctor, has been carried out under my supervision at the Department of Chemical Engineering of this university and that meets the requirements to qualify for the European Mention.

Tarragona, 04/09/2018

Doctoral Thesis Supervisor

Table of content

1. SUMMARY	1
2. INTRODUCTION AND MOTIVATIONS.....	7
2.1. MEMBRANE CONTACTORS FOR CO₂ CAPTURE PROCESSES	8
2.1.1. Membrane contactors	10
2.1.2. Membranes	11
2.1.2.1. Ceramics	11
2.1.2.2. Polymers	13
2.1.2.3. Bio – composite	14
2.1.3. Absorbents	16
2.2. CARBON DIOXIDE HYDROGENATION IN CO₂ UTILIZATION TECHNOLOGIES	17
2.2.1. Metal-catalyzed hydrogenation to formic acid	17
2.2.2. Photocatalytical reduction of CO₂	18
2.2.3. Electrochemical conversion	19
2.3. MOTIVATION	20
REFERENCES.....	21
3. OBJECTIVES AND HYPOTHESIS.....	27
I. PRISTINE AND NANOCOMPOSITE POLYSULFONE MEMBRANE CONTACTORS	31
I.1. INTRODUCTION	33
I.2. EXPERIMENTAL.....	35
1.2.1. Materials	35
1.2.2. Membranes preparation.....	36
1.2.3. Characterization methods.....	37
I.3. RESULTS AND DISCUSSION	42
I.4. CONCLUSIONS	57
References	57
II. STUDIES OF POLYSULFONE MEMBRANE CONTACTORS IN STATIC MODULE	63
II.1. INTRODUCTION	65
II.2. EXPERIMENTAL.....	67
II.2.1. Materials.....	67
II.2.2. Flat sheet membranes preparation.....	67
II.2.3. Morphology analysis	67
II.2.4. Membrane wetting estimation	68
II.2.5. CO₂ absorption studies	69
II.2.6. Statistical analysis	70
II.3. RESULTS AND DISCUSSION	70
II.3.1. Morphology analysis	70
II.3.2. Membrane wetting estimation	72
II.3.3. CO₂ absorption results	74

II.3.3.1.	Influence of the membrane thickness and stirring rate on the contactor absorption capacity	74
II.3.3.2.	PH influence.....	75
II.3.3.3.	Change of absorption in time.....	76
II.3.3.4.	The comparison of performances	77
II.4.	CONCLUSIONS.....	77
	REFERENCES.....	78
III.	POLYSULFONE MEMBRANE CONTACTORS MODIFIED WITH ACTIVATED CARBON ...	83
III.1.	INTRODUCTION	85
III.2.	EXPERIMENTAL.....	85
III.2.1.	<i>Materials</i>	85
III.2.2.	<i>Membrane preparation</i>	86
III.2.3.	<i>Membrane characterization</i>	87
III.2.4.	<i>CO₂ capture studies</i>	89
III.2.5.	<i>Statistical analysis</i>	90
III.3.	RESULTS AND DISCUSSION	90
III.3.1.	<i>Membrane characteristics</i>	90
III.3.2.	<i>CO₂ absorption studies</i>	95
III.4.	CONCLUSIONS.....	97
	REFERENCES.....	97
IV.	BIOMIMETIC POLIMERIC MEMBRANES	101
IV.1.	INTRODUCTION	103
IV.2.	EXPERIMENTAL.....	105
IV.2.1.	<i>Materials</i>	105
IV.2.2.	<i>Synthesis and functionalization of magnetic nanoparticles (MNPs)</i>	106
IV.2.3.	<i>Characterization of MNPs</i>	106
IV.2.4.	<i>Membrane preparation</i>	107
IV.2.5.	<i>Enzyme immobilization</i>	107
IV.2.6.	<i>Characterization of the enzyme and the membrane</i>	108
IV.3.	RESULTS AND DISCUSSION	111
IV.3.1.	<i>Nanoparticles and membranes physico-chemical characterization</i>	111
IV.3.2.	<i>Protein evaluation in terms of structural changes and CO₂ sorption capacity induced by the immobilization on :</i>	116
IV.3.2.1.	<i>Polysulfone based membrane</i>	116
IV.3.2.2.	<i>PVA based membranes</i>	130
IV.4.	CONCLUSIONS.....	140
	<i>References</i>	141
V.	BICARBONATE ELECTRO-REDUCTION TO FORMIC ACID	143
V.1.	INTRODUCTION	145
V.2.	EXPERIMENTAL.....	145
V.2.1.	<i>Materials</i>	145
V.2.2.	<i>Working electrode preparation</i>	146

V.2.3.	<i>Electrochemical behavior</i>	146
V.2.4.	<i>Electro-reduction experiments</i>	147
V.3.	RESULTS AND DISCUSSION	149
V.4.	CONCLUSIONS	150
	<i>References</i>	151
4.	GENERAL CONCLUSIONS	153
	APPENDIX	159
	LIST OF FIGURES	160
	LIST OF TABLES	164
	THESIS OUTCOMES	166
	CURRICULUM VITAE	169

Acknowledgments

The last four years were full of incredible experiences, hard work and constant development. Here I would like to show my appreciation to all of the people that accompanied me though these years and directly or indirectly contributed to the dissertation.

First of all I have to acknowledge my supervisor, Dr. Ricard Garcia-Valls. I am utterly grateful for all the time he dedicated me, and the advices, guidance, and encouragements you gave me.

I am also thankful to the former members of Meteor group and current members of MemTec who I had pleasure to meet and work with: Prof. Tania Gumi, Prof. Marta Giamberini, Prof. José Antonio Reina Lozano, Mario, Gianmarco, Mimmo, Jie, Rita, Ania, Monika, Xavi, Ruben, Joandiet, Cristina, Cinta. My special gratitude goes to Kamila and Krzysztof for our brainstorming sessions, and to Martin, who was not an official member of the group but he was always there to get our minds away from work; to Pepa for always finding solutions to my problems and for spending a lot of time with me buying lab supplies; to Bartek, for all the opportunities he gave me, all the publications we shared and that he helped making more appealing to reviewers.

I would also like to thank all of the students who were working with me on the project as interns: Yuki, Guillaume, Ada, Mikolaj, Amadeusz and master students Lorenza, Mario, Carmen, Omar. I really appreciate their work and dedication.

I am very grateful to prof. João Crespo for hosting me in his group and all the kind people I met during my research stay, especially Carla Brazinha, Carla Portugal, Carla Rodrigues, Ana Carina. Moreover, I acknowledge my Casa de Parque mates and the coordinator of this structure Carla for providing a cozy and friendly atmosphere during my stay in Lisbon.

I thank Servicio de Recursos Científicos y Técnicos workers, in particular Lukas and Mariana – the AFM, ESEM and SEM specialists, Ramon for his patience with NMR analysis and Ernest for manufacturing all of my modules.

I thank Nuria for help with all the administrative issues.

I thank Alberto, a square-head perfectionist, for helping me to shape this thesis. I also thank my friends, both the ones I shared my life with during this period, Kasia, Kamila, Ania, Monika, Keks, Justynka, thanks whom I can call Tarragona my home; and ones far away, Agata, Maka, Iga, Natalia, who always believed in me and although living 2k km away never made me feel the distance.

I want to express my deepest gratitude to all my family for the support and patience, help at distance and unconditional love.

Last but not least, for the financial support I would like to acknowledge Universitat Rovira I Virgili Marti Franquez scholarship 2015PMFPIPF and Centre Tecnològic de la Química de Catalunya.

1. SUMMARY

1. Summary

Ambient carbon dioxide capture and conversion via membranes

The climate change caused by the increased CO₂ content in the atmosphere is raising a lot of concern nowadays. The constant need for sustainable green energy generation inspired us to develop an artificial photosynthetic system. The system works as a leaf, where CO₂ is captured directly from air through the membrane pores and passes to the next compartments to be finally converted to methanol or other hydrocarbons and to be further used as fuel in fuel cells.

The main scope of the work is to reveal the influence of polysulfone - based membrane contactors on atmospheric CO₂ capture rate by chemical sorption into absorbent aqueous solutions. Flat sheet membranes that vary in morphology were prepared by immersion precipitation and undergo internal morphology and surface characterization. Moreover, the compatibility between membranes and absorbent solution was evaluated in terms of swelling and contact angle measurements. According to the results, it can be concluded that polysulfone membranes is suitable for use with potassium hydroxide solutions. The study indicates that the CO₂ flux increases when increasing the absorbent flow rate over the range of liquid velocities investigated. Moreover, the flux grows with the increase of membrane macrovoids size, due to decrease of the membrane mass transfer resistance. Results obtained during dynamic module operations revealed a superior CO₂ assimilation abilities of the unit as compared to a natural leaf.

In order to evaluate the impact of liquid flow on the system performance, the subsequent experiments were carry out in static conditions – without the use of a pump, with the solution being mixed only by a stirrer. The influence of the solution's mass transfer resistance during static operation of the module is low, as the solution remains in the same container. Still, the CO₂ assimilation results were similar to a leaf performance.

The polysulfone membrane was modified with a number of additives. Copper-ferrite nanoparticles were firstly added to the membrane bulk in the concentration of 5%. Studies showed that the incorporation of nanoparticles does not change the membrane internal morphology. However, it increased surface roughness and CO₂ permeability. CuFeO₃ nanoparticles proved to be capable of capturing CO₂, but when introduced to the polymeric membrane and tested in contactor systems they influenced the CO₂ flux negatively.

1. Summary

The polysulfone flat sheet membranes were modified with activated carbon following two approaches: i) bulk modification by adding AC into the polymeric solution used for membrane preparation and ii) spraying of the carbon-containing ink on the blank polysulfone membrane top surface. In the case of surface modification, the amount of introduced AC was determined by elemental analysis and calculation of change in membrane mass and thickness. The incorporation of AC into the polymeric bulk caused an increase of the membrane thickness and contributed to pores formation on the bottom surface of the membrane. The hydrophilicity was not improved and the gas absorption test results showed no improvement of the membrane performance.

Modification of the polysulfone surface by coating it with active carbon layer was accomplished. The cross section images of the modified membranes showed that the layer was not penetrating into the membrane. Unfortunately, the additional layer increased membrane mass transfer resistance without no active passage of the CO₂ to absorbent solution, which decreased its effectiveness as a membrane contactor.

Another tested solution for improving CO₂ capture was the combination of the polymeric membrane with enzymes involved in the nature carbon fixation: RuBisCo and CA. Two approaches were studied: physical attachment by adsorption and chemical attachment by covalent binding to amine terminated magnetic nanoparticles dispersed within the membrane. In order to evaluate the real influence of covalent binding on the immobilization, the adsorption studies were performed on both blank and nanocomposite membranes. The structural changes of the enzyme induced by the immobilization, as well as its activity and CO₂ solubility was determined. It was observed that RuBisCo immobilization is favourable to more hydrophilic surfaces. The solubilized CA was attached to the hydrophilic membrane and -NH₂ terminated nanoparticles, but there was no evidence of covalent binding. Fluorescence analyses did not reveal any structural changes in the case of CA immobilization, while the RuBisCo structure was altered during the process. Nevertheless, polysulfone based bio-mimetic membranes showed slight increase in the nanocomposite membrane CO₂ absorption, although the blank membrane still shows the best performance.

In addition, PVA-based membranes were studied for the development of the biomimetic membranes. The PVA membranes were found to be good supports for enzyme immobilization due to their high

Ambient carbon dioxide capture and conversion via membranes

hydrophilicity. Unfortunately, enzyme immobilization did not improve the CO₂ sorption of the membrane, independently on the enzyme used – CA or RuBisCo - or its concentration. Moreover, both enzymes show signs of a molecular unfolding, which could change the availability of the active center and cause the decrease of activity.

As the captured CO₂ takes form of bicarbonate or carbonate accordingly to the pH, bicarbonate conversion to fuel was also studied. The working electrode was prepared by electro-polishing copper foil followed by annealing, and characterized by LSV. The conversion of bicarbonate to formic acid by electro-reduction was achieved in potentiostatic conditions at -1.6 V.

An artificial stomata for ambient CO₂ capture was designed and developed. Studies showed that the polysulfone based system has superior CO₂ assimilation compared to a leaf performance. Moreover, the best results were obtained using blank and unmodified membrane, providing a low production cost. Furthermore, the conversion of bicarbonate to formic acid was achieved, giving a promising start to be improved in future work.

1. Summary

2. INTRODUCTION AND MOTIVATIONS

2. Introduction and motivations

2.1. Membrane contactors for CO₂ capture processes

(*based on: Adrianna Nogalska, Anna Trojanowska, Ricard Garcia – Valls, *Membrane contactors for CO₂ capture processes – critical review*, Physical Sciences Reviews, Volume 2, 2017)

The content of carbon dioxide in the atmosphere has increased since the industrial revolution (started in 1750) by 40 % according to The International Panel of Climate Change (**Fig. 2. 1**) [1]. The major human activity sources of CO₂ emission are in the power and industry sectors, which generate 60% of total emission. Burning fossil fuels in power plants, oil refineries and other large industrial facilities release the biggest amount of carbon dioxide to the air. Besides the combustion, emission occur during petrochemical processes, manufacture of metals from ores using carbon, thermal decomposition of limestone in cement production and fermentation processes in alcohol making. Even if natural sources of CO₂ emissions are larger than human ones, increased content of carbon dioxide affects the balance in nature and causes climate changes [1]. More than 100 countries have adopted a global warming limit of 2° C or lower as a guiding principle for it mitigation efforts to reduce climate change risks, impacts and damages [2]. Unfortunately, simulations shows that even stopping emissions, the consequence would be an irreversible change for the next 1000 years of atmosphere warming, precipitations or sea level rise [3].

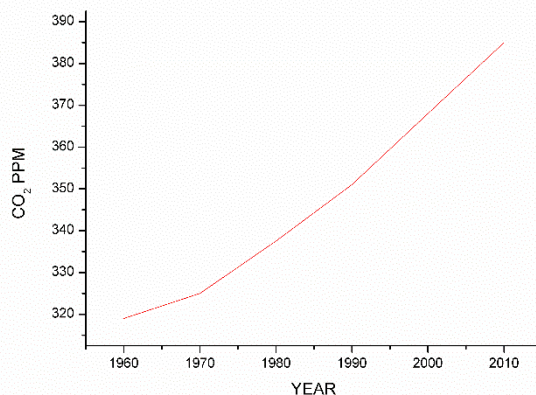


Figure 2. 1. Chart of increase of atmospheric CO₂ concentration during years 1958 – 2010 [1].

CO₂ capture is an efficient process when considering CO₂ emission sources at high concentration. In order to contribute to the wellness of the

Ambient carbon dioxide capture and conversion via membranes

environment, few ways for eliminating the CO₂ excess from air were proposed, like use of algal cultures and sea weed as negative emission technologies [4] or use of CO₂ directly captured from the air as a reagent in green synthetic strategies [5]. Due to low efficiency, the low concentration carbon dioxide capture process is still a rarely discussed subject and requires developments.

A very effective CO₂ capture method is the amine base scrubbing, widely commercially used in flue gas purification CO₂ capture method is the amine base scrubbing [6]. This system is based on chemical absorption of CO₂ into methanolamine (MEA). The process takes place in a two compartments system: firstly, CO₂ from the flue gas stream is absorbed in the amine and then desorbed in a stripper as concentrated gas. The stripped amine is regenerated and sent back to the first compartment. The heat needed for desorption is very high and it is the most expensive part of the process. In any case, researchers are coming with new ideas constantly searching for improvements.

There is a number of patents released during the last decade with inventions concerning CO₂ removal from the gas streams by precipitation techniques [7-9] or by separation with membranes [10-14]. The absorbent systems for removing CO₂ from exhaust gases by precipitation is based on absorbents such as a mixture of amine and aminoacid salts, metal oxides or bicarbonates, which are contacted with a CO₂ containing gas stream, resulting in a precipitation of different solids. The bicarbonates salts formed are then moved from the absorbing compartment to the desorbing one and CO₂ is regenerated for example by applying heat. The inventors claim that the CO₂ capture efficiency is higher than conventional amine scrubbing with higher CO₂ removal ability per cycle and less solvent vaporization loss. The membrane technology used for the CO₂ capture is based on separation processes for mixed gases - CO₂/N₂ and CO₂/CH₄ in flue gas and nature gas. The inventors came up with new composite materials for membrane preparation, e.g. Polyimide-poly(ethylene glycol) copolymer membrane polyvinylamine/polyaniline mixed matrix membranes or a metal organic framework membrane among others. Membranes work as selective barriers which allow the passage of CO₂ and contribute to the formation of a CO₂ reach permeate on the other side.

The captured CO₂ can be later used for several applications and further processes depending on its form. For example the precipitated product can be used as a material for constructions, cement or to produce

2. Introduction and motivations

aggregates so that CO_2 cannot escape back to the atmosphere. At the same time, pure gaseous CO_2 is used in chemical synthesis. The scientific world drew attention to the potential use of the CO_2 as source of green energy production, especially for recycling carbon dioxide by converting it to methanol or hydrocarbons, and its further use as a fuel e.g. in direct methanol fuel cells [15].

Lately, interest on membrane contactors grew as a consequence to the possibility of decreasing the size of the absorber unit, thus the lower prize of system production and exploration. This section focuses on the use of gas – liquid membrane contactor systems in CO_2 capture processes. The state of art in the technology, including novel materials and process improvement approaches, is summarized. Three different membranes types, ceramic, polymeric and bio – composite, as well as variety of absorbents solutions, are presented.

2.1.1. Membrane contactors

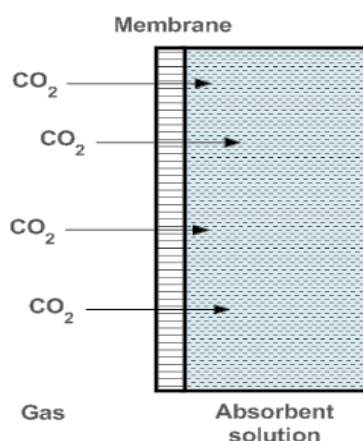


Figure 2. 2. Schematic representation of gas liquid membrane contactor for CO_2 capture.

Membrane contactors (**Fig. 2. 2**) are used in separation processes for their features: large gas–liquid contact area, helping to reduce the contactor size and weight; easy scale-up and compact configuration; the driving force is a difference in the concentration gradient, thus no applied pressure is needed, excluding flooding problems.

Ambient carbon dioxide capture and conversion via membranes

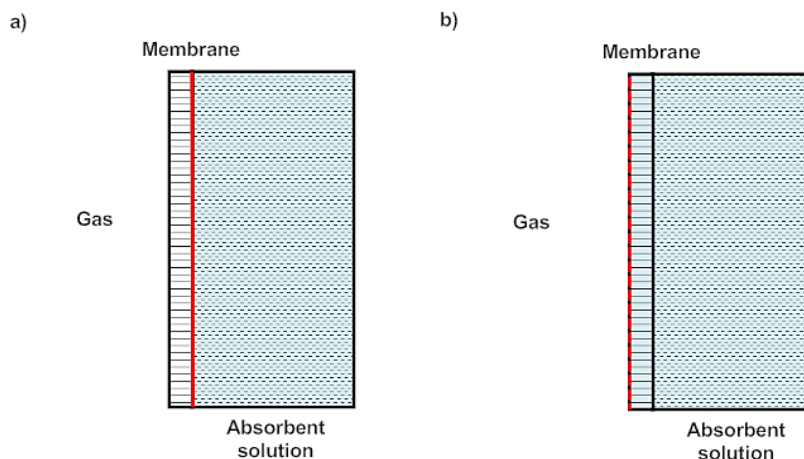


Figure 2. 3. Gas - liquid membrane contactors in dry (a) and wet (b) mode. The contact surface area is marked with red color.

The selection of compatible membranes and absorbents is crucial for the system efficiency. The membranes have to stand both physical and chemical degradation. But the most important factor to overcome is the wetting problem. While it is true that high porosity and open structure are good for flux, these can contribute to membrane wetting. For a good performance, membrane pores should stay dry and open for the gas, as this helps to keep large the contact area (**Fig. 2. 3**). Therefore, the best solution is a membrane with high hydrophobicity and an absorbent solution with high surface tension. Besides, the absorbent should exhibit high affinity to the gas, so its gas absorption capacity and selectivity will be high. The absorbent should also be compatible with the rest system components and having non-corrosive properties. On the other hand, the membrane mostly has to provide high gas permeability with large open spaces within the structure.

2.1.2. Membranes

2.1.2.1. Ceramics

Ceramic membranes possess superior chemical and thermal stability over polymeric ones. The most common materials used for the fabrication of ceramic membranes for CO₂ capture systems are metal oxides, in particular alumina and silica. The hydroxide groups situated on their surface results in high hydrophilicity of the material. Thus, research is mostly focused on improving membrane hydrophobicity, in order to overcome the

2. Introduction and motivations

wetting problem. This brought to the production super-hydrophobic ceramic (SC) membrane contactors. Fluoroalkyl silane (FAS) grafting is the method usually used for the hydrophobicity improvement. The FAS reacts with OH- groups of the metal oxide and increases surface hydrophobicity (Fig. 2. 4).

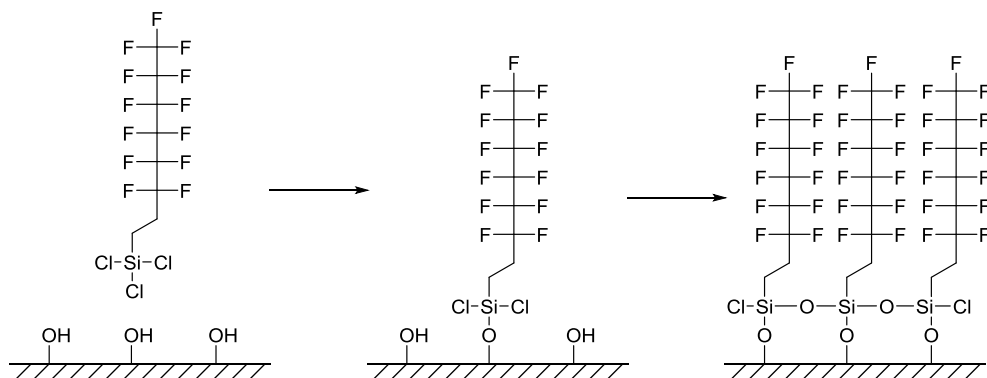


Figure 2. 4. Model reaction of surface hydroxyl groups with fluoroalkyl silanes.

As an example, Magnone et al. [16] performed the grafting directly on an alumina hollow fibre membrane contactor with a high-symmetric distribution of morphological elements. The modified membrane achieved a CO_2 absorption flux of about $5.4 \times 10^{-3} \text{ mol/m}^2\text{s}$ at room temperature with a single symmetric ceramic membrane, which is considerably higher compared to other conventional polymeric membrane for CO_2 absorption into MEA solutions.

Lin et al. [17] reported that pore wetting by amine solution was decreasing CO_2 absorption flux into an alumina membrane. The author's approach consisted in coating a macroporous alumina tubular membrane surface with mesoporous silica aerogel by sol – gel reaction and shrunk of the pore size. Subsequently, the membrane undergoes FAS grafting: the contact angle achieved with four grafting reached the value of 139° . The prepared membranes had a high CO_2 flux ($0.6 \text{ mmol/m}^2\text{s}$) and were stable for 24 h. Compared to the analogue flat membranes, the tubular membranes provide larger surface area, which results in higher CO_2 recovery up to 100 %.

Another material for SC preparation is mullite ($3\text{Al}_2\text{O}_3\cdot 2\text{SiO}_2$), which combines alumina and kaolin. Abdulmunen et al. [18] disclosed the preparation of grafted kaolin - alumina hollow fibres membrane. Using a

Ambient carbon dioxide capture and conversion via membranes

low cost material membranes with high performance were obtained, thanks to the high porosity and hydrophobicity. The membrane was prepared by extrusion and sintering technique from a suspension of kaolin and alumina mixture followed by grafting with FAS, obtaining a membrane with a contact angle of 142°.

In order to overcome wetting and fouling problems in liquid gas membrane contactor systems, Yu et al. [19] prepared an SC membrane from alumina tube with ZrO₂ layer introduction followed by grafting of the surface. The authors suggested that a periodic drying of the membrane ensures a constant and high CO₂ removal efficiency. The ceramic membrane is considered a cheap material which gives improved results thanks to anti-wetting and anti-fouling features because of the drying. After grafting with FAS, the ceramic membrane exhibited a contact angle value of 153°, and a slightly lower permeance as the grafted FAS reduces the pore sizes of the membrane.

2.1.2.2. Polymers

A comparison between different polymeric membranes was done by the Fabien Porcheron's group. The authors studied a number of polymers: Polypropylene (PP), Nylon, Polytetrafluoroethylene (PTFE) and Polyvinylidene fluoride (PVDF). The studies show that the membranes are hydrophobic, yet they noticed a decrease of contact angle up to 0° on Nylon and PVDF after aging with absorbent solutions at high temp for one week. The results are in agreement with TGA, TMA and IR analysis in which only PP and PTFE membranes did not reveal any changes caused by aging. Gas permeability tests show that more porous material give the best results thus taking into consideration structure and stability of PTFE membrane it was applied in CO₂ capture studies in a contactor system and provided a good performance with high efficiency [20].

The main research goal is the invention of new materials for membrane preparation or improving existing ones. The most important membrane feature to improve in gas – liquid contactors operation is its hydrophobicity. A research group from China [21] tried to improve it by incorporating graphene nanosheets into a polyvinylidene fluoride (PVDF) membrane. The modification induced a more porous sublayer structure, where the particles were visible and the surface roughness increased. Hence, the contact angle increased only on the bottom surface. The hybrid membrane had an enhanced CO₂ absorption only when the more

2. Introduction and motivations

hydrophobic surface was facing the absorbent. The wetting problem was overcome, also the long term efficiency of system was achieved.

Fashand et al. [22] decided to use PVC for the first time in gas-liquid contacting processes for CO₂ capture. The relatively cheap material provides membrane with high hydrophobicity and a structure adequate for its use in the process, with large macrovoids and reduced wall thickness. Thanks to the good processability, high absorption efficiency was achieved by optimization of the take – up speed during spinning process.

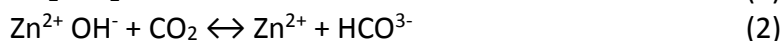
Besides, focusing on materials, researchers also studied the use of different modules. Paul's group [23] disclosed a theoretical study on difference in CO₂ removal performance by flat sheet (FSMC) and hollow fiber (HFMC) polymeric membrane contactors by using amine aqueous solutions. At the studied conditions, flat sheet membrane contactors showed better results. Nevertheless, the authors admit that before choosing a suitable module a number of factors should be considered, such as membrane properties and operating parameters. Francis Bougie [24] has studied a possibility of using more than one FSMC for CO₂ removal from a gas mixture. The author designed an experiment consisting in connecting up to 3 polymeric membrane contactors, so that the outlet absorbent liquid was directed to the inlet of next compartment. The generated results indicated that there is a proportional increase in CO₂ flux with the number of membranes. Moreover, the author demonstrated that there is a possibility of adding as many membranes as needed to achieve the absorbent solution saturation.

2.1.2.3. Bio – composite

According to Fick's law, an increase of local CO₂ concentration on the membrane side will result in enhanced CO₂ absorption by the system. To achieve it, scientists are modifying the membrane surface, for example by incorporation of biomolecules. The most commonly used enzyme for CO₂ capture studies is carbonic anhydrase (CA). This protein can be found in leaves and it is responsible for catalysis of CO₂ hydration (1) in natural photosynthesis. Moreover, it can be found in blood, where it helps to keep the pH balance. The catalyzed reaction involves a two-step mechanism. The first step (2) is the nucleophilic attack of a zinc – bound hydroxide ion to CO₂. The second step (3) is the regeneration of the active site by ionization

Ambient carbon dioxide capture and conversion via membranes

of the zinc – bound water molecule and removal of a proton from the active site.



The biomimetic systems suffer one main disadvantage: enzyme incorporation into a synthetic support usually results in decrease in its activity caused mostly by structural or functional changes. The researchers are studying the application of different incorporation techniques to overcome this issue.

One option is to use nanoparticles for covalently binding the enzyme. This approach was investigated by Jingwei Hou et al. [25] Bio - catalytic TiO₂ nanoparticles with covalently immobilized carbonic anhydrase were used to prepare super hydrophobic PP membrane by sol-gel coating and surface modification with a silan. Results showed that the enzyme stayed highly active and that the bio - catalytic membrane contactor has a reusability of 10 cycles.

Another method, used by Joel K. J. Yong et al. [26], includes electrostatic adsorption of carbonic anhydrase by layer – by – layer assembly on polymeric membrane surface. The films were applied to the shell side of hollow fiber membranes by static mode where membrane remains in solution and polyelectrolites are forced across the membrane. The results show the formation of thin films only on the surface, without penetration into the inside pores. This lead to another improvement, the pores wetting was significantly reduced and the CO₂ hydration was enhanced in all eximined cases.

Ya-Tao Zhang et al. [27] studied the performance of membrane reactors consisting of PVDF hollow fiber membranes aligned in parallel with nanocomposite hydrogel, with immobilized CA between them. As the porous network of the hydrogel contained free water, crucial for proper functioning of the enzyme, the enzymatic activity remained up to 76 %. The designed reactor effectively separate CO₂ from mixed gas streams of low concentration with a 30 h durability.

2. Introduction and motivations

2.1.3. Absorbents

Absorbents play crucial role in membrane contactor systems as they are the only selective part of the compartment. The effectiveness of the system depends mostly on the affinity of the liquid to CO₂. A number of solutions were studied (**Fig. 2. 5**), in particular bases and amines and their salts. Monoethanolamine (MEA) solution is the most commonly used reference absorbent.

The theoretical study conducted by Subham Paul's group [23] about the use of pure and blended amines included aqueous solutions of MEA, DEA, MDEA and AMP as absorbent solutions for CO₂ capture by flat sheet membrane contactor (FSMC). It was proven that MEA has the highest absorption flux rate among single amines and that the increase in its concentration in blends results in increase of absorption rate as well.

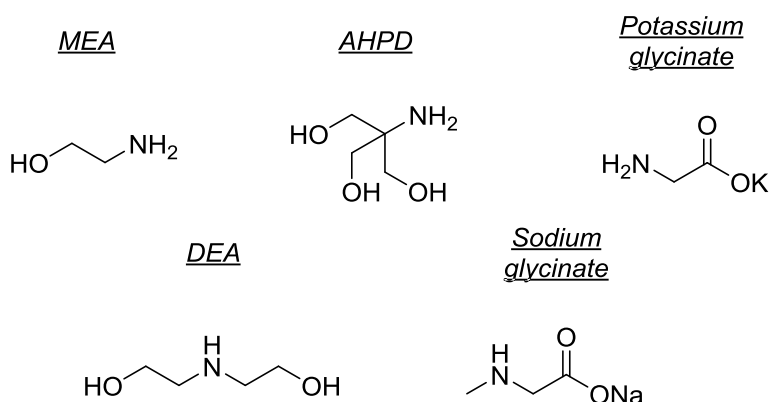


Figure 2. 5. Amines used in CO₂ absorption studies.

The use of aqueous amine solution was investigated also by Francis Bougie [24]. Piperazine (Pz) was incorporated as activator of CO₂ removal from CO₂/N₂ gas mixture with aqueous 2-amino-2-hydroxymethyl-1,3-propanediol (AHPD) in polymeric FSMC, comparing the obtained results with an MEA solution. Pz is a secondary diamine activator with good absorption and regeneration capacities and, thanks to its high surface tension, a potential to decrease the membrane wetting. The activated absorbent solution showed a better performance than single AHPD solution, but similar absorption flux to the MEA solution.

Amino acid salts (AAS) such as potassium glycinate, sodium glycinate, potassium sarcosine and sodium sarcosine were compared with MEA and NaOH by Nihmiya Abdul Rahim et al. [28]. The AAS solutions show

better CO₂ absorption performance but only at low molar ratios, because the decreased pH enhance the release of CO₂.

Muhammad Saeed [29] used Zinc complexes to promote K₂CO₃ absorption in a contactor system. The Zn – cyclen complex mimics carbonic anhydrase (the enzyme mentioned in bio – composite membranes section), but the studies show that it is more stable and has a longer life time as compared to the natural enzyme. Promotion of the absorbent results in a 10-fold improvement of the adsorption rate.

2.2. Carbon dioxide hydrogenation in CO₂ utilization technologies

Once CO₂ is captured, it can be converted to useful products by a number of technologies. The mostly applied utilization methods are: Enhanced oil recovery (EOR) & Enhanced coal bed methane (ECBM), mineral carbonation, biofuels production from microalgae cultivation, chemical CO₂ conversion to fuel, enhanced geothermal systems and food processing. An analysis of patents search conducted by Norhasyima et al. [30] covering the years 1980-2017 shows that the majority (53 %, 1592 patents) corresponds to technologies focused on chemicals and fuels production. This is because CO₂ can be converted to many useful products, such as CO, syngas, hydrogen, methane, methanol, formic acid, dimethyl ether, formaldehyde, urea and others. Moreover, it can be directly used as a reagent for the synthesis of more complex organic compounds.

2.2.1. Metal-catalyzed hydrogenation to formic acid

The metal-catalyzed CO₂ hydrogenation first involves a dissociative chemisorption of H₂ on the metal surface, as seen in **Fig. 2. 6**. Once the CO₂ is also chemisorbed, it reacts with a hydrogen atom producing a metal-formate. Further reaction of this with another hydrogen releases formic acid.

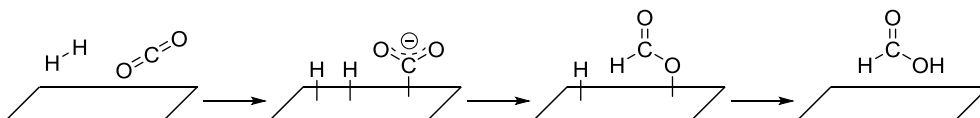


Figure 2. 6. CO₂ hydrogenation mechanism on a metallic catalyst.

The most commonly used catalyst are transition metal-based. Nickel is a metal commercially exploited in hydrogenation reactions such as reductions of unsaturated organic compounds in food industry or petrochemistry. Wang et al. [31] used nickel based catalyst in form of nanoparticles to transform bicarbonate and CO₂ to formate. An alloy of Ni:Pd in the proportion of 7:3 was identified to be

2. Introduction and motivations

the most active catalyst, achieving TOF of 2.8 h^{-1} in mild reaction conditions. The bimetallic catalyst revealed a superior activity due to the small size of the metallic particles and the stabilizing effect of Pd to Ni. Furthermore, hydrogen was found to be easily activated by the catalyst.

2.2.2. Photocatalytic reduction of CO_2

Photoreduction happens via light-induced electrons excitation, which produces electron-hole pairs (Fig. 2. 7). This is a fundamental step of the process, with the energy band gap being characteristic for each catalyst. The mostly studied catalysts are transition metal catalysts because of their high activity and ability to suppress hydrogen generation in aqueous conditions. In particular, rhenium (I) and ruthenium (II) complexes [32, 33] were found to reduce CO_2 to CO and formic acid with a very low yield of H_2 .

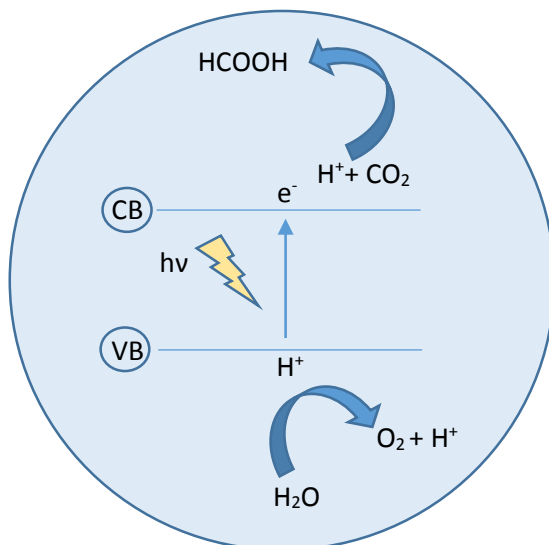


Figure 2. 7. CO_2 hydrogenation mechanism in photocatalytic reduction.

For the sake of cost reduction, research has been focused on the production noble metal-free catalysts: manganese [34] or $\text{CoSn}(\text{OH})_6$ [35] were found suitable for the reaction. TiO_2 based photo-catalysts have been extensively studied due to their stability, non-toxicity and low production cost. Liu et al. [36] studied CO_2 adsorption/dissociation, the charge transfer mechanism, and the reaction pathways/product selectivity of the TiO_2 photo-catalyst. The author concluded that the crystal phase, surface defects and the modifications are the primary factors affecting the photoreduction efficiency of the catalyst.

Electrolyte effects have also been investigated beyond the metal characteristics. Lin et al. [37] reported that the transportation of photo-induced

Ambient carbon dioxide capture and conversion via membranes

charges of CO₂ conversion photocatalysis can be accelerated by selecting an appropriate solvent. Their results using cobalt complexes showed that the CO₂ solubility in the solvent have a strong effect on the performance, whereas other parameters such as solvent viscosity do not have a clear influence.

2.2.3. Electrochemical conversion

The electrochemical conversion of carbon dioxide to organic fuels is carried in a cell where the water splitting at the anode forms the protons needed at the cathode for the reduction (**Fig. 2. 8**). Some cell configurations include a proton permeable membrane in between the electrodes to prevent the oxidation of the reduced products while ensuring the proton diffusion to catholyte.

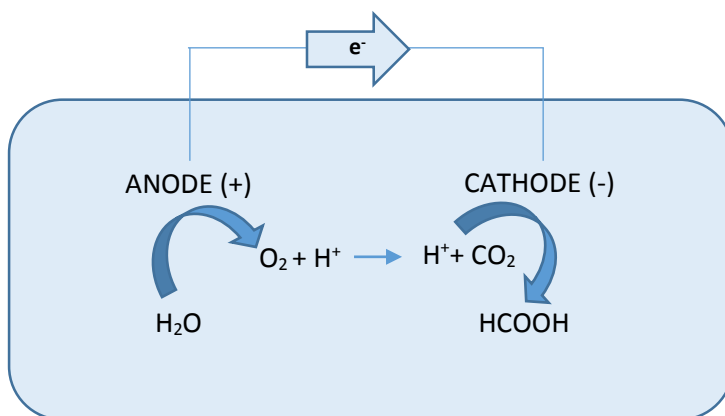


Figure 2. 8. CO₂ electro chemical conversion mechanism.

A number of metallic electro-catalysts were studied in terms of activity and product selectivity. Among them, Cu exhibits a distinct catalytic ability to produce a wide range of CO₂ reduction products, maintaining high faradic efficiency [38]. Hydrogen evolution in aqueous electrolyte is a competitive reaction which contributes to the loss of the reaction efficiency. Hydrogen can be originated from the reduction of water or from protons [39]. To overcome the hydrogen evolution, a high overpotential must be applied during the electrolysis. The electro-reduction is a pH dependent process as the form CO₂ will be present in solution depends on this parameter (**Fig. 2. 9**): CO_{2 (aq)} < HCO₃⁻ < CO₃²⁻. Studies were conducted on CO₂ saturated electrolytes, in which CO₂ was purged to KHCO₃ solutions until a stable pH was obtained. It was found that the bicarbonate improves

2. Introduction and motivations

the conversion, providing high concentrations of CO_2 species near to the cathode. Following these observations, Hosseini et al. [40] performed a direct conversion of bicarbonate to formate. They used bicarbonate as both electrolyte and CO_2 source. The composite electrode made up of tin, nanodiamond and carbon nanotube gave a faradic efficiency of 67% toward formic acid production.

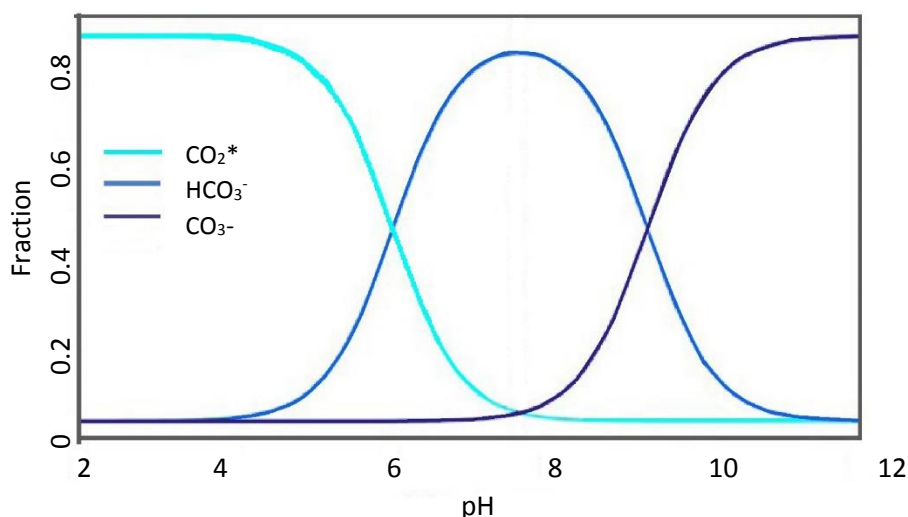


Figure 2. 9. CO_2/pH equilibrium diagram.

2.3. Motivation

Taking into consideration that the CO_2 excess in the atmosphere is a good and free source of CO_2 which can be converted to a fuel, our group conceived design of a system capable of recirculating carbon dioxide and produce energy, mimicking photosynthetic organisms. The system consist of 3 parts combining different operations (Fig. 2. 10): 1) CO_2 capture; 2) bicarbonate hydrogenation to formate; 3) energy production in Direct Formic Acid Fuel Cell (DFAFC).

The first compartment is a container in which one of the walls consist of a membrane allowing the passage of CO_2 to the absorber (1). The captured CO_2 converts to bicarbonate and carbonate and it is used as a substrate for formate production (2). Hydrogenation of carbon dioxide is the result of the electro-reduction at the cathode, while the proton is supplied from water electrolysis at the anode. The proton exchange membrane facilitates the transport of protons and prevents oxidation of reduced species. Furthermore, the obtained formic acid is moved to a

Ambient carbon dioxide capture and conversion via membranes

DFAFC and used as a fuel: the system generates electrical energy (3). For the unit to be self-sufficient, the energy needed for electrolysis is provided from sunlight and it is captured with a solar panel.

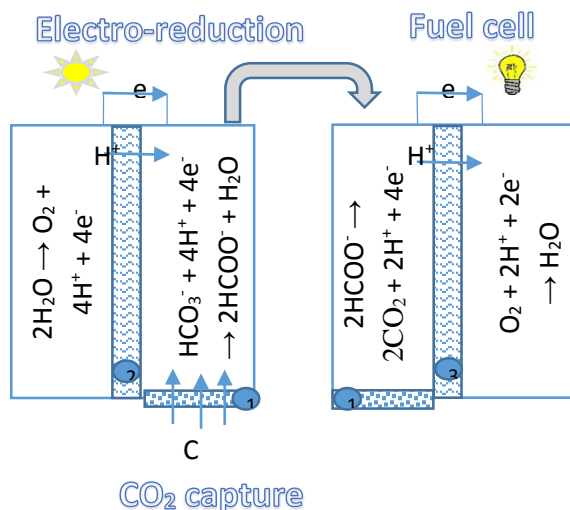


Figure 2. 10. Schematic representation artificial photosynthetic device.

The thesis focuses on the development of the first part of the whole project (1), which consist on a preparation and characterization of a polymeric membrane contactor for CO₂ capture. Moreover, preliminary results on the electrochemical reduction of bicarbonate to formic acid (2) are discussed.

References

- [1] IPCC, Climate Change 2013: The Physical Science Basis, ed. T.F. Contribution of Working Group I to the Fifth Assessment Report of the Intergovernmental Panel on Climate Change [Stocker, D. Qin, G.-K. Plattner, M. Tignor, S.K. Allen, J. Boschung, A. Nauels, Y. Xia, V. Bex and P.M. Midgley (eds.)]2013, Cambridge University Press, Cambridge, United Kingdom and New York, NY, USA. Chapters: 6, TPM.
- [2] Malte Meinshausen, N.M., William Hare, Sarah C. B. Raper, Katja Frieler, Reto Knutti, David J. Frame & Myles R. Allen, Greenhouse-gas emission targets for limiting global warming to 26°C. Nature, 2009. 458: p. 1158 - 1163.

2. Introduction and motivations

[3] Susan Solomon, G.-K.P., Reto Knutti, and Pierre Friedlingstein, Irreversible climate change due to carbon dioxide emissions. PNAS, 2009. 102(6): p. 1704–1709.

[4] Diana Moreira, J.C.M.P., Atmospheric CO₂ capture by algae: Negative carbon dioxide emission path. Bioresource Technology, 2016. 215: p. 371 - 379.

[5] Wendong Zhang, F.D., Wei Zhang, Capture of atmospheric CO₂ into (BiO)₂CO₃/graphene or grapheneoxide nanocomposites with enhanced photocatalytic performance. Applied Surface Science, 2015. 358: p. 75-83.

[6] Anand B. Rao, E.S.R., A Technical, Economic, and Environmental Assessment of Amine-Based CO₂ Capture Technology for Power Plant Greenhouse Gas Control. Environmental Science Technology, 2002. 36: p. 4467 - 4475.

[7] DONALD W (CA) WAY J DOUGLAS (US) BARD ALLEN J (US) DANZIGER ROBERT (US) RYAN CECILY (US) FERNANDEZ MIGUEL (US) , C.B.U.Y.A.U.T.P.B.U.O.S.U.F.K.U.G.R.J.U.D.V.U.K., METHODS OF SEQUESTERING CO₂ E.P. Application, Editor 2010.

[8] (US), C.B.R.U.B.M.U.S.J.U.C.C., CARBON SEQUESTRATION METHODS AND SYSTEMS, AND COMPOSITIONS PRODUCED THEREBY, E.P. Application, Editor 2016, BLUE PLANET LTD. .

[9] Dakhil, F.R., IT) Carbon dioxide capture and storage system 2016, DAKHIL FAROUK United States

[10] RYUL[KR], L.J.W.K.L.K.S.K.P.S., METHOD FOR CAPTURING AND CONVERTING CARBON DIOXIDE FROM EXHAUST GAS AND APPARATUS FOR CAPTURING AND CONVERTING CARBON DIOXIDE FROM EXHAUST GAS, L.C. CORP[KR], Editor 2013.

[11] +, W.Z.Z.S.Z.J.Q.Z.W.J., Preparation of polyvinylamine/polyaniline mixed matrix membranes used for separation of gas containing carbon dioxide, U.T. +, Editor.

[12] DEHONG, Y.J.Y.H.W.J.X.Z.B.J.L.J.Z.Y.Y., Preparation method of metal organic framework membrane for CO₂ separation, U.D. TECH, Editor 2013.

[13] Guohua Jing, F.P., Bihong Lv, Zuoming Zhou, Immobilization of carbonic anhydrase on epoxy-functionalized magnetic polymer

Ambient carbon dioxide capture and conversion via membranes

microspheres for CO₂ capture. *Process Biochemistry*, 2015. 50: p. 2234-2241.

[14] HIRANABE Ryuichiro (Toray Industries Inc., -, Sonoyama 1-chome, Otsu-sh, Shiga 58, 〒5208558, JP) HANAKAWA Masayuki (Toray Industries Inc., 1-1, Sonoyama 1-chome, Otsu-sh, Shiga 58, 〒5208558, JP) KAWAKAMI Tomonori (Toray Industries Inc., 1-1, Sonoyama 1-chome, Otsu-sh, Shiga 58, 〒5208558, JP) CARBON-DIOXIDE-SEPARATING MEMBRANE W.P. Application, Editor 2013, TORAY INDUSTRIES, INC. (1-1 Nihonbashi-Muromachi 2-chome, Chuo-ku Tokyo, 66, 〒1038666, JP) Japan.

[15] George A. Olah, A.G., G. K. Surya Prakash, *Chemical Recycling of Carbon Dioxide to Methanol and Dimethyl Ether: From Greenhouse Gas to Renewable, Environmentally Carbon Neutral Fuels and Synthetic Hydrocarbons*. *Journal of Organic Chemistry*, 2009. 74(2): p. 487–498.

[16] Edoardo Magnone, H.J.L., Jin Woong Che, Jung Hoon Park, High-performance of modified Al₂O₃ hollow fiber membranes for CO₂ absorption at room temperature. *Journal of Industrial and Engineering Chemistry*, 2016. 42: p. 19-22.

[17] Yi-Feng Lin, J.-M.C., Qian Ye, Kuo-Lun Tung, Hydrophobic fluorocarbon-modified silica aerogel tubular membranes with excellent CO₂ recovery ability in membrane contactors. *Applied energy*, 2015. 154: p. 21-25.

[18] Mohammed Abdulmunem Abdulhameed, M.H.D.O., Ahmad Fauzi Ismail, Takeshi Matsuura, Zawati Harun, Mukhlis A. Rahman, Mohd Hafiz Puteh, Juhana Jaafar, Masoud Rezaei, Siti Khadijah Hubadillah, Carbon dioxide capture using a superhydrophobic ceramic hollow fibre membrane for gas-liquid contacting process. *Journal of Cleaner Production*, 2017. 140: p. 1731 - 1738.

[19] Xinhai Yu, L.A., Jie Yang, Shan-Tung Tu, Jinyue Yan CO₂ capture using as superhydrophobic ceramic membrane contactor. *Journal of Membrane Science*, 2015. 496: p. 1-12.

[20] Fabien Porcheron, D.F., Eric Favre, Phuc Tien Nguyen, Olivier Lorain, Régis Mercier, Laurent Rougeau, Hollow fiber membrane contactors for CO₂ capture: from lab-scale screening to pilot-plant module conception. *Energy procedia*, 2011. 4: p. 763-770.

2. Introduction and motivations

[21] Xiaona Wu, B.Z., Liang Wang, Zhaohui Zhang, Hongwei Zhang, Xinhua Zhao, Xingfei Guo, Hydrophobic PVDF/graphene hybrid membrane for CO₂ absorption in membrane contactor. *Journal of Membrane Science*, 2016. 520: p. 120 - 129.

[22] Hossein Fashandi, A.G., Reza Saghafi, Mohammad Zarrebini, CO₂ absorption using gas-liquid membrane contactors made of highlyporous poly(vinyl chloride) hollow fiber membranes. *International Journal of Greenhouse Gas Control*, 2016. 52: p. 13-23.

[23] Subham Paul, A.K.G., Bishnupada Mandal, Theoretical studies on separation of CO₂ by single and blended aqueous alkanolamine solvents in flat sheet membrane contactor (FSMC). *Chemical Engineering Journal*, 2008. 144: p. 352 - 360.

[24] Francis Bougie, I.I., Maria C. Iliuta, Flat sheet membrane contactor (FSMC) for CO₂ separation using aqueous amine solutions. *Chemical Engineering Science*, 2015. 123: p. 255 - 264.

[25] Jingwei Hou, M.Y.Z., Munirah Mohammada, Yatao Zhang, Amir Razmjou, Vicki Chen, Biocatalytic gas-liquid membrane contactors for CO₂ hydration with immobilized carbonic anhydrase. *Journal of Membrane Science*, 2016. 520: p. 303 - 313.

[26] Joel K. J. Yong, G.W.S., Frank Caruso, Sandra E. Kentish, In situ layer-by-layer assembled carbonic anhydrase-coated hollow fiber membrane contactor for rapid CO₂ absorption. *Journal of Membrane Science*, 2016. 514: p. 556 - 565.

[27] Ya-Tao Zhang, L.Z., Huan-Lin Chen, Hong-Man Zhang, Selective separation of low concentration CO₂ using hydrogel immobilized CA enzyme based hollow fiber membrane reactors. *Chemical Engineering Science*, 2010. 65: p. 3199 - 3207.

[28] Nihmiya Abdul Rahim, N.G., Mohamed Al-Marzouqi, Absorption of CO₂ from natural gas using different amino acid salt solutions and regeneration using hollow fiber membrane contactors. *Journal of Natural Gas Science and Engineering*, 2015. 26: p. 108-117.

[29] Muhammad Saeed, L.D., Post-combustion CO₂ membrane absorption promoted by mimic enzyme. *Journal of Membrane Science*, 2016. 499: p. 36-46.

Ambient carbon dioxide capture and conversion via membranes

- [30] R.S. Norhasyimaa, T.M.I.M., Advances in CO₂ utilization technology: A patent landscape review. *Journal of CO₂ Utilization*, 2018. 26: p. 323*335.
- [31] Mengnan Wang, J.Z., Ning Yan, Transformation of sodium bicarbonate and CO₂ into sodium formate over NiPd nanoparticle catalyst. *Frontiers in Chemistry: Inorganic Chemistry*, 2013. 1(17): p. 1-8.
- [32] Mark D. Doherty, D.C.G., James T. Muckerman, Dmitry E. Polyansky, Etsuko Fujita, Toward more efficient photochemical CO₂ reduction: Use of scCO₂ or photogenerated hydrides. *Coordination Chemistry Reviews*, 2010. 254: p. 2472 - 2482.
- [33] Mark D. Doherty, D.C.G., James T. Muckerman, Dmitry E. Polyansky, Etsuko Fujita, Toward more efficient photochemical CO₂ reduction: Use of scCO₂ or photogenerated hydrides. *Coordination Chemistry Reviews*, 2010. 254: p. 2472 - 2482.
- [34] Alessandro Sinopoli, N.T.L.P., Jose F. Martinez, Michael R. Wasielewski, Muhammad Sohail, Manganese carbonyl complexes for CO₂ reduction. *Coordination Chemistry Reviews*, 2018: p. 60-74.
- [35] Xiahui Lina, b., Yilin Gaoa, Min Jianga, Yongfan Zhanga, Yidong Houa, Wenxin Daia, Sibowanga, Zhengxin Ding, Photocatalytic CO₂ reduction promoted by uniform perovskite hydroxide CoSn(OH)₆ nanocubes. *Applied Catalysis B: Environmental*, 2018. 224: p. 1009 - 1016.
- [36] Lianjun Liu, Y.L., Understanding the Reaction Mechanism of Photocatalytic Reduction of CO₂ with H₂O on TiO₂-Based Photocatalysts: A Review. *Aerosol and Air Quality Research*, 2014. 14: p. 453-469.
- [37] Jinliang Lin, B.Q., Guanglian Zhao, Effect of solvents on photocatalytic reduction of CO₂ mediated by cobalt complex. *Journal of Photochemistry and Photobiology A: Chemistry*, 2018. 354: p. 181-186.
- [38] Qi Lu, F.J., Electrochemical CO₂ reduction: Electrocatalyst, reaction mechanism, and process engineering. *Nano Energy*, 2016. 29: p. 439 - 456.
- [39] Hideshi Ooka, M.C.F., Marc T. M. Koper, Competition between Hydrogen Evolution and Carbon Dioxide Reduction on Copper Electrodes in Mildly Acidic Media. *Langmuir*, 2017. 33: p. 9307 - 9313.
- [40] Soraya Hosseini, S.K., Salman Masoudi Soltani, Mohamed Kheireddine Aroua, Houyar Moghaddas, Rozita Yusoff, Improvement of product selectivity in bicarbonate reduction into formic acid on a tin-based

2. Introduction and motivations

catalyst by integrating nano-diamondparticles. Process Safety and Environmental Protection, 2018. 116: p. 494 - 505.

3. OBJECTIVES AND HYPOTHESIS

3. Objectives and hypothesis

Ambient carbon dioxide capture and conversion via membranes

The objectives of the doctoral dissertation are:

1. Polysulfone and polysulfone-nanocomposite membrane contactors studies:
 - Preparation and characterization of flat sheet polymeric membranes by immersion-precipitation processes with different structural features and addition of CuFe_2O_4 nanoparticles. Application of the obtained membranes as contactors in a gas/liquid system for CO_2 capture from air and examination of the influence of the membrane structure and composition on CO_2 flux in dynamic module.
2. Polysulfone membrane contactors in static module:
 - Implementation of the obtained polysulfone membranes as contactors in a gas/liquid system for CO_2 capture from air and examination of the influence of the membrane structure and on CO_2 flux in static module.
3. Modification of polysulfone membrane contactors with activated carbon:
 - Preparation and characterization of flat sheet polysulfone membranes modified with activated carbon. Introduction of the obtained composite membranes as contactors in a gas/liquid system for CO_2 capture from air and examination of the influence of the membrane structure and composition on CO_2 flux in dynamic module.
4. Enzyme immobilization on polymeric membranes:
 - Preparation and characterization of polysulfone and PVA based membranes containing enzymes for carbon fixation, such as: carbonic anhydrase and RubisCo. Studies of different immobilization methods influence on the attachment efficiency, enzyme activity and its structural changes.
5. Conversion of the bicarbonate formed in the previous process to formic acid by electro-reduction with copper – preliminary studies:
 - Electro-catalyst characterization and electro-reduction experiments.

3. Objectives and hypothesis

The main hypothesis are:

1. Polysulfone membrane used as a contactor will facilitate the CO₂ capture from the air by absorbent aqueous solution thanks to open porous structure.
2. The CO₂ capture efficiency of polysulfone membrane contactors in static module operations will be lower but it will be compensate by the lower energy consumption by the system.
3. The introduction of compounds with known affinity to CO₂ capture (e.g. activated carbon, magnetic nanoparticles, enzymes) will allow us to use lower pH values in the absorbing solution and thus to have more durable system working as artificial trees.
4. The absorbing solution can be used directly to produce formic acid or methanol by electro – catalytic reduction.

I. PRISTINE AND NANOCOMPOSITE POLYSULFONE MEMBRANE CONTACTORS

*based on: Adrianna Nogalska, Mario Ammendola, Bartosz Tylkowski, Veronica Ambrogi, Ricard Garcia-Valls, *Ambient CO₂ adsorption via membrane contactors – Value of assimilation from air as nature stomata*, Journal of Membrane Science 546 (2018) 41–49

1. Pristine and nanocomposite polysulfone membrane contactors

The scope of the Chapter I is revealing the influence of polysulfone membrane contactors on atmospheric CO₂ capture rate by chemical adsorption into absorbents aqueous solutions. In this study, polysulfone based membranes were prepared by a Phase Inversion Precipitation method using different polymeric solutions (N,NDimethylformamide or 1-Methyl-2-pyrrolidone). Obtained asymmetric fingerlike, droplike, or spongy morphologies were characterized: by SEM and ESEM equipped with EDX, while their surfaces were investigated by: AFM, dynamic and static contact angle, swelling measurement. Finally, membranes were tested as contactors for CO₂ absorption flux from ambient air into potassium hydroxide aqueous solutions. Moreover, copper - ferrite nanoparticles, used for preparation of composite membranes was characterized by TEM, and X-ray diffraction. Their influence on material CO₂ solubility, membrane surface morphology and wettability were deeply investigated, and demonstrated influence of membranes roughness on their performance.

I.1. Introduction

The content of carbon dioxide in the atmosphere has increased by 40% since industrial revolution, which started around year 1750 and reached a value of 400 ppm in 2010 [1]. CO₂ Emission occurs mainly during fossil fuel combustion, petrochemical processes, manufacture of metals from ores with use of carbon, thermal decomposition of limestone in cement production and fermentation process in alcohol preparation. Even if natural sources of CO₂ emissions are larger than human, increased content of carbon dioxide affects the balance in nature and changes the climate. Due to warming of the atmosphere, Earth surface and oceans, ice sheets are losing mass and sea level is rising. On the other hand, oceans absorb most of CO₂ what cause its acidification [1]. There are few ways for reduction of the emissions like reducing the energy consumption or increasing use of natural renewable energy sources, but in order to eliminate or recirculate the CO₂ that already exists in atmosphere, it has to be captured. The best approach is to take the inspiration from the nature, which since billions of years is improving the CO₂ capture process in photosynthesis by leaves. The main organs used to control the gas exchange in leaves are stomata. Stomata are small adjustable pores situated on the leaf surface and during photosynthesis it allows CO₂ to diffuse into the leaf [2]. According to Nature [3] stomata are small pores on the surfaces of leaves and stems, bounded by a pair of guard cells that control the exchange of gases -most importantly water vapour and CO₂ -between the interior of the leaf and the atmosphere. Very recently Chi Hoon Park et al. [4] reported a study concerning a concept of self-humidifying membranes analogous to vapour exchange mechanism of stomata. By deposition of a thin hydrophobic layers with narrow water channels with controlled thickness and morphology, author obtained a nanocracked surface which opens under humidifying conditions allowing water and ion molecules to pass. Whereas, our approach is focused on the stomata role in CO₂ assimilation process. Currently CO₂ capture processes are using physical or chemical solvents and membrane technology. Recently, new hybrid systems that combine membranes and absorbent solutions have been developed [5,6]. These are very compact systems, where the membrane contactor is a gas permeable barrier between liquid solutions and gas [7]. This hybrid system, named as membrane contactor, combines an advanced membrane with an effective absorbing aqueous solution. The selective sorbent performs as the separator function, while the membrane facilitates the mass exchange process by expanding the phase contact surface area [8].

1. Pristine and nanocomposite polysulfone membrane contactors

This membrane contactor system mimics the leaf structure for carbon dioxide capture process, where the pores play the role of stomata. Moreover the membrane contactor system possesses the following advantages: (1) it provides large contact surface area between phases, without need to disperse one phase into another; (2) it is modular; (3) it is not sensitive to flooding, channelling or back-mixing; (4) its operational flow rates are wide; (5) the system footprint can be custom designed and modified; and (6) the overall system size is small.

Polysulfone (PSf) has been widely used as a membrane material due to its mechanical strength, thermo-stability, stability against chemicals and relative hydrophobicity [9,10]. Furthermore, the membrane internal morphology is easy to control by simply changing preparation conditions [11]. Because of the above properties, this polymer provides a potential application in the membrane gas absorption processes [12]. Several studies on PSf with different additives have shown that is possible improve CO₂ flux, by modifying morphology and characteristics of the membranes. M. Rahbari-Sisakht et al. investigated the effects of surface macromolecules on the morphology of PSf hollow fiber membrane contactor for CO₂ absorption. They used SMM, macromolecules with an amphipathic structure, with their main chain composed by polyurea or polyurethane polymer (hydrophilic part), which is end-capped with two low polarity fluorine-based polymer (oligomer) chains (hydrophobic part). In this case, also, the results shows that CO₂ absorption flux was enhanced [13].

Spinel materials, such as ferrites, attracted research interest because of their special properties, e.g. catalytic, magnetic, gas sensing, and electronic conductivity [14]. Positively charged copper particles have shown improving influence in copper surface activity what enhances CO₂ complexation. J.H. Lee et al. performed experiments, in which Cu nanoparticles in ionic liquid were applied to CO₂ separation membranes. Experimental results show their good selectivity and gas permeance, and revealed that partially positively charged Cu nanoparticles facilitate CO₂ transport [15]. It is expected that CuFe₂O₄ nanoparticles will facilitate membrane contactor absorption properties.

Published studies are mostly focused on CO₂ absorption from flue gas, thus in absorption experiments of pure CO₂ or its mixture with N₂. The approach of the present article is to capture CO₂ from atmosphere, such as photosynthetic organisms do. Therefore, we could describe our research as

the development of artificial stomata's (the pores that are present in the leaves of the trees and are responsible from the exchange of gases). The novelty of this study is the use of MC in ambient CO₂ fixation. Flat sheet contactors are less frequently described in the literature than hollow fiber membranes. However, they possess some advantages compared with hollow fibers, for instance they are easy to prepare, characterize, and the module is easy to assemble and scale up. Some authors report the linear relationship between the absorption rate and the liquid flow rate within the module [16]. Besides, CO₂ flux increases directly with the pore size, which is also related to a decrease in the membrane wetting and, therefore, asymmetric membranes are favorable [17]. The hydrophobic character of the membrane in gas/ liquid contactor system was found to be highly important. Studies on influence of polymeric membrane hydrophobicity on CO₂ recovery show an increase of CO₂ flux when membrane hydrophobicity also grows [18]. Membrane wetting causes an enhancement on membrane mass transfer resistance. Moreover, absorbent surface tension also has an effect on the membrane wetting, high surface tension can increase the water contact angle [19].

I.2. Experimental

I.2.1. Materials

Polysulfone (Mw 35.000 Da) in transparent pellet form; N,N-Dimethylformamide (DMF, 99%); and 1-Methyl-2-pyrrolidone (NMP, ACS) were purchased from Sigma Aldrich and used for flat sheet membrane manufacture. Distilled water was used as coagulation bath in membrane preparation. 2-propanol (99.8%, extra dry) from Acros Organics was added to the coagulation bath in case of preparation of M5. Hollytex non-woven made of polyester with a density of 34 g/m² was acquired from Servicios Tecnicos y Equipamientos para Museos (Stem) and used as support in the module. Extra pure potassium hydroxide in pellets (Sharlab) was dissolved in deionized water to prepare absorptive solutions. Carbon dioxide ion selective electrode and all needed solutions were purchased from Thermo Scientific: 1000 ppm as CaCO₃ standard solution for the calibration, Carbon Dioxide Buffer Solution to adjust solution pH to the operating range of the electrode and the electrode internal filling solution. CO₂ used for permeability and solubility tests was provided by Carburos metalicos company, Spain. All chemicals were used without any further purification.

I. Pristine and nanocomposite polysulfone membrane contactors

I.2.2. Membranes preparation



Figure I. 1. Casting Knife Film Applicator.

Table I. 1. Polymeric solutions composition and pristine and nanocomposite polysulfone membranes preparation parameters.

Membrane	Polysulfone content (%wt)	Solvent (80% wt)	Additive CuFe ₂ O ₄ (%wt)	Coagulation bath	Casting knife [μ m]
M1	20	DMF	-	Water	300
M2	20	DMF	-	Water	250
M3	20	NMP	-	Water	250
M4	20	NMP	-	Water	200
M5	20	DMF	-	i-propanol: DMF 2:1	250
M6	19	DMF	1 %	Water	300
M7	19	DMF	1 %	Water	250
M8	19	NMP	1 %	Water	250
M9	19	NMP	1 %	Water	200

All membranes were prepared by phase inversion precipitation in ambient conditions. The proper amount of polymer was dissolved in an organic solvent and mixed with additives if added. Copper ferrite na-

nanoparticles were prepared according to literature [20]. The resulting solution was stirred for 48 h and left overnight for degasification. Solutions containing nanoparticles were sonicated for 1 h before the membrane preparation. Obtained mixture was cast on a glass with use of casting knife (**Fig. I.1**) (knife thickness: 200 μm or 250 μm or 300 μm), and immediately immersed into coagulation bath. Membrane precipitates instantly, except M5, which had to be left in coagulation bath over night to precipitate. Prepared flat sheet membranes were taken out from water and left overnight to dry on air. The characteristics of each membrane preparation process conditions are given in **Table I. 1**.

Prepared membrane diversity allows to examine influence of membrane morphology, thickness and addition of CuFe_2O_4 nanoparticles on CO_2 absorption rate.

I.2.3.Characterization methods

Scanning electronic microscopy (JEOL JSM-6400 Scanning Microscopy Series) was used to examine the membranes morphology. The samples were immersed into liquid nitrogen, fractured and coated with gold particles (sputtering). The membrane cross-section micrographs were taken by using a magnification value of 350. Images obtained from SEM were analyzed with ImageJ and IFME software [21], in order to obtain information about membrane asymmetry, mean pore size and thickness. The membrane overall porosity (ϵ) was determined from the bulk and the polysulfone density, by using the following equation:

$$\epsilon = \left(1 - \frac{\rho_m}{\rho_{psf}}\right) 100\% \quad (1)$$

where ρ_m and ρ_{psf} correspond to membrane and polysulfone density respectively.

The membrane surface morphology and roughness were analyzed by Atomic Force Microscopy (AFM) -Molecular Imaging model Pico SPM II (Pico+), together with the WsxM software. The membrane surfaces were imaged in a scan size of 2 μm \times 2 μm . The surface roughness parameters of the membranes expressed in terms of the mean roughness (Ra), and the root mean square of the Z data (Rq) were obtained by roughness analysis calculated by the software.

1. Pristine and nanocomposite polysulfone membrane contactors

The chemical stability tests included contact angle and swelling. Contact angle measurements employing Dataphysics OCA 15EC. A 3- μ L droplet of milli-q water or 0.6 M KOH, was placed on to the bottom surface of the membrane. The contact angle was calculated from a digital image by SCA software included in the apparatus. The measurements were repeated three times and the final result was the mean value. Dynamic contact angle was analyzed by advancing and receding contact angle measurements (ARCA) in dynamic sessile drop (needle in) mode. The dosing volume was adjusted to 2 μ L and two cycles were performed. The hysteresis, defined as the difference between advancing and receding angles, was calculated based on average angle values.

In order to verify the chemical stability of membrane in the presence of strong absorptive solutions, two 5 cm² pieces of membranes were immersed one into the absorbing solution and the other in distilled water for 24 h. After one day, they were taken out, washed with distilled water and dried with filter paper. The swelling tests were made to state if the membranes are capable to soak up any amount of the absorbent. It was calculated based on change in mass before and after immersion according to following equation:

$$Swelling = \frac{(w_2 - w_1)}{w_1} 100\% \quad (2)$$

where w_1 and w_2 refer to membrane weight before and after swelling.

Transmission Electron Microscopy (TEM) was used to determine the morphology and the size of the nanoparticles [22]. TEM images were obtained by JEOL 1011 and the nanosize was confirmed by ImageJ. The physical characterization was done by X-ray diffraction (Siemens EM – 10110BU model D5000). Environmental Scanning Electron Microscope (FEI Quanta 600) equipped with PentaFETx3 Link Dispersive Energy Xray Spectroscopy EDXS system managed by IncaOxford. It was used to examine the nanoparticles composition and its distribution in membrane. Surface microanalyses were performed on top and bottom side of the membranes.

In order to carry out the CO₂ absorption test from ambient air by polysulfone membrane contactor a home-made module was applied. The resulting membranes [9 cm²] were used for CO₂ absorption experiments conducted in a gas-liquid membrane contactor. A volume of 100 ml of 0.64 M KOH solution was employed as liquid absorbent in contact with bottom

Ambient carbon dioxide capture and conversion via membranes

side of a flat sheet membrane placed in a cross-flow module where the upper part was opened to the air (**Fig. I. 2**). The effect of the liquid flow rate was tested within a range of 35–438 ml/min. The absorption experiments were performed during 1 h with stirring. Samples were collected and examined for CO₂ content. All experiments were carried out in 25 °C, 1013 hPa and each one was repeated three times.

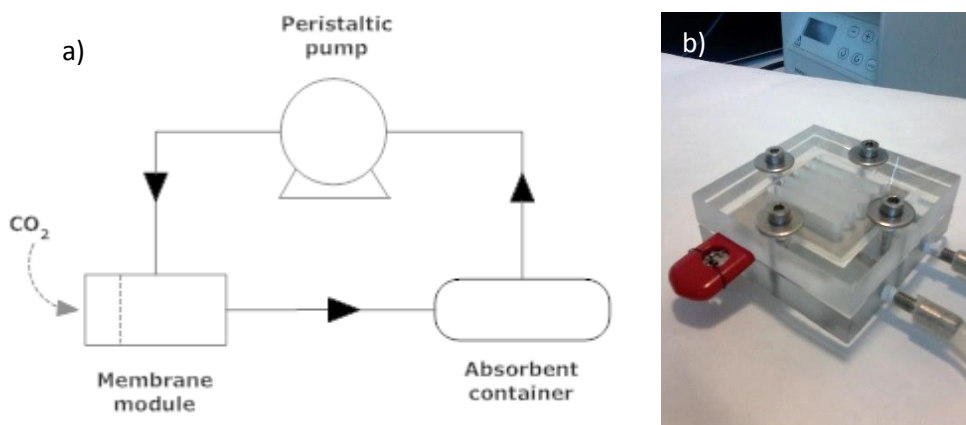


Figure I. 2. System for CO₂ absorption (a) with dynamic module (b).

With the purpose of determining the absorbed CO₂ amount, carbon dioxide ion selective electrode (Thermo Scientific connected with Thermo Scientific Orion Dual Star pH/ISE Benchtop meter) was used. Diluted sample (1 ml sample + 45 Milli-Q water) was mixed with CO₂ buffer (5 ml) in order to adjust the pH to the electrode working pH at 4.8–5.2. The apparatus was set to auto read mode and the stable value of CO₂ concentration was recorded. The results enable to calculate CO₂ flux J [mol/m²*s] in the membrane contactor by equation:

$$J_{CO_2} = \frac{Q_i * M_{CO_2}}{A} * 1000 \quad (3)$$

where Q_i is the absorbent flow rate [m³/s], M_{CO_2} is CO₂ concentration in the absorbent [mol/L] obtained from the measurements and A is the area of the flat sheet membrane [m²].

Gas permeation test was carried out using a self-made stainless steel dead-end apparatus containing a membrane to measure the carbon dioxide permeance. The effective membrane area in the module was 12.6 cm². **Fig. I. 3** shows a schematic representation of the system used in the process. Pure CO₂ was injected into the module. Permeated gas flow was measured

1. Pristine and nanocomposite polysulfone membrane contactors

at 1 bar, 2 bar and 3 bar, respectively, using a precision gas mass flow controller (Alicat scientific MC-500SCCM-D).

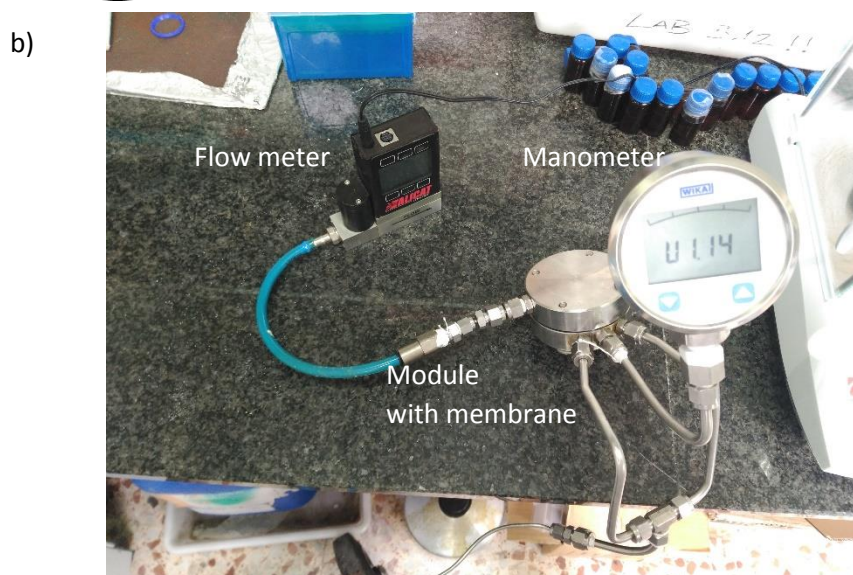
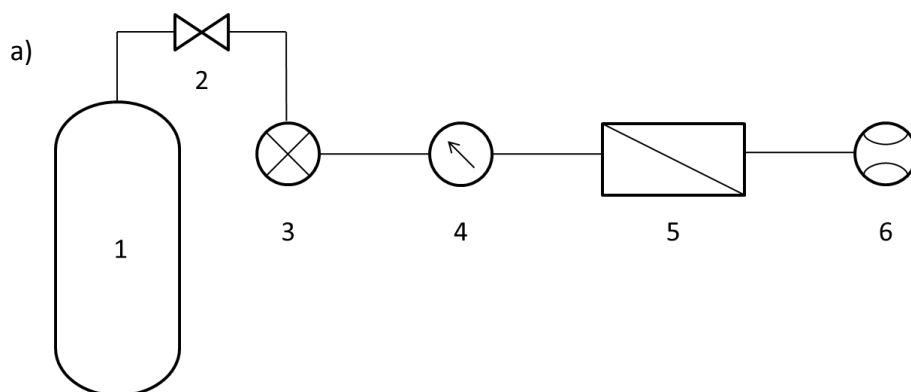


Figure 1. 3. Gas permeability system on scheme (a) and on photo (b): 1) CO₂ gas bottle, 2) valve, 3) pressure transducer, 4) manometer, 5) steel module containing membrane, 6) gas flow meter.

Finally, a mass transfer coefficient k [mol/s*m²*Pa], was calculated following the equation:

$$k = \frac{n}{A\Delta P} \quad (4)$$

where n stays for mass transfer [mol/s], A is membrane area [m²] and ΔP driving force pressure gradient [Pa].

Ambient carbon dioxide capture and conversion via membranes

The solubility of CO₂ into studied materials: polymeric membrane, nanocomposite membrane and nanoparticles themselves, was studied by measurements of the pressure decay using the system described in **Fig. I. 4**. Analyzed material was placed in the module and the valve 2 was open to introduce the CO₂ to the system. When the pressure reached 2 bar, the valve (2) was closed and pressure decrease was measured. The solubility was calculated according to the Eq. (5):

$$n_{CO_2} = \frac{(p_i - p_f)V}{RT} \quad (5)$$

where n is the adsorbed moles of CO₂, p_i and p_f are the initial and final pressures [Pa], respectively, V is gas volume of gas [m³], R is gas constant (8.314 [J/K/mol]) and T [K] is temperature.

The solubility coefficient, S_{CO_2} , expressed in [m³ (STP)/m³ polymer atm] units, which are commonly used when referring to the solubility of gases, is calculated respectively through:

$$S_{CO_2} = \frac{V_{CO_2m}(STP)}{V_m \cdot p_{established}} \quad (6)$$

where V_{CO_2m} (STP)[m³], is the volume of CO₂ corresponding to n_{CO_2} at STP conditions (1 atm, 273.15 K), V_m is the analyzed material volume [m³] and $P_{established}$ [atm] is the pressure measured at equilibrium conditions.

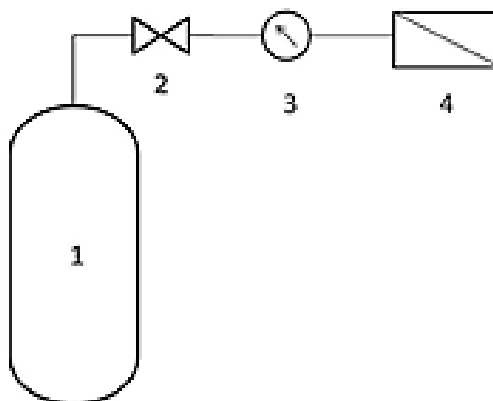


Figure I. 4. CO₂ solubility system: 1) CO₂ gas bottle, 2) valve, 3) manometer, 4) steel module containing membrane.

1. Pristine and nanocomposite polysulfone membrane contactors

1.3. Results and discussion

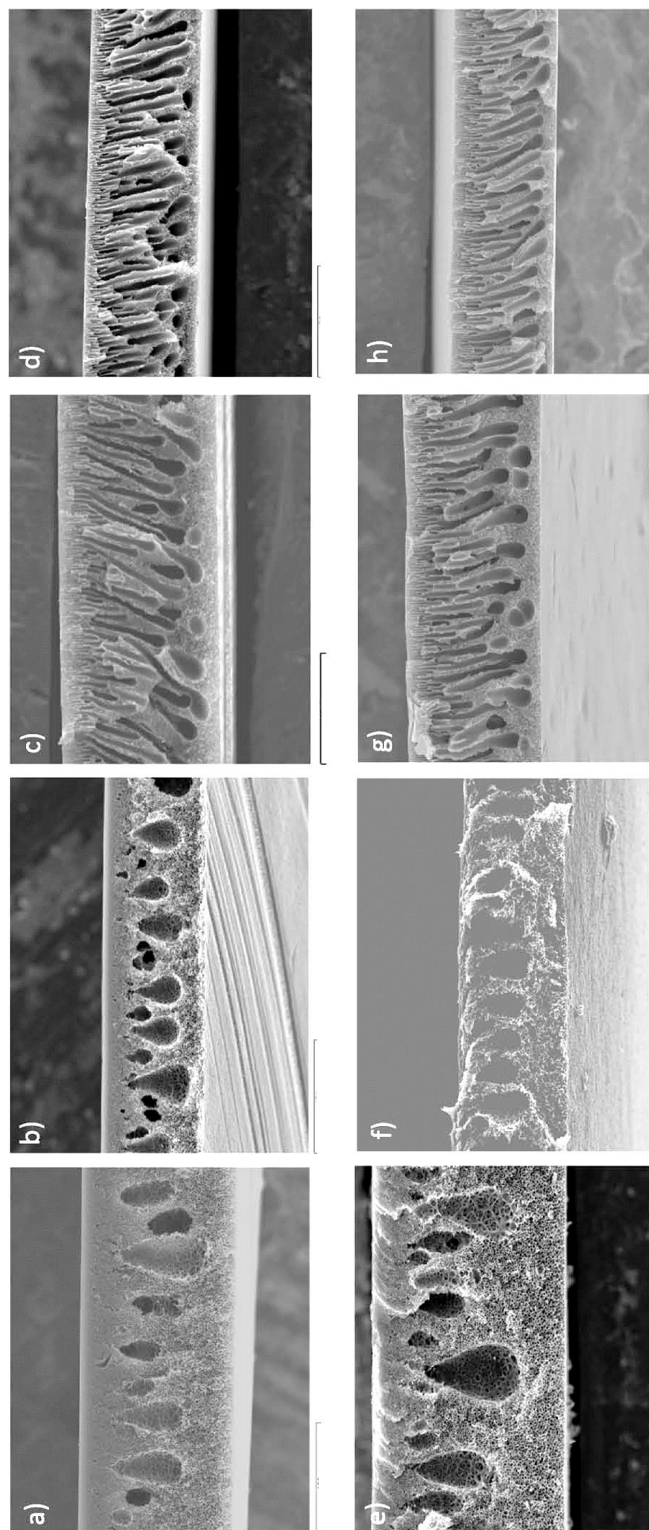
The velocity of precipitation is the factor, which affects mainly the membrane morphology in immersion precipitation process. Fast penetration of coagulant into polymer solution results in asymmetric membranes formation. The slower the process is, the more leads towards to a symmetrical structure. The composition of the coagulation bath also influences the rate of previously mentioned velocity. Thus, if bath contains a weak nonsolvent or addition of a solvent, it slows the precipitation down. The resulting membrane thickness depends on several factors like the precipitation kinetics but also the viscosity and the casting knife preselected thickness. For instance, the membrane obtained by a fast precipitation process, contains fingerlike macrovoids (M3), is thicker, than the one obtained by a slower process (M5). This makes sense, as for the same amount of polymeric material, as the rate of precipitation is higher and the positioning of the polymer is more random, the process leaves a number of large voids.

Table 1. 2. *Characteristics of the resulting pristine and nanocomposite polysulfone membranes.*

Membrane	Thickness [μm]	Assymetry [%]	Porosity (ε) [%]	Mean pore size [μm]
M1	138.4 ±0.5	11	65.3	5.3 ±0.1
M2	90 ±1	9	66.9	3.6 ±0.1
M3	142.2 ±0.3	12	77.4	4.6 ±0.1
M4	99 ±1	5	72.9	1.8 ±0.2
M5	76 ±3	9	57.3	4.2 ±0.2
M6	176.3 ±0.6	12	73.0	2.2 ±0.1
M7	100 ±2	4	71.2	4.9 ±0.2
M8	123 ±1	6	71.3	5.0 ±0.1
M9	92 ±1	13	69.8	4.8 ±0.2

Ambient carbon dioxide capture and conversion via membranes

Figure I. 5. SEM micrographs of the fabricated flat sheet membranes cross section, respectively pristine polysulfone membranes: a) M1, b) M2, c) M3, d) M4 and nanocomposite membranes: e) M6, f) M7, g) M8, h) M9. *scale bar corresponds to 100 μm



1. Pristine and nanocomposite polysulfone membrane contactors

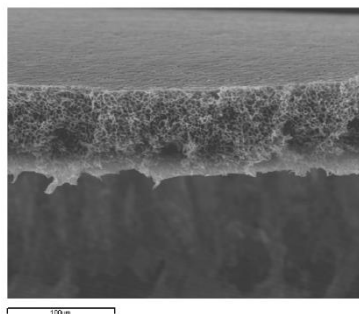


Figure I. 6. Internal morphology of the pristine membrane M5.

The characterization results (**Table I. 2**) together with analysis of morphological structures (**Fig. I. 4**) give full information about membrane qualities. The membranes obtained by dissolution of the polymer in DMF and precipitating in water (M1, M2) contain droplet like voids in the middle of cross section. Around those voids, it can be observed a sponge structure (**Fig. I. 5**) with low asymmetry and large macrovoids. On the other hand, the membranes precipitated from polysulfone and NMP solutions (M3, M4) resulted to have a fingerlike structure on top of a sponge like bulk matrix (**Fig. I. 5**). Besides, incorporation of nanoparticles does not change significantly the internal membrane morphology with respect to blank polysulfone membranes and they possess characteristic macrovoids structure. The absorption studies will show the clear influence of the additives on the CO₂ absorption rate. The thinnest membrane is M5 that has a sponge like structure without any macrovoids formed (**Fig. I. 6**). Almost half of its volume corresponds to pores. This membrane was hard to produce with lower thickness as it did not make a solid film. Moreover, nanoparticles incorporation did not succeed, probably due to use of the solvent in the coagulation bath.

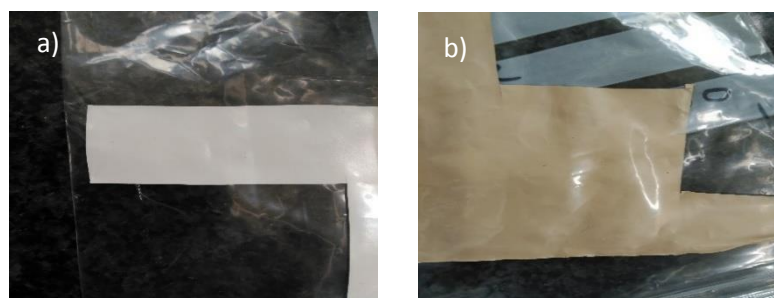


Figure I. 7. Pristine (a) and nanocomposite (b) membrane photo.

Ambient carbon dioxide capture and conversion via membranes

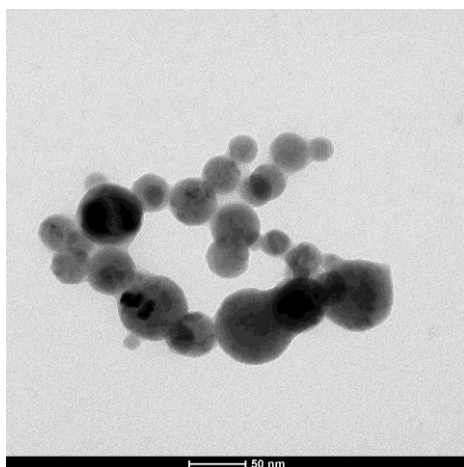


Figure I. 8. TEM micrograph of CuFe_2O_4 nanoparticles.

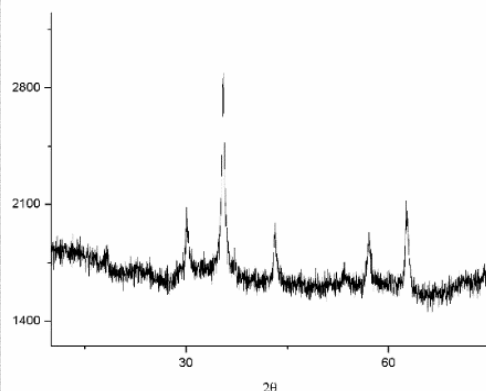


Figure I. 9. XRD analysis of the produced CuFe_2O_4 powder.

Fig. I. 8 shows physical appearance of obtained CuFe_2O_4 particles. As it is observed the synthesized particles are within 20–50 nm nanometer size and spherical shape. X-ray diffraction analysis results confirm the formation of copper ferrite nanoparticles with cubic structure (**Fig. I. 9**), which consist on CuFe_2O_4 as major phase and Fe_2O_3 as minor phase [23]. In particular, diffraction peaks at $2\theta = 30.1, 35.1, 43.4, 54.6, 57.1$ and 63.7 which represent the Bragg reflections from the (220), (311), (400), (422), (511) and (440) planes, are present in the diffraction patterns of both spectra [24]. The obtained peaks and their relative intensities are, in both cases, in agreement with literature data [20, 25]. ESEM analysis was carried out on CuFe_2O_4 nanoparticles. The relative amount of the main elements is: O 62 ± 2, Fe 25 ± 1 and Cu 13.5 ± 0.5 wt%, showing a good agreement with the expected stoichiometry.

The composition of the membranes was determined by (**Table I. 3**) EDX microanalysis integrated in the ESEM. The results show that the amount of Fe and Cu are similar on the top and bottom of each membrane, thus we can conclude that nanoparticles are homogeneously dispersed in the bulk, without significant differences between the surfaces.

I. Pristine and nanocomposite polysulfone membrane contactors

Table I. 3. *Composition of the pristine and nanocomposite polysulfone membranes analyzed by EDX.*

Membrane	Surface	The elements (weight %)				
		C	O	S	Fe	Cu
M1	<i>Top</i>	71.9 ± 0.7	17.5 ± 0.2	9.66 ± 0.03	-	-
	<i>Bottom</i>	72.8 ± 0.7	18.3 ± 0.2	8.87 ± 0.03	-	-
M2	<i>Top</i>	73.4 ± 0.7	18.2 ± 0.2	8.38 ± 0.03	-	-
	<i>Bottom</i>	73.8 ± 0.7	17.4 ± 0.2	8.82 ± 0.03	-	-
M3	<i>Top</i>	73.4 ± 0.7	17.7 ± 0.2	8.82 ± 0.03	-	-
	<i>Bottom</i>	73.7 ± 0.7	18.7 ± 0.2	8.96 ± 0.03	-	-
M4	<i>Top</i>	73.1 ± 0.7	19.1 ± 0.2	7.82 ± 0.03	-	-
	<i>Bottom</i>	73.6 ± 0.7	18.6 ± 0.2	7.81 ± 0.03	-	-
M5	<i>Top</i>	74.4 ± 0.7	16.5 ± 0.2	9.10 ± 0.03	-	-
	<i>bottom</i>	73.2 ± 0.7	17.9 ± 0.2	8.94 ± 0.03	-	-
M6	<i>Top</i>	71.1 ± 0.7	17.2 ± 0.2	8.73 ± 0.03	1.99 ± 0.01	1.02 ± 0.01
	<i>Bottom</i>	70.6 ± 0.7	18.5 ± 0.2	7.85 ± 0.03	1.88 ± 0.01	1.18 ± 0.01
M7	<i>top</i>	70.3 ± 0.7	17.8 ± 0.2	8.69 ± 0.03	1.96 ± 0.01	1.23 ± 0.01
	<i>bottom</i>	70.2 ± 0.7	18.7 ± 0.2	8.19 ± 0.03	1.87 ± 0.01	1.08 ± 0.01
M8	<i>top</i>	70.6 ± 0.7	17.2 ± 0.2	8.65 ± 0.03	1.97 ± 0.01	1.56 ± 0.01
	<i>bottom</i>	70.6 ± 0.7	18.2 ± 0.2	7.98 ± 0.03	1.94 ± 0.01	1.22 ± 0.01
M9	<i>top</i>	70.8 ± 0.7	17.5 ± 0.2	8.48 ± 0.03	1.93 ± 0.01	1.19 ± 0.01
	<i>bottom</i>	70.5 ± 0.7	18.6 ± 0.2	8.18 ± 0.03	1.63 ± 0.01	1.13 ± 0.01

Ambient carbon dioxide capture and conversion via membranes

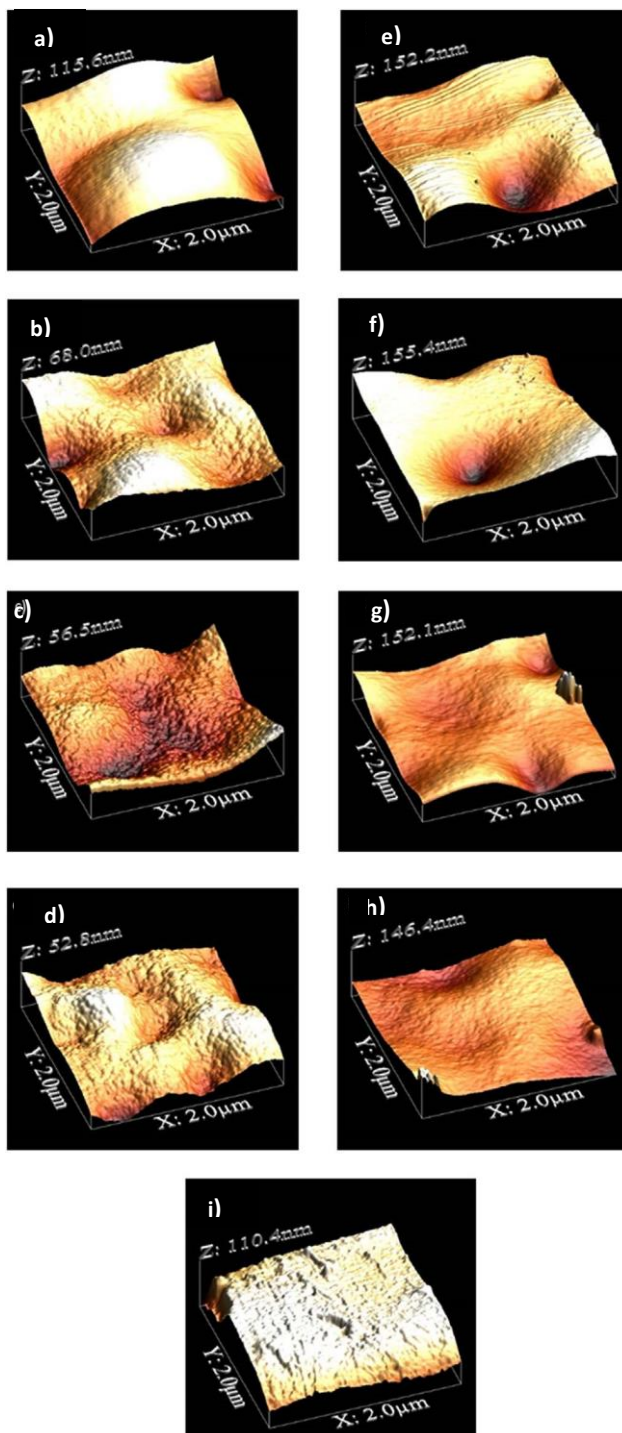


Figure I. 10. AFM 3D micrographs representing bottom surfaces of pristine and nanocomposite membranes: a) M1, b) M2, c) M3, d) M4, e) M6, f) M7, g) M8, h) M9, i) M5.

1. Pristine and nanocomposite polysulfone membrane contactors

Table I. 4. *Pristine and nanocomposite polysulfone membrane surfaces roughness parameters.*

Membrane	Average roughness (Ra)	Root mean square (Rq)
M1	11.0 ± 0.2	13.5 ± 0.4
M2	9.6 ± 0.3	11.9 ± 0.3
M3	4.4 ± 0.1	9.1 ± 0.5
M4	6.6 ± 0.1	8.2 ± 0.3
M5	9.2 ± 0.2	12.7 ± 0.4
M6	19.4 ± 0.4	25.1 ± 0.7
M7	21.9 ± 0.6	29.0 ± 0.6
M8	11.8 ± 0.2	15.6 ± 0.5
M9	12.6 ± 0.4	16.3 ± 0.5

In order to deeply understand the membrane wettability phenomena an exhaustive characterization by means of AFM and contact angle (both static and dynamic) were performed. By carrying out the AFM investigation the mean roughness (Ra), defined as the arithmetic average of the absolute values of the surface height deviations, and the root mean square roughness (Rq), the standard deviation from the mean surface, were measured. The three-dimensional surface images and surface roughness parameters of the M1–M9 membranes are given in **Fig. I. 10** and **Table I. 4**, respectively. Incorporation of nanoparticles in the membrane structure has a significant influence on the average roughness value. Comparing the Ra values of the membranes M1–M4 with their modified equivalents M6–M9, it can be seen that the membranes with nanoparticles have a greater surface roughness (approximately double) than pristine ones as shown in Table 4. This behaviour was previously reported by [26]. Moreover, our studies shown that the membrane obtained with NMP (M3-4), used as a solvent for polymeric solution preparation, have lower roughness values than the one made with DMF (M1-2), due to different membranes morphologies caused by solvent/non-solvent interaction during the polymer precipitation. It well known that the roughness parameter is related to the contact angle of the membrane and its wettability [27]. Letellier et al. [28] and Long et.al. [29] reported that highest values of static contact angle on modified roughness, (including: micro patterned, machined or etched hydrophobic surface) is caused by inhibition of the liquid spreading into grooves, scratches and/or cavities on the rough surface. According to the authors a spreading of such drop can be

Ambient carbon dioxide capture and conversion via membranes

“arrested” by the edges of the grooves. **Table I. 5** provides the static contact angle results measured on M1–M9 membranes. The contact angle results show that all studied membranes are hydrophilic (69 ± 7); however, the static contact angle of the M6-M9 nanocomposite membranes are higher than the values of M1–M4 membranes which possess lower surface roughness, what it is in accordance with literature findings.

Table I. 5. *The contact angle measurements results of pristine and nanocomposite polysulfone membranes surface (where: adv - advancing, rec – receding).*

Membrane	Static contact angle		Dynamic Contact angle			
	Water drop	KOH drop		I cycle°	II cycle°	Hysteresis°
M1	60 ± 2	84 ± 2	adv	79 ± 1	77 ± 5	28.3
			rec	55 ± 4	45 ± 4	
M2	76 ± 3	91 ± 3	adv	73 ± 4	72 ± 5	36.5
			rec	35 ± 2	37 ± 4	
M3	66 ± 3	91.0 ± 0.8	adv	66 ± 4	74 ± 6	24.7
			rec	48 ± 5	43 ± 3	
M4	63 ± 5	92 ± 2	adv	73 ± 2	78 ± 2	17.0
			rec	61.6 ± 0.7	55.5 ± 0.3	
M5	69 ± 3	85 ± 4	adv	79 ± 4	77 ± 2	25.3
			rec	53 ± 4	53 ± 3	
M6	72 ± 1	78 ± 2	adv	84 ± 7	82 ± 8	17.0
			rec	65 ± 10	66 ± 9	
M7	66 ± 2	89 ± 6	adv	74 ± 5	72 ± 5	35.8
			rec	36.6 ± 0.9	37 ± 4	
M8	70 ± 3	83 ± 6	adv	85 ± 12	78 ± 11	35.5
			rec	47 ± 9	46 ± 11	
M9	83 ± 3	86 ± 4	adv	75.4 ± 0.2	73.9 ± 0.4	30.2
			rec	44 ± 1	45 ± 1	

The phenomenon of wetting is more than just a static state. According to Yuan and Lee [30] the measurement of a single static contact angle to characterize wetting behaviour does not provide sufficient

1. Pristine and nanocomposite polysulfone membrane contactors

information. For this reason, in order to understand the wetting behaviour of investigated membrane, further analyses of dynamic contact angle were studied. The difference between advancing and receding contact angles is called contact angle hysteresis. A high advancing /receding contact angle and low contact angle hysteresis is responsible for the low wettability of a material surface [31]. **Table I. 5** gives the dynamic contact angle results, including advancing and receding contact angles in both cycles and the hysteresis values. Generated results demonstrated that all calculated hysteresis are in a range of 17.0–36.5°. The values of advancing and receding contact angle in second cycle are smaller than in the first measurements due to previous wetting of the surface. Membranes containing nanoparticles show higher contact angle degrees but also higher hysteresis, what makes them more susceptible to eventual wetting of the membrane. Monticelli et al. [32] modified polysulfone membranes with nanoclay and demonstrated that the nanoparticles increase membrane wettability.

Next, we evaluated the chemical resistance of the membranes to the alkaline media (0.64 M KOH) in order to ensure a long-term stability during gas/liquid contactor operations. Conducted tests demonstrated that membrane swelling is limited for the absorbent solution (around 1%) in all M1–M9 membranes. On the other hand, M3 and M4 membranes, with fingerlike macrovoids morphologies, show capabilities to water swelling up to 50%. Moreover, water contact angle measurements, performed on the bottom side of the membrane before and after immersion, are not significantly different. This reveals that potassium hydroxide solution does not have a clear influence on the membrane hydrophobicity even after 24 h of exposure. Indeed, the contact angle values measured with KOH solution were higher than those ones obtained for water (see **Table I. 5**). This indicates the compatibility of the chosen absorptive solution with the membranes. Besides, the results of chemical stability test confirm that the investigated membranes are stable under the tested operating conditions (room temperature 25 °C, and atmospheric pressure).

Ambient carbon dioxide capture and conversion via membranes

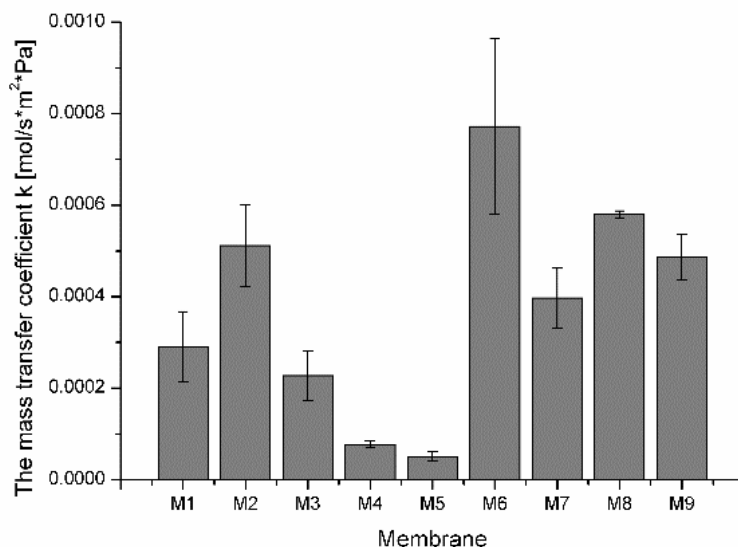


Figure I. 11. CO₂ mass transfer coefficient of pristine and nanocomposite membranes.

Membrane mass transfer coefficient was determined in order to evaluate the influence of membrane mass transfer resistance on the absorption into the system. **Fig. I. 11** shows the membrane mass transfer coefficient calculated from CO₂ permeation through the M1–M9 membranes. Kubica and co-workers [33] reported that heterogeneous polysulfone membranes containing copper terephthalate nanoparticles exhibit significantly higher CO₂ permeation comparing to that of pure polysulfone. According to the authors the porosity of the CuTPA particles play an important role in the increase of the gas permeability. Indeed, as it is shown in **Fig. I. 11**, the CO₂ permeation through the M6–M9 nanocomposite membranes is approximately 40% higher than through the pure M1–M5 membranes. In our opinion, it occurs due to the porous CuFe₂O₄ nanospheres structure [34], as Kubica et al. reported.

Table I. 6. CO₂ solubility studies results of pristine and nanocomposite polysulfone membranes and nanoparticles.

Material	n _{CO2} [mmol]	S [m ³ STP/m ³ atm]
Polysulfone membrane	0.32 ± 0.05	4.79 ± 0.01
Nanocomposite polysulfone membrane	0.23 ± 0.05	5.00 ± 0.02
Magnetic nanoparticles	0.14 ± 0.02	11.41 ± 0.05

1. Pristine and nanocomposite polysulfone membrane contactors

To verify the CO₂ solubility in the studied materials CO₂ adsorption studies were performed for the blank membranes, nanocomposite membranes and nanoparticles (**Table I. 6**). The mole of CO₂ adsorbed by unmodified polysulfone membrane is 50% higher than these adsorbed by the modified membrane, but this value depends on the amount of used material [35]. For this reason the CO₂ solubility in the material (*S*) has to be calculated. The analyses put into evidence that CO₂ solubility in the nanoparticles is two times higher than into the polymeric membranes. However, by comparing the CO₂ solubility into nanocomposite membrane and unmodified one we see, that the presence of the nanoparticles does not influence the membrane CO₂ adsorption.

As it is reported in literature [36], in membrane contactor systems mass transfer is limited by resistance of the gas phase, liquid phase and the membrane itself. In our case the gas phase resistance is not taken into consideration, because of the use of ambient air as CO₂ source, thus the gas concentration is constant in all cases. Hence, the contribution of the liquid boundary layer and the membrane mass transfer resistance can be analyzed. The only driving force for CO₂ diffusion through the membrane is the difference in carbon dioxide concentration in gas and liquid phases, where liquid phase is selective for CO₂ absorption. Our hypothesis is that there is a condensation of CO₂ on top of the surface and that makes this driving force much higher than it would be without the presence of the membrane contactor.

The absorption performance expressed as CO₂ absorption flux, obtained for potassium hydroxide aqueous solution using polysulfone flat sheet membrane contactor (FSMC) in cross flow module is shown as a function of the liquid flow rate (**Fig. I. 12**). CO₂ flux increase with the absorbent flow rate over the range of liquid velocities investigated, always at laminar flow. For the slowest values the mass transfer is mainly influenced by the liquid flow rate [36]. Examined liquid velocities rise up to 400 ml/min, thus by increasing absorbent flow rate, reduction of the resistance occurs, what facilitates the transport.

The CO₂ absorption is increasing slowly with the absorbent flow rate at low velocities. Potassium hydroxide, which reacts with CO₂, is slowly moved to make space for free absorbent. Thus, until a speed of 230 ml/min,

Ambient carbon dioxide capture and conversion via membranes

the increase of CO₂ flux is not significant. As the solution velocity is increasing, unreacted KOH is floating faster, what results in good contact with CO₂ and rise of the flux.

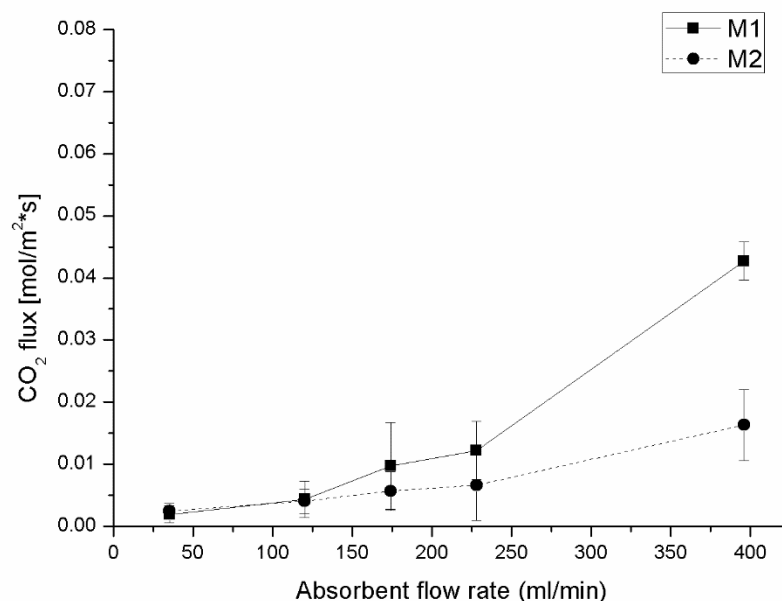


Figure I. 12. Effect of pristine membranes thickness on CO₂ absorption flux.

To verify an influence of membrane thickness on the absorption (**Fig. I. 12**), several experiments were performed with membranes of the same morphology but different thickness. We can conclude that the thicker the membrane, the better is CO₂ flux. There is a lot of free space in membrane, so the resistance in membrane mass transport is becoming lower with increasing of macrovoids size.

In high liquid velocities, mass transport depends mostly on the membrane resistance factor [10]. To study the membrane morphology influence on CO₂ absorption flux, three membranes were chosen: M2, M4, M5, which have similar thickness but different internal structure. Membrane morphology affects CO₂ absorption for velocities higher than 230 ml/min. The flux decreases with the macrovoids size as follow: M4 > M2 > M5 (**Fig. I. 13**). Membrane M5, which possess sponge like structure without macrovoids, exhibits very poor absorption efficiency.

I. Pristine and nanocomposite polysulfone membrane contactors

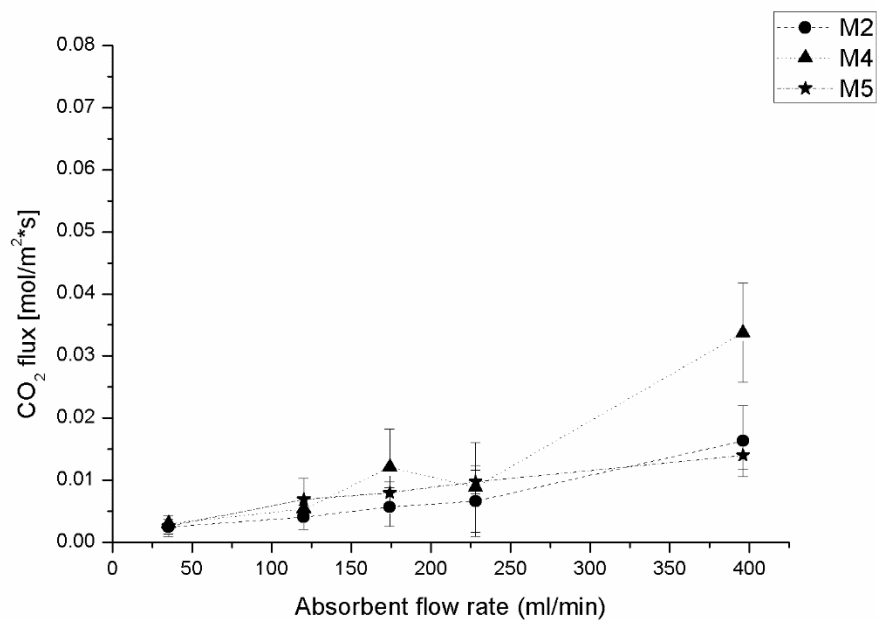


Figure I. 13. CO₂ absorption flux into pristine membranes of different morphologies as a function of liquid flow rate.

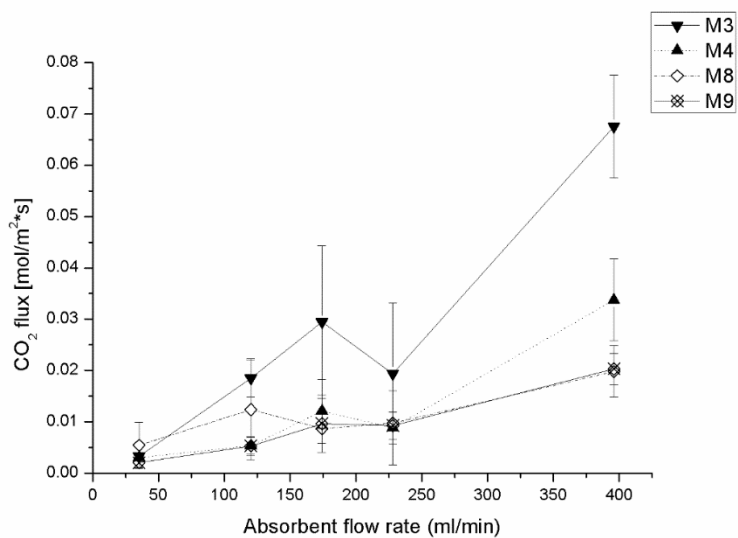


Figure I. 14. Difference in CO₂ absorption abilities of pristine and nanocomposite membrane contactors.

It was expected that CuFe_2O_4 nanoparticles would enhance membrane contactor absorption properties. The results do not show any improvement on the absorption. The absorption results are overlapping for both thicknesses, even at high velocities, where the membrane resistance influence is the highest. The additional factor added to membrane mass transfer resistance is overcoming the influence of polarized copper particles. There is a study in the literature [15] on partially polarized Cu particles absorption properties. In the present article CuFe_2O_4 nanoparticles contain copper which is partially stabilized by ferrite. The nanoparticles should enhance the transport through the membrane by absorbing CO_2 from the air and passing it to the alkaline solution. Comparing obtained values with the CO_2 flux values for each membrane we can see that the membranes with nanoparticles have generally better mass transfer properties (**Fig. I. 11**), but the CO_2 flux into alkaline solution through those membrane (**Fig. I. 14**) is worst.

Finally, a comparison of developed membranes to stomatal CO_2 assimilation efficiency was done. According to the literature the maximum plant stomatal CO_2 assimilation rate is in a range $15\text{--}40 \mu\text{mol}/\text{m}^2\cdot\text{s}$ [37–40] depending on the plant species used for investigation. For example, the value of $20 \mu\text{mol}/\text{m}^2\cdot\text{s}$ of CO_2 assimilation, reported by J. Martínez-Lüscher et al. achieved for grapevine, means that 20 micro moles of CO_2 is captured by 1m^2 of the leaf during 1 s. In order to compare the CO_2 capture capacity of the plant stomata with the artificial one, the results generated in the laboratory should be recalculated using the Eq. (7) where n is moles of CO_2 , A is membrane area [m^2] and t is experimental time [s].

$$J = \frac{n}{A \cdot t} \quad (7)$$

The absorption results for all prepared membranes gives the assimilation value of $27.7\text{--}284.2 \mu\text{mol}/\text{m}^2\cdot\text{s}$. It means that the artificial membrane contactor, designed and developed in our laboratory, is able to absorb even higher amount of CO_2 than the natural stomata. To our knowledge, we also highly improved CO_2 absorption from ambient air in comparison to commercially available membranes (**Table I. 7**).

I. Pristine and nanocomposite polysulfone membrane contactors

Table I. 7. *The artificial stomata CO₂ assimilation rate in range of 35-400 ml/min liquid flow velocities for pristine and nanocomposite polysulfone membranes.*

Absorbent flow [ml/ min]	Membrane contactor CO ₂ assimilation [$\mu\text{mol}/\text{m}^2\cdot\text{s}$]								
	M1	M2	M3	M4	M5	M6	M7	M8	M9
35	95.6	117.4	157.1	143.8	122.8	58.7	149.1	259.6	96.8
120	91.9	78.1	256.7	74.0	95.9	56.2	38.4	172.1	73.7
174	93.0	54.5	281.9	115.6	76.7	56.5	86.9	83.2	92.5
228	89.3	48.5	141.7	64.8	71.3	52.0	85.2	71.3	67.8
396	179.7	68.7	284.2	142.0	58.9	27.7	70.8	83.4	85.5

I.4. Conclusions

Inspired by nature, we designed and developed the artificial stomata for CO₂ absorption based on polysulfone membrane contactor. By using the phase inversion precipitation method and applying different membrane preparation parameters (such as: different solvents, coagulation bath composition, casting knife thickness), we successfully fabricated membrane contactors (76 – 176 μm thickness range) with different morphologies (from a spongy-like to open microvoids one). AFM and Contact angle studies demonstrated that incorporation of nanoparticles in membrane structures increases not only their roughness but also their wettability and CO₂ permeability; however their presence does not improved CO₂ flux. Low swelling and high contact angle values (91° ± 2°) of aqueous potassium hydroxide solutions on polysulfone membranes confirmed excellence process efficiency due the materials compatibility. Furthermore, CO₂ solubility test shown that incorporation of nanoparticles does not changes the membrane adsorption abilities. Beside, generated results show that the highest CO₂ absorption flux (67.5 mmol/m²*s) was obtained by using a fringelike macrovoids membrane, which can assimilate (284.2 μmol/m²*s) a higher amount of CO₂ than the natural stomata (40 μmol/m²*s). To our knowledge this value is also the highest one which have been measured for an artificial system and reported in literature. Furthermore, presented results concern the first membrane contactor established for ambient CO₂ capture. From the study, we can indicate that CO₂ flux increases with increase of absorbent flow rate over the range of liquid velocities investigated. The flux grows with increase of membrane macrovoids size, due to decrease of the membrane mass transfer resistance.

References

- [1] IPCC, Climate change 2013: the physical science basis, in: T.F. Stocker, D. Qin, G.K. Plattner, M. Tignor, S.K. Allen, J. Boschung, A. Nauels, Y. Xia, V. Bex, P.M. Midgley (Eds.), Contribution of Working Group I to the Fifth Assessment Report of the Intergovernmental Panel on Climate Change, 2013 Cambridge University Press, Cambridge, United Kingdom and New York, NY, USA, 2013.
- [2] P.I. Hemesley, A. R, The evolution of Plant Physiology: from Whole Plants to Ecosystems, Linnean Society of London, London, 2004.

1. Pristine and nanocomposite polysulfone membrane contactors

[3] W.F. Hetherington AM, The role of stomata in sensing and driving environmental change, *Nature* 424 (2003) 901–908.

[4] S.Y.L. Chi Hoon Park, Doo Sung Hwang, Dong Won Shin, Doo Hee Cho, Kang Hyuck Lee, Tae-Woo Kim, Tae-Wuk Kim, Mokwon Lee, Deok-Soo Kim, Cara M. Doherty, Aaron W. Thornton, Anita J. Hill, Michael D. Guiver, Young Moo Lee, Nanocrack-regulated self-humidifying membranes, *Nature* 532 (2016) 480–483.

[5] P.H.M.F. Shuaifei Zhao, Liyuan Deng, Eric Favre, Elodie Chabanon, Shuiping Yan, Jingwei Hou, Vicki Chen, Hong Qi, Status and progress of membrane contactors in post-combustion carbon capture: a state-of-the-art review of new developments, *J. Membr. Sci.* 511 (2016) 180–206.

[6] J.G.W. Pingjiao Hao, Jay Kniep, Richard W. Baker, Gas/gas membrane contactors – an emerging membrane unit operation, *J. Membr. Sci.* 462 (2014) 131–138.

[7] IPCC, IPCC special report on carbon dioxide capture and storage, in: B. Metz, O. Davidson, D.C. de Coninck, M. Loos, L.A. Meyer (Eds.), Prepared by Working Group III of the Intergovernmental Panel on Climate Change, Cambridge University Press, Cambridge, United Kingdom and New York, NY, USA, 2005.

[8] A.D. Anna Witek-Krowiak, Szymon Modelski, Daria Podstawczyk, Carbon dioxide removal in a membrane contactor – selection of absorptive liquid/membrane system, *Int. J. Chem. Eng. Appl.* 3 (2012).

[9] M. Mulder, *Basic Principles of Membrane Technology*, Kluwer Academic Publisher, Dordrecht, Boston, London, 1996.

[10] B. Tylkowski, F. Carosio, J. Castañeda, J. Alongi, R. García-Valls, G. Malucelli, M. Giamberini, Permeation behavior of polysulfone membranes modified by fully organic layer-by-layer assemblies, *Ind. Eng. Chem. Res.* 52 (2013) 16406–16413.

[11] C. Torras, Obtenció de membranes polimèriques selectives, in: Chemical Engineering Dep., Universitat Rovira i Virgili, Tarragona, 2005. *Journal of Membrane Science* 546 (2018) 41–49

[12] A.D.A. Witek-Krowiak, S. Modelski, D. Podstawczyk, Carbon dioxide

Ambient carbon dioxide capture and conversion via membranes

removal in a membrane contactor -selection of absorptive liquid/membrane system, *Int. J. Chem. Eng. Appl.* 3 (2012).

[13] A.F. Ismail, M. Rahbari-Sisakht, D. Rana, T. Matsuura, Effect of novel surface modifying macromolecules on morphology and performance of Polysulfone hollow fiber membrane contactor for CO₂ absorption, *Sep. Purif. Technol.* 99 (2012) 61–68.

[14] L.L. Zhipeng Sun, Dian zeng Jia, Weiyu Pan, Simple synthesis of CuFe₂O₄ nanoparticles as gas-sensing materials, *Sens. Actuators* 125 (2007) 144–148.

[15] J.H. Jung Hyun Lee, Jong Hak Kim, Yong Soo Kang, Sang Wook Kang, Facilitated CO₂ transport membranes utilizing positively polarized copper nanoparticles, *Chem. Commun.* 48 (2012) 5298–5300.

[16] I.I. Francis Bougie, Maria C. Iliuta, Flat sheet membrane contactor (FSMC) for CO₂ separation using aqueous amine solutions, *Chem. Eng. Sci.* 123 (2015) 255–264.

[17] S.-H.L. Shia-Chung Chena, Rean-Der Chiend, Ping-Shun Hsua, Effects of shape, porosity, and operating parameters on carbon dioxide recovery in polytetrafluoroethylene membranes, *J. Hazard. Mater.* 179 (2010) 692–700.

[18] K.-L.T. Su-Hsia Lin, Hao-Wei Chang, Kueir-Rarn Lee, Influence of fluorocarbon flatmembrane hydrophobicity on carbon dioxide recovery, *Chemosphere* 75 (2009) 1410–1416.

[19] D.W.F.Bb. V.Y. Dindore, F.H. Geuzebroek c, G.F. Versteeg, Membrane – solvent selection for CO₂ removal using membrane gas – liquid contactors, *Sep. Purif. Technol.* 40 (2004) 133–145.

[20] E.A.P. Alvaro Cruz-Izquierdo, Carmen Lopez¹, Juan L. Serra¹, Maria. J. Llama, Magnetic cross-linked enzyme aggregates (mCLEAs) of *Candida antarctica* Lipase: an efficient and stable biocatalyst for biodiesel, *Synthesis* 9 (2014) 1–22.

[21] R.G.-V. Carles Torras, Quantification of membrane morphology by interpretation of scanning electron microscopy images, *J. Membr. Sci.* 233 (2004) 119–127.

1. Pristine and nanocomposite polysulfone membrane contactors

- [22] B. Tylkowski, I. Tsibranska, Overview of main techniques used for membrane characterization, *J. Chem. Technol. Metall.* 50 (2015) 3–12.
- [23] R.M. Mohamed, M.M. Rashad, M.A. Ibrahim, L.F.M. Ismail, E.A. Abdel-Aal, Magnetic and catalytic properties of cubic copper ferrite nanopowders synthesized from secondary resources, *Adv. Powder Technol.* 23 (2012) 315–323.
- [24] Jeevan M. Bhojane, Jayashree M. Nagarkar, Sachin A. Sarode, An efficient magnetic copper ferrite nanoparticle catalysed ligand and solvent free synthesis of N-aryl amide from aldoximes and iodobenzene, *RSC Adv.* 5 (2015) 105353–105358.
- [25] R.M. Mohamed, M.M. Rashad, M.A. Ibrahim, L.F.M. Ismail, E.A. Abdel-Aal, Magnetic and catalytic properties of cubic copper ferrite nanopowders synthesized from secondary resources, *Adv. Powder Technol.* 23 (2012) 315–323.
- [26] R.W. Yuan Zhang, Novel method for incorporating hydrophobic silica nanoparticles on polyether imide hollow fiber membranes for CO₂ absorption in agas–liquid membrane contactor, *J. Membr. Sci.* 452 (2014) 379–389.
- [27] I.T. Bartosz Tylkowski, Overview of main techniques used for membrane characterization, *J. Chem. Technol. Metall.* 50 (2015) 3–12.
- [28] A.M.P. Letellier, M. Turmine, Drop size effect on contact angle explained by nonextensive thermodynamics, Young's equation revisited, *J. Colloid. Interface Sci.* 314 (2007) 604–614.
- [29] M.N. Hyder, J. Long, R.Y.M. Huang, P. Chen, Thermodynamic modeling of contact angles on rough, heterogeneous surfaces, *Adv. Colloid Interface Sci.* 118 (2005) 173–190.
- [30] Y. Yuehua, Contact angle and wetting properties, in: H.B. Bracco Gianangelo (Ed.), *Surface Science Techniques*, Springer-Verlag Berlin Heidelberg, Berlin, 2013, pp. 3–34.
- [31] D.R.X.M. Li, M. Crego-Calama, What do we need for a super hydrophobic surface? A review on the recent progress in the preparation of super hydrophobic surfaces, *Chem. Soc. Rev.* 36 (2007) 1350–1368.

Ambient carbon dioxide capture and conversion via membranes

- [32] O. Monticelli, A. Bottino, I. Scandale, G. Capannelli, S. Russo, Preparation and properties of polysulfone–clay composite membranes, *J. Appl. Polym. Sci.* 103 (2007) 3637–3644.
- [33] P. Kubica, A. Wolinska-Grabczyk, E. Grabiec, M. Libera, M. Wojtyniak, S. Czajkowska, M. Domański, Gas transport through mixed matrix membranes composed of polysulfone and copper terephthalate particles, *Microporous Mesoporous Mater.* 235 (2016) 120–134.
- [34] M. Zhu, D. Meng, C. Wang, G. Diao, Facile fabrication of hierarchically porous CuFe_2O_4 nanospheres with enhanced capacitance property, *ACS Appl. Mater. Interfaces* 5 (2013) 6030–6037.
- [35] A.P.F. Carla Brazinha, Helena Pereira, Orlando M.N.D. Teodoro, Joao G. Crespo, Gas transport through cork: modelling gas permeation based on the morphology of a natural polymer material, *J. Membr. Sci.* 428 (2013) 52–62.
- [36] A.F.I. Gh Bakeri, M. Rezaei DachtArzhandi, T. Matsuura, Porous PES and PEI hollow fiber membranes in gas-liquid contacting process -a comperative study, *J. Membr. Sci.* 475 (2015) 57–64.
- [37] F.M.J. Martínez-Lüschera, M. Sánchez-Díaza, S. Delrotc, J. Aguirreoleaa, E. Gomèsc, I. Pascuala, Climate change conditions (elevated CO_2 and temperature) and UV-Bradiation affect grapevine (*Vitis vinifera* cv. Tempranillo) leaf carbonassimilation, altering fruit ripening rates, *Plant Sci.* 236 (2015) 168–176.
- [38] V.J. Mitchell, W. Tezara, S.D. Driscoll, D.W. Lawlor, Water stress inhibits plant photosynthesis by decreasing coupling factor and ATP, *Nature* 401 (1999) 914–917.
- [39] K. Radoglou, Environmental control of CO_2 assimilation rates and stomatal conductance in five oak species growing under yeld conditions in Greece, *Ann. Sci. For.* 53 (1996) 268–278.
- [40] M.K. Péter Teszláka, Krisztián Gaál, Martin Pour Nikfardjam, Regulatory effects of exogenous gibberellic acid (GA3) on water relations and CO_2 assimilation among grapevine (*Vitis vinifera* L.) cultivars, *Sci. Hortic.* 159 (2013) 41–51.

II. Studies of polysulfone membrane contactors in static module

II. STUDIES OF POLYSULFONE MEMBRANE CONTACTORS IN STATIC MODULE

*based on: Adrianna Nogalska, Adrianna Zukowska, Ricard Garcia-Valls, *Atmospheric CO₂ capture for the artificial photosynthetic system*, Science of the Total Environment, 621 (2018) 186–192

II. Studies of polysulfone membrane contactors in static module

The aim of the studies shown in Chapter II is to evaluate the ambient CO₂ capture abilities of the membrane contactor system in the same conditions as leafs, such as ambient temperature, pressure and low CO₂ concentration, where the only driving force is the concentration gradient. The prepared membranes were introduced into a static module and used as contactors between CO₂ and the absorbing media, a potassium hydroxide solution. The influence of the membrane thickness, absorbent stirring rate, solution pH and absorption time on CO₂ capture were evaluated. The polysulfone membranes employed were made by a phase inversion process and characterized by ESEM micrographs which were used to determine the thickness, asymmetry and pore size. Besides, the porosity of the membrane was measured from the membrane and polysulfone density correlation and the hydrophobicity was analysed by contact angle measurements. Moreover, the compatibility of membrane and absorbent was evaluated, in order to exclude wetting issues by meaning of swelling, dynamic contact angle and AFM analysis.

II.1. Introduction

Growth in carbon dioxide concentration of Earth's atmosphere is one of the main issues troubling the modern world. Since the Industrial Revolution started, global average level of CO₂ concentration rose from 280 ppm to 404 ppm (as of May 2016) and it is the highest recorded in last 650,000 years. Another important issue is its growth rate [1].

At present almost half of CO₂ emission is absorbed by lands and oceans [2]. Studies show that global increase in total carbon dioxide concentration will enhance the storage, but simultaneously climate change will tend to release land's and ocean's carbon to atmosphere [3]. Fossil fuel combustion emission, which is the main cause of the carbon dioxide atmospheric growth, is increasing year by year. In the past 50 years the fraction of CO₂ that remains in atmosphere grew from 40 to 45% (2009) [4]. These factors require the invention of new technologies as well as development of the ones already existing to reduce global warming effects. The best inspiration for scientists has always been nature. Our planet had been taking care of the balance of CO₂ for billions of years through, among others, photosynthesis.

The approach of the present work is to capture CO₂ from atmosphere, such as photosynthetic organisms do. The system works as a leaf, where CO₂ is captured directly from air through the membrane pores and passes to the next compartments to be finally converted to methanol or other hydrocarbons to be used as fuel in fuel cells [5, 6]. The electrochemical device converts the chemical energy of a fuel directly into electrical energy, through a chemical reaction.

The first step, which is the CO₂ fixation, is the process rate determining step. CO₂ assimilation rate in stomata reaches between 15 and 40 μmol/m²·s [7, 8, 9, 10]. Stomata are small adjustable pores located on the leaf surface. The main role of stomata is regulating gas exchange between the inside of the leaf and the external environment, e.g. during photosynthesis it allows CO₂ to diffuse into the leaf. The system designed for carbon dioxide capture process mimics stomata function. It consists of a porous polysulfone membrane contactor which uses a basic solution to absorb carbon dioxide. The membrane contactor is permeable for the gas and provides high contact surface area. Recently they started to be used for carbon dioxide capture as a hybrid of membrane separator and chemical absorption.

II. Studies of polysulfone membrane contactors in static module

In the membrane contactor, the porous membrane separates the gas and liquid phases and the absorption process is driven by pressure or concentration gradient. The mass transfer process includes following steps: convective-diffusive transport of the solute from the bulk gas to the membrane surface, transfer through the membrane pores to the liquid membrane surface and a convective-diffusive transfer of a solute to the bulk liquid followed by physical or chemical absorption. The overall mass transfer coefficient takes in account every individual resistances. The resistances are: the gaseous phase boundary layer ($1/k_G$), the membrane ($1/k_m$) and the liquid phase boundary layer ($1/k_L$). The overall process is well-known as a “resistance in series” model and overall mass transfer resistance ($1/K_o$) can be obtained by adding the individual resistances [11].

$$\frac{1}{K_o} = \frac{1}{k_G} + \frac{1}{k_m} + \frac{1}{k_L} \quad (1)$$

A precise knowledge of mass transfer coefficient is essential for simulation, industrial design and use of membrane contactors. Simplified equation for its theoretical value is:

$$k_m = \frac{D * \varepsilon}{\tau * z} \quad (2)$$

In this equation D stands for effective diffusion coefficient of CO_2 , ε is the membrane porosity, z is membrane thickness and τ is a tortuosity coefficient. It is essential to know that this is simplified equation and deviations from reality are highly possible to appear [12].

A great number of polymers have been studied as materials for membranes in CO_2 capture studies including polyacetylenes [13], polyaniline [14], poly(ethylene oxide) [15], polyolefin [16], polypropylene [17] and others [18]. Polysulfone, chosen in the study, is a thermally and chemically stable polymer, easy to handle. Besides, control of polysulfone membrane morphology is easily achieved by changing preparation conditions, a useful feature for membranes [19].

Previous studies on polysulfone membrane contactors for ambient CO_2 capture were performed in the system equipped with a peristaltic pump in order to decrease the absorbent mass transfer resistance by increase of the liquid flow rate (Chapter I) [20]. In the current study, experiments are carry out in static conditions in which the liquid flow is zero to evaluate the impact of the pump. Membranes of the same

morphology with different thickness, macrovoids size and the hydrophobicity were used in the research. The influence of the membrane characteristics, absorbent liquid resistance and absorption time were analyzed.

II.2. Experimental

II.2.1. Materials

Polysulfone (SIGMA-ALDRICH) in form of pellets was used for membrane preparation with N-Methyl-2-pyrrolidone (NMP) $\geq 99,0\%$ (SIGMA-ALDRICH). Potassium Hydroxide (85%, pellets) (SIGMA-ALDRICH) were used as absorption liquid for CO₂.

II.2.2. Flat sheet membranes preparation

Polysulfone membranes were made via phase inversion method. The preparation conditions are summarized in **Table II. 1**. Polymeric solution used for the fabrication consisted of 20% wt. polysulfone dissolved in 1-Methyl-2-pyrrolidone after 48 h stirring. The resulting solution was cast on a glass support by using a casting knife of particular thickness and immediately immersed into water, where the membrane precipitates as a result of exchanging solvent (NMP) with non-solvent (water). Prepared flat sheet membranes were dried at ambient conditions. As the only changed factor in the process is thickness, further membranes names will be associated with the size of the casting knife used in the preparation as follows: membrane 250, membrane 200 and membrane 100.

Table II. 1. Blank polysulfone membrane preparation parameters.

Process	Immersion precipitation
Polymeric solution	20 % Polysulfone in NMP
Coagulation bath	Distilled water
Casting knife [μm]	250, 200, 100
Support	Glass

II.2.3. Morphology analysis

The morphology of fabricated membranes was investigated with Environmental Scanning Electron Microscopy (FEI Quanta 600). Membranes were fractured in liquid nitrogen and fixed to the support suitable for the cross-section analysis. The ESEM micrographs were recorded with 350 magnification.

II. Studies of polysulfone membrane contactors in static module

Obtained micrographs were analyzed with Ifme [21] and ImageJ software, where membrane asymmetry, mean pore size, microvoid size and thickness is calculated based on the cross section structure of the membrane. Moreover, the overall porosity was determined by using densities of the membrane and the polymer, according to the equation [22]:

$$\varepsilon = \left(1 - \frac{\rho_m}{\rho_p}\right) 100\% \quad (3)$$

where ρ_m corresponds to the membrane density and ρ_p to the polysulfone density (1.24 g/cm³).

Atomic Force Microscopy (Molecular Imaging model Pico SPM II (Pico+)) together with the WsxM [23] software were used to analyse the bottom surface roughness. The images were taken over of 2 μm^2 area. The surface roughness parameters of the membranes are expressed in terms of the mean roughness (Ra), the root mean square (Rq) and Skewness (Rsk).

II.2.4. Membrane wetting estimation

As membrane wetting is an unwanted phenomena in gas-liquid membrane contactor operations, membrane hydrophobicity and its affinity to the absorbent solution needs to be evaluated. Therefore, membrane swelling and static and dynamic contact angle measurements of both water and absorbent solution were performed.

Membrane (2 cm²) was immersed into the water and absorbent solution for 24 h and swelling was calculated based on the membrane weight before (w_1) and after immersion (w_2) by the following equation:

$$Swelling = \frac{(w_2 - w_1)}{w_1} 100\% \quad (4)$$

Hydrophobicity was analyzed by contact angle measurements (Dataphysics OCA 15EC). A 3 μL droplet of milli-q water or potassium hydroxide solution was placed on the bottom surface of the membrane. The measurements were performed only on the bottom surface of the membranes, as it is the part in contact with the solvent during operation. A contact angle was calculated from a digital image by SCA software included in the apparatus as average of 6 measurements. Hysteresis ϑ_{hys} was calculated based on dynamic contact angle measurements. Advancing ϑ_A

Ambient carbon dioxide capture and conversion via membranes

and receding ϑ_R angle of 2 μL droplet was recorded and applied in the equation:

$$\theta_{\text{hys}} = \theta_A - \theta_R \quad (5)$$

II.2.5. CO₂ absorption studies

Experiments were performed to determine the influence of solution stirring rate and pH, membrane thickness and time of exposition of the membrane contactor on the CO₂ absorption rate from ambient air. A cross section of a module used for the studies is schematically presented in **Fig. I 1**. It consists of two parts separated by membrane. The bottom part has a capacity of 100 cm³ and it is filled with absorbent solution. The upper part has holes allowing CO₂ to pass through it. Both compartments are tightly closed with the membrane in between them. Thus the bottom side of the membrane was in contact with the absorbent solution while the top was exposed to the air with a contact area of 19 cm².

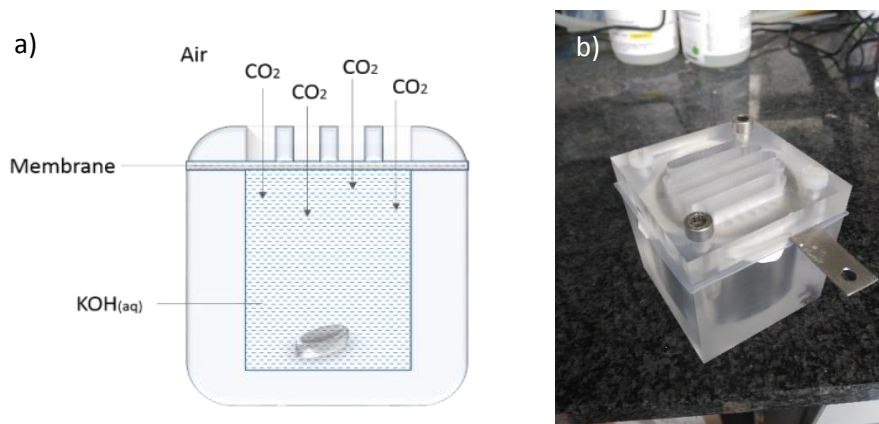


Figure II. 1. Static module cross section scheme (a) and photo (b).

Firstly, membranes of different thickness were placed and examined in the module. The absorbent used was a 100 mL aqueous solution of KOH with a concentration of 0.64 M. It was stirred with different RPM rates ranging from 0 to 1000. The time of experiment was fixed to 1 h. Samples were collected and analyzed for CO₂ content by using a CO₂ ion-selective electrode (Thermo Scientific connected with Thermo Scientific Orion Dual Star pH/ISE Benchtop meter). The absorption flux J [mol/m²*s] was calculated based on the following equation:

II. Studies of polysulfone membrane contactors in static module

$$J_{CO_2} = \frac{n_{CO_2}}{t * A} \quad (6)$$

where n_{CO_2} is the number of CO₂ moles in the absorbent solution of 100 mL [μmol] obtained from the measurements, t is the time of experiment [s] and A is the area of the flat sheet membrane [m²].

Then, the membrane with the best combination of membrane thickness and stirring rate for the absorption was used to analyse the absorption in function of time and solution pH. For the purpose, chosen membrane was placed into the system and experiments firstly were conducted without stirring during 1 h using absorbent solution of pH 11–14 and water (pH 7). After that, the solution with the highest pH was tested in the same conditions but after time of: 15, 30, 45, 60, 120 min. Collected samples were analyzed in the same way as previously.

II.2.6. Statistical analysis

Statistical analysis was performed by Xlstat software, consisting of ANOVA tool for comparison of variables between groups with significance level α of 0.05 and regression for correlation. Tested results were measurements of 3 independent experiments. Errors provided together with the numerical results are corresponding to standard deviation.

II.3. Results and discussion

II.3.1. Morphology analysis

Resulting membranes have finger-like macrovoids in porous media (**Fig. II. 2**). Membranes characteristics obtained from the analysis of ESEM micrographs together with porosity values calculated based on Eq. (3) are listed in **Table II. 2**. It shows that membranes vary in thickness and have increasing macrovoids size respectively to the thickness. The porosity and asymmetry do not change significantly.

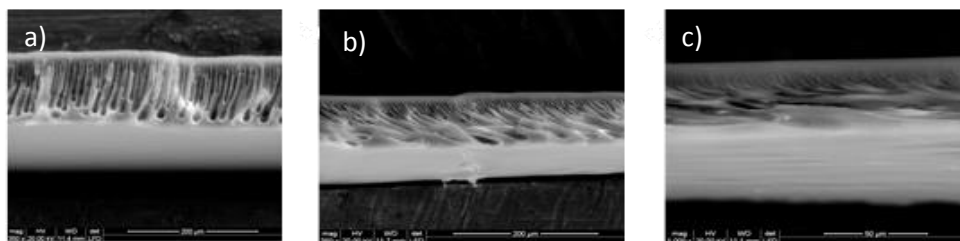


Figure II. 2. ESEM micrographs of the blank polysulfone membranes cross section: a) 250, b) 200, c) 100. *scale bar in a), b) is 200 μm and c) is 50 μm.

Ambient carbon dioxide capture and conversion via membranes

Table II. 2. Characteristics of the resulting blank polysulfone membranes.

Membrane	Thickness [μm]	Asymmetry [%]	Mean pore diameter [μm]	Mean macrovoids size [μm ²]	Porosity [%]
100	45 ± 1	15	17 ± 2	40 ± 26	66.73
200	88 ± 2	14	18 ± 2	400 ± 271	72.53
250	124 ± 3	15	12.0 ± 0.3	610 ± 228	73.70

Additionally AFM analysis was performed in order to evaluate the surface roughness. The three-dimensional surface images (**Fig. II. 3**) and surface roughness parameters (**Table II. 3**) of the membranes were obtained with WSxM software. Within the roughness parameters, the average roughness (R_a) is defined as the arithmetic mean of the absolute values of the surface departures measured from the mean plane, the root mean square roughness (R_q) represents the standard deviation of the profile and surface skewness (R_{sk}) - asymmetry of the profile above mean plane.

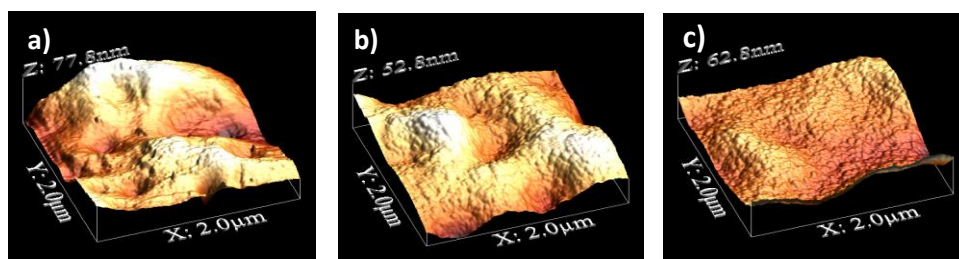


Figure II. 3. AFM 3D images of bottom membrane surface of blank polysulfone membranes: a) 100, b) 200, c) 250.

Table II. 3. Blank polysulfone membranes surface roughness parameters.

Membrane	Average roughness R_a [nm]	Root square R_q [nm]	Skewness R_{sk}
100	11.82	14.75	0.80
200	6.59	8.23	-0.15
250	5.98	7.90	0.13

The roughness parameters are generally low (**Table II. 3**) which indicate that the bottom surface is smooth. Positive skewness refers to “hills”

II. Studies of polysulfone membrane contactors in static module

on the smooth surface, while negative value represents the “valleys” in the surface. Thus the more positive the skewness value is, the smaller are the pores located on the surface [24]. As we can see the negative Rsk value characterize membrane 200. According to the analysis, we can conclude that membrane 200 possesses bigger pores on the surface than the rest of membranes.

II.3.2. Membrane wetting estimation

Pores wetting is an undesirable phenomena in gas – liquid membrane contactor operations. For that reason we need to exclude the blocking influence of the absorbent solution on the pores. The analysis was performed with water as reference and absorbent solution. Swelling (**Table II. 4**) and contact angle of the water and KOH solution (**Table II. 5**) were measured. Analysis was followed by dynamic contact angle measurements.

Table II. 4. Swelling test measurements results of blank polysulfone membranes (n. d. – not detected).

Absorbed liquid	Membrane	Swelling [%]
Water	100	11.0 [± 0.6]
	200	55 [± 3]
	250	39 [± 2]
KOH	100	1.21 [± 0.06]
	200	n. d.
	250	n. d.

Swelling test results shows that membranes are capable to absorb water but not absorbent solution which is in agreement with contact angle measurements.

Static contact angle measurement is suitable to analyse the membrane hydrophobicity but it is not enough to estimate the wetting properties. In order to examine the membrane wettability the dynamic contact angle by meaning of contact angle hysteresis must be measured [25].

Table II. 5. *Water and KOH solution contact angle measurements results of blank polysulfone membranes.*

Contact angle liquid	Membrane	Contact angle [°]
Water	100	67 [±3]
	200	81.9 [±0.8]
	250	68 [±2]
KOH	100	71 [±7]
	200	87 [±5]
	250	76 [±5]

Prepared membranes are hydrophilic with average contact angle value of 72°, the same value for polysulfone membranes was reported by Kibechu et al. [26]. The membrane hydrophilic character is in agreement with AFM studies, in which we confirmed that surfaces are smooth [27]. Nevertheless, water contact angle is lower than absorbent solution contact angle (**Table II. 5**). The significance of the difference was confirmed by statistical analysis, where obtained p-value was 0.04. This occurs due to difference in liquid surface tension, which influence its interaction with the membrane surface. The tests demonstrate that the absorbent solution is adequate for working with polysulfone membranes.

Similar tendency was obtained in dynamic contact angle measurements. The hysteresis results are gather in **Table II. 6**. A high advancing/receding contact angle and low contact angle hysteresis are responsible for the low wettability of a material surface [28].

Table II. 6. *Dynamic contact angle measurements results of blank polysulfone membranes.*

Membrane	Water contact angle hysteresis [°]	Absorbent solution contact angle hysteresis [°]
100	19.98	16.26
200	17.29	12.71
250	21.67	14.13

The absorbent solution contact angle hysteresis is again lower than water ($p = 0.03$). What is more, the smallest value was obtained for membrane 200. It also has the highest static contact angle value, which indicates that the membrane possess the best non-wetting properties among tested membranes.

II. Studies of polysulfone membrane contactors in static module

II.3.3. CO₂ absorption results

II.3.3.1. Influence of the membrane thickness and stirring rate on the contactor absorption capacity

It was expected that increasing the mixing of absorbent solution would have a positive influence on the absorption rate, as the fluctuation of the absorbent below the membrane could increase the amount of unreacted potassium hydroxide molecules in the contact with the surface. Nevertheless, studies show that the impact of the mixing is not significant (p-value 0.97). It looks like the influence of the solutions mass transfer resistance during the static operation of the module is low as the solution remains in the same container. A previously studied case, where the absorbent solution was in a separated flask, and it was circulated through the contactor by the use of pump, revealed the positive influence of the absorbent fluctuations on the absorption rate.

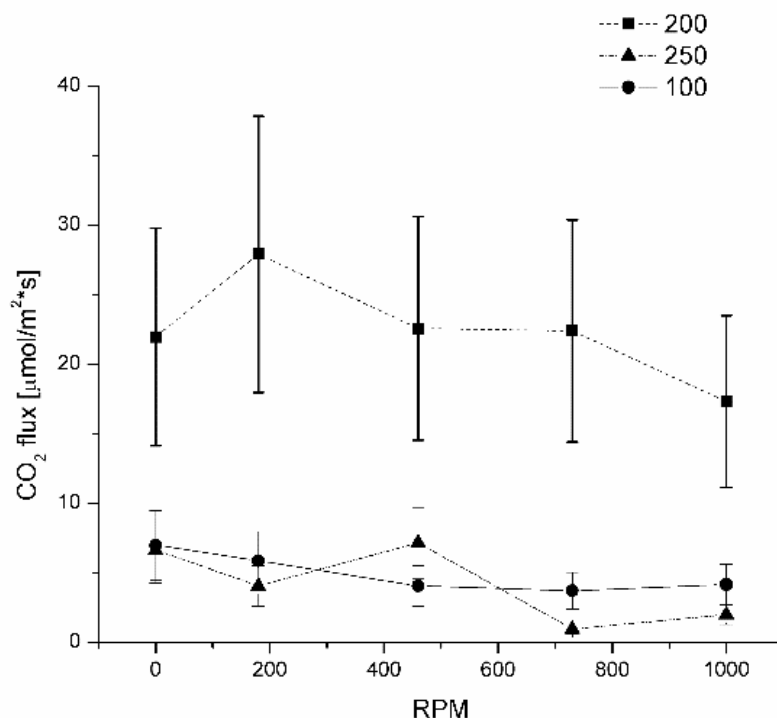


Figure II. 4. CO₂ absorption as a function of RPM by different blank polysulfone membranes in static module.

Ambient carbon dioxide capture and conversion via membranes

The mass transfer resistance in the membrane can be studied by using of different thickness and hence macrovoids size, as the obtained membranes possess similar internal morphology. The CO₂ passage rate through the membrane phase depends on the distance (membrane thickness), free space (macrovoids and pores size) and the material interaction with the absorbent solution. From the study we can conclude that the membrane 200 shows the best results in absorption capacity over the rest of studied membranes (**Fig. II. 4**). The p-value ($2.9 \cdot 10^{-7}$) obtained by ANOVA analysis reveals that the difference in absorption between membranes is high. We conclude that the distinct properties of the membrane contributed to its high effectivity in the process and not the thickness itself. This membrane shows the lowest hydrophilicity and the best non-wetting properties among the other membranes. According to the negative skewness value, the membrane possesses the biggest pores on the surface what cause an increment in the size of the contact area.

II.3.3.2. PH influence

The best conditions from previous experiments were chosen to study the membrane contactor system abilities to absorb CO₂ at different pH values. Thus membrane 200 was chosen for the studies based on the previous analysis. Experiments were performed during 1 h and without use of stirrer, as its impact was proved to be negligible.

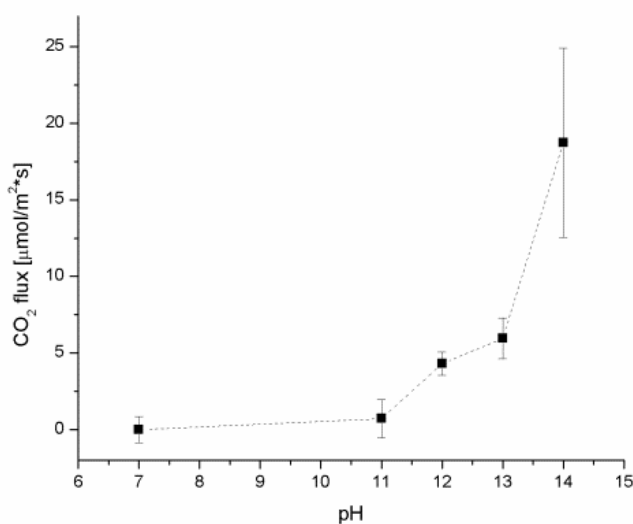


Figure II. 5. CO₂ absorption flux by membrane 200 in static module as function of pH.

II. Studies of polysulfone membrane contactors in static module

The natural stomata work at neutral pH. We wanted to see how our system will behave if we decrease the absorbent solution pH to get closer to the real conditions. The change of absorption in function of pH rise exponentially (**Fig. II. 5**) (nonlinear regression fitting $R^2 = 0.982$ for equation $y = 6.29 * 10^{-05} * e^{-0.9x}$). The flux increases with pH as the absorbent solution is more concentrated and there is more potassium hydroxide available to react with CO_2 .

II.3.3.3. Change of absorption in time

The same conditions were applied to study the flux over time with potassium hydroxide solution at the highest concentration. In the plot (**Fig. II. 6**) the change in CO_2 content in the final absorbent solution and its flux through the contactor are displayed together.

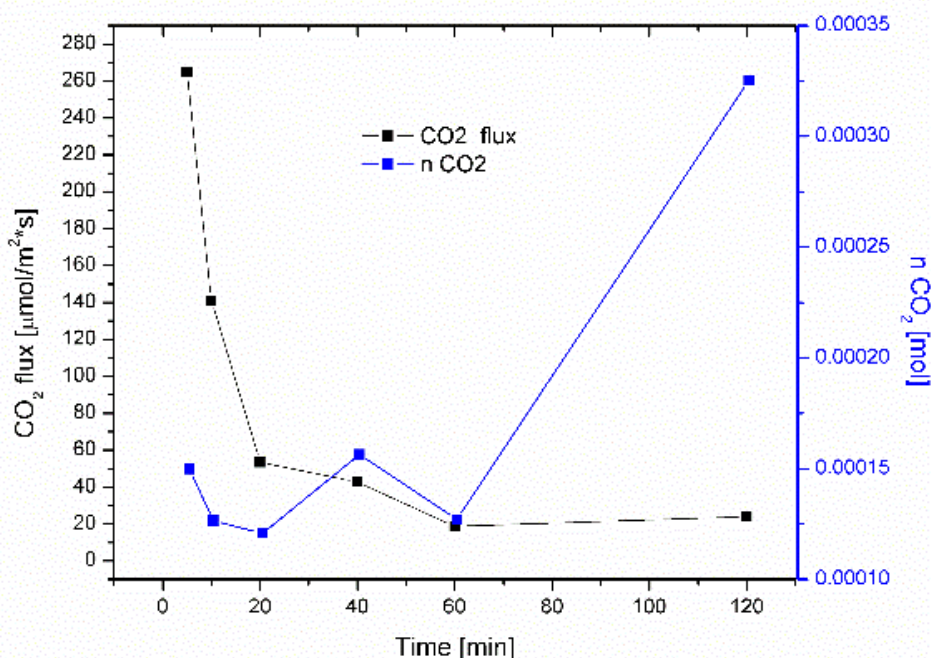


Figure II. 6. CO_2 absorption flux and CO_2 content change by membrane 200 in static module as a function of time.

The absorbed CO_2 amount is rising within the studied range of time (polynomial regression of 3rd order $R^2 = 0.961$, $y = 3 * 10^{-10} x^3 - 3 * 10^{-08} x^2 + 6 * 10^{-07} x + 0.0001$). The system would keep increasing the CO_2 content

until the saturation state. Absorption is low at the beginning but after 1 h it experiences an increase. By extrapolating forward to the regression equation we can observe that all the potassium would be consumed after 9 h. On the other hand, the CO₂ flux is decreasing over time and a plateau was reached after 1 h of experiment ($R^2 = 0.990$, $y = 1287.07 * x^{-0.98}$). The results are logical and coherent with our expectations as according to the Eq. (6), the flux is proportional to moles and inversely proportional to time and area.

II.3.3.4. The comparison of performances

As the system is designed based on the natural leaf structure, the obtained results will be compared to the natural stomatal CO₂ assimilation rate. As a reference we choose the grape vine leaf with an assimilation rate value of 20 $\mu\text{mol}/\text{m}^2 * \text{s}$, as reported by J. Martínez-Lüscher et al. [7]. The range obtained by us depends on the experimental conditions ranging in 6-160 $\mu\text{mol}/\text{m}^2 * \text{s}$. Nevertheless, in the studies of the influence of time presented above, we can observe that the system achieved stabilization with membrane 200 after 1 h of experiment reaching the value of 20 $\mu\text{mol}/\text{m}^2 * \text{s}$, which should be used as the reference. Results show that the CO₂ assimilation rate in our artificial system is in the same range as in natural stomata.

The developed CO₂ capturing unit, finally will be incorporated into a leaf mimicking system used for green energy production. If we assume that all of the captured CO₂ (max of 0.0016 M) is converted to methanol and used as fuel for direct methanol fuel cell the energy obtained will be 0.75 V [29] which is enough to supply a diode.

II.4. Conclusions

Porous polysulfone membranes with different thickness were fabricated and characterized with the purpose of using them as contactors in ambient carbon dioxide capture studies. Compatibility of the membranes and absorbent solutions was evaluated by swelling tests and contact angle measurements and surface roughness analysis. According to the results, we can conclude that polysulfone membranes are compatible to be used with potassium hydroxide solution. Furthermore, the influence of membrane thickness, absorbent solution mixing rate, its pH and experimental time on the system absorption capacity were investigated. From the study we can conclude that the membrane 200 shows visible superiority in absorption capacity over the rest of studied membranes, due to its distinct properties

II. Studies of polysulfone membrane contactors in static module

such as big surface pore size providing high contact area and the best non wetting properties. Nevertheless, the results showed that the impact of the absorbent solution mixing is not significant. It looks like the influence of the solutions mass transfer resistance during the static operation of the module is low as the solution remains in the same container. The system absorption capacity rises with increase of the sorbent concentration at the same pH. As expected, the absorbed CO₂ amount was rising within the studied range of time. The comparison between natural and the artificial stomata reveals that the CO₂ assimilation is within the same range. Thus, the designed stomata mimicking unit can be used further in artificial photosynthetic systems.

References

- [1] Josep G. Canadell CLQr, Michael R. Raupach, Christopher B. Field, Erik T. Buitenhuis, Philippe Ciais, Thomas J. Conway, Nathan P. Gillett, R. A. Houghton, Gregg Marland, *Contributions to accelerating atmospheric CO₂ growth from economic activity, carbon intensity, and efficiency of natural sinks*, Proceedings of the National Academy of Sciences of the United States of America, 2007, **104**: p 18,866–18,870.
- [2] P. Ballantyne CBA, J. B. Miller, P. P. Tans, J. W. C. White, *Increase in observed net carbon dioxide uptake by land and oceans during the past 50 years*, Nature, 2012, **488**: p 70-73.
- [3] P. Friedlingstein PC, R. Betts, L. Bopp, W. von Bloh, V. Brovkin, P. Cadule, S. Doney, M. Eby, I. Fung, G. Bala, J. John, C. Jones, F. Joos, T. Kato, M. Kawamiya, W. Knorr, K. Lindsay, H. D. Matthews, T. Raddatz, P. Rayner, C. Reick, E. Roeckner, K.-G. Schnitzler, R. Schnur, K. Strassmann, A. J. Weaver, C. Yoshikawa, N. Zeng, *Climate–Carbon Cycle Feedback Analysis: Results from the C4MIP Model Intercomparison*, Journal of Climate, 2006, **19**: p 3337-3353.
- [4] Corinne Le Quéré MRR, Josep G. Canadell, Gregg Marland, *Trends in the sources and sinks of carbon dioxide*, Nature Geoscience, 2009, **2**: p 831 - 836.
- [5] George A. Olah AG, G. K. Surya Prakash, *Chemical Recy-cling of Carbon Dioxide to Methanol and Dimethyl Ether: From Green-house*

Ambient carbon dioxide capture and conversion via membranes

Gas to Renewable, Environmentally Carbon Neutral Fuels and Synthetic Hydrocarbons, Journal of Organic Chemistry, 2009, **74**: p 487–498.

- [6] Wei Wang SW, Xinbin Ma, Jinlong Gong, *Recent advances in catalytic hydrogenation of carbon dioxide*, Chemical Society Reviews, 2011, **40**: p 3703 – 3727.
- [7] F.M. J. Martínez-Lüschera MS-D, S. Delrotc, J. Aguirreoleaa, E. Gomèsc, I. Pascuala, *Climate change conditions (elevated CO₂ and temperature) and UV-B radiation affect grapevine (Vitis vinifera cv. Tempranillo) leaf carbon assimilation, altering fruit ripening rates*, Plant Science, 2015, **236**: p 168-176.
- [8] M.K. Peter Teszlaka KG, Martin Pour Nikfardjam, *Regulatory effects of exogenous gibberellic acid (GA3) on water realtions and CO₂ assimilation among grapevine (Vitis vinifeera L.) cultivars*, Scientia Horticulturae, 2013, **159**: p 41-51.
- [9] W. Tezara VJM, S. D. Driscoll & D. W. Lawlor, *Water stress inhibits plant photosynthesis by decreasing coupling factor and ATP*, Nature, 1999, **401**: p 914-917.
- [10] Radglou K. *Environmental control of CO₂ assimilation rates and stomatal concuctance in five oak species growing under yield conditions in Greece*, Annales des sciences forestieres, 1996, **53**: p 268 - 278.
- [11] V.Y. Dindore DWFB, F.H. Geuzebroek, G.F. Versteeg, *Membrane-solvent selection for CO₂ removal using membrane gas-liquid contactors*, Separation and Purification Technology, 2004, **40**: p 133-145.
- [12] E. Favre, HFS, *Membrane contactors for intensified post-combustion carbon dioxide capture by gas-liquid absorption processes*, Journal of Membrane Science, 2012, **407**: p 1-7.
- [13] Stern SA, *Polymers for gas separations: the next decade*, Journal of Membrane Science, 1994, **94**: p 1-65.

II. Studies of polysulfone membrane contactors in static module

- [14] G. Illing KH, R.J. Wakeman, A. Jungbauer, *Preparation and characterisation of polyaniline based membranes for gas separation*, Journal of Membrane Science, 2001, **184**: p 69-78.
- [15] H. Lin BDF, *Gas solubility, diffusivity and permeability in poly(ethylene oxide)*, Journal of Membrane Science, 2004, **239**: p 105-117.
- [16] Paul H.M. Feron AEJ, *CO₂ separation with polyolefin membrane contactors and dedicated absorption liquids: performances and prospects*, Separation and Purification Technology, 2002, **27**: p 231-242.
- [17] Witek-Krowiak AD, S. Modelski, D. Podstawczyk, *Carbon Dioxide Removal in a Membrane Contactor - Selection of Absorptive Liquid/Membrane System*, International Journal of Chemical Engineering and Applications, 2012, **3**.
- [18] Hongqun Yang ZX, Maohong Fan, Rajender Gupta, Rachid B Slimane, Alan E Bland, Ian Wright, *Progress in carbon dioxide separation and capture: A review*, Journal of Environmental Sciences, 2008, **20**: p 14-27.
- [19] Torras C., *Obtenció de membranes polimèriques selectives*, Chemical Engineering Dep. Universitat Rovira i Virgili, Tarragona, 2005.
- [20] Adrianna Nogalska MA, Bartosz Tylkowski, Veronica Ambrogi, Ricard Garcia Valls, *Ambient CO₂ adsorption via membrane contactors – value of assimilation from air as nature stomata*, Journal of membrane science, 2018, **546**: p 41-49.
- [21] Carles Torras RG-V., *Quantification of membrane morphology by interpretation of scanning electron microscopy images*, Journal of Membrane Science, 2004, **233**: p 119-127.
- [22] Yuan Zhang RW., *Novel method for incorporating hydrophobic silica nanoparticles on polyether imide hollow fiber membranes for CO₂ absorption in a gas-liquid membrane contactor*, Journal of Membrane Science, 2014, **452**: p 379 - 389.

Ambient carbon dioxide capture and conversion via membranes

- [23] Horcas I. FR, Gómez-Rodríguez J. M., Colchero J., Gómez-Herrero J., Baro A. M., *WSXM: A software for scanning probe microscopy and a tool for nanotechnology*, Review of scientific instruments, 2007, **78**.
- [24] Shirazi, M.M.A., Kargari, A., Bazgir, S., Tabatabaei, M., Shirazi, M.J.A., Abdullah, M.S., Matsuura, T., Ismail, A.F., *Characterization of electrospun polystyrene membrane for treatment of biodiesel's water-washing effluent using atomic force microscopy*, Desalination, 2013, **329**: p 1–8.
- [25] Yuehua Y., *Contact Angle and Wetting Properties*, In: Bracco Gianangelo HB, editor. Surface Science Techniques. Springer-Verlag Berlin Heidelberg, 2013, p 3-34.
- [26] Rose Waithiegeni Kibechu DTN, Titus Alfred Makudali Msagati, Bhekie Briliance Mamba, S. Sampath, *Effect of incorporating graphene oxide and surface imprinting on polysulfone membranes on flux, hydrophilicity and rejection of salt and polycyclic aromatic hydrocarbons from water*, Physics and Chemistry of the Earth, 2017, **100**: p126-134.
- [27] K. Boussu BVdB, A. Volodin, J. Snauwaert, C. Van Haesendonck, C. Vandecasteele, *Roughness and hydrophobicity studies of nanofiltration membranes using different modes of AFM*, Journal of Colloid and Interface Science, 2005, **286**: p 632-638.
- [28] X.M. Li DR, M.Crego-Calama, *What do we need for a super hydrophobic surface? A review on the recent progress in the preparation of super hydrophobic surfaces*, Chemical Society Reviews, 2007, **36**: p 1350 - 1368.
- [29] K.A.I.L.Wijewardena Gamalath BMPP, *Theoretical Approach to the Physics of Fuel Cells*, International Letters of Chemistry, Physics and Astronomy, 2012, **2**: p 15-27

III. Polysulfone membrane contactors modified with activated carbon

III. POLYSULFONE MEMBRANE CONTACTORS MODIFIED WITH ACTIVATED CARBON

III. Polysulfone membrane contactors modified with activated carbon

In Chapter III, polysulfone flat sheet membranes were modified with activated carbon following these two approaches: i) bulk modification by adding AC into the polymeric solution used for membrane preparation and ii) spraying of the carbon-containing ink on blank the polysulfone membrane top surface. The prepared membranes were characterized by contact angle, SEM and ESEM with EDX. In the case of surface modification, the amount of introduced AC was determined by elemental analysis and simple calculation of change in membrane mass and thickness. The obtained membranes were examined for CO₂ absorption flux in potassium hydroxide aqueous solutions in the membrane contactor system. The influence of the additive, membrane thickness and absorbents flow rate on the CO₂ absorption rate were investigated.

III.1. Introduction

Activated carbon (AC) is a highly microporous material with a large surface area [1]. AC is known as carbonaceous adsorbent and have been widely used for CO₂ capture due to its wide properties, like low cost, high thermal stability, low sensitivity to moisture [2], excellent porous structure, specific surface properties, reusability and environmentally being nature [3]. It can be formed from a variety of precursors: coals, industrial by products, wood or other biomass sources [4]. As most of the AC precursors come from organic and natural sources, its utilization is ecologically attractive. Rajiv et al. studied the use of biomass-derived activated carbons for CO₂ adsorption [5]. The obtained carbon was treated with KOH and carbonized. Different precursors gave different textures of AC, but they showed sensitivity to adsorption temperature and pressure. The group of Nor Adilla Rashidi synthesized and activated palm kernel shell-based carbon and used it for atmospheric pressure CO₂ adsorption, which was never reported before [6]. The obtained AC was proven to have an adequate CO₂ physisorption capacity comparable to commercial one. Activated carbons are most efficient around room temperature [4].

The purpose of this study is to improve the polysulfone membrane CO₂ capture abilities in gas/liquid contactor systems by introducing activated carbon to the membrane. An increase of the local concentration of CO₂ on the membrane would accelerate the absorption into the liquid. For this purpose, the membrane bulk can be modified by adding the AC into the matrix [7-9]. This can be accomplished by addition of carbon into the polymeric solution before membrane is cast. Another approach is surface modification, where the additive is spread just on the top surface of the membrane. This kind of membrane coating with carbon is widely used in MEA fabrication [10, 11]. The carbon ink is prepared by mixing activated carbon with a catalyst, alcohol and Nafion glue. The mixture is then sprayed on the paper in order to fabricate the electrode.

III.2. Experimental

III.2.1. Materials

Polysufone (Mw 35,000) in transparent pellet form and 1-Methyl-2-pyrrolidone (NMP, ACS) were purchased from Sigma Aldrich and used for flat sheet membrane fabrication. Distilled water was used as coagulation bath in membrane preparation. The activated carbon (activated charcoal Norit) added to membranes was purchased in Sigma Aldrich. For carbon ink

III. Polysulfone membrane contactors modified with activated carbon

preparation, besides the AC, i-propanol (99.8%, extra dry) from Acros Organics and Nafion 117 solution ~5 % in a mixture of lower aliphatic alcohols and water (Sigma Aldrich) were used. Hollytex non-woven made of polyester with density 34 g/m² was acquired in Stem and used as support in the module. Extra pure potassium hydroxide in pellets (Sharlab) was dissolved in deionized water to prepare the absorptive solutions. Carbon dioxide ion selective electrode and all needed solutions was purchase from Thermo Scientific: 1000 ppm as CaCO₃ standard solution for the calibration, Carbon Dioxide Buffer Solution to adjust solution pH to the operating range of the electrode and the electrode internal filling solution. All chemicals were used without any further purification.

III.2.2. Membrane preparation

The membranes were prepared by phase inversion precipitation process in ambient conditions. A proper amount of polymer was dissolved in NMP (80 wt%) mixed with activated carbon, if added (**Table III. 1**). The resulting solution was stirred for 48 h and left overnight for degasification. The solutions containing additives were sonicated for 30 min before the membrane preparation. The obtained mixture was cast on a glass using a casting knife of a specific thickness, and immediately immersed into the coagulation bath containing water, where membrane precipitates instantly. The prepared flat sheet membranes were taken out from water and left overnight to dry in air.

Table III. 1. Polymeric solutions composition and carbon modified polysulfone membranes preparation parameters.

Membrane	Polysulfone content (%wt)	Active carbon (wt%)	Casting knife [μm]
M200	20	-	200
M250	20	-	250
MAC100	19	1	100
MAC200	19	1	200
MAC250	19	1	250

The obtained blank polymeric membranes (M200, M250) were used for surface modification with carbonic ink. The ink started by wetting 0.6 g of activated carbon with 2 g of distilled water. Then, AC was dispersed in isopropyl alcohol (13 g) while stirring, and sonicated for 1 h. A total of 4.4 g of the Nafion solution was added dropwise with a funnel. The obtained

Ambient carbon dioxide capture and conversion via membranes

solution was further sonicated for 30 min and left to cool down to room temperature. The polysulfone membranes were cut in pieces of 4x4 cm² and immobilized on glass. The top surfaces of the membranes were covered with carbon ink by airbrush and left overnight to dry in air (**Fig III. 1**) (M200_LAC_1, M200_LAC_2, M250_LAC_1, M250_LAC_2). The resulting layer consists just on activated carbon and Nafion due to evaporation of the solvents. The various prepared surfaces were coated with different amounts of activated carbon in order to examine its influence on CO₂ absorption rate.



Figure III. 1. Airbrush used for the membrane surface modification.

III.2.3. Membrane characterization

In the case of membranes with the carbon layer, internal morphology was determined by Scanning Electronic Microscopy (JEOL JSM-6400 Scanning Microscopy Series) in order to achieve high resolution. The samples were immersed into liquid nitrogen, fractured and coated with gold (sputtering). The micrographs were taken on the cross-section of membranes with a magnification of 350. The bulk – modified membranes morphology was examined by cross section micrographs obtained with an

III. Polysulfone membrane contactors modified with activated carbon

Environmental Scanning Electron Microscope (ESEM, FEI Quanta 600). All the cross-section images were analysed with ImageJ and Ifme software [12], in order to obtain information about membrane asymmetry, mean pore size, microvoid size and thickness.

Furthermore, ESEM was used to examine membranes surface composition. Microanalyses, together with the micrographs, were performed on top and bottom surfaces of membranes. Besides, the coated membranes were weighed before and after brushing, in order to calculate the amount of carbon added to membrane. The difference in membrane thickness, before and after coating, was also measured as well as the thickness of the carbon layer on each membrane.

Hydrophobicity was analysed w contact angle measurements using Dataphysics OCA 15EC. A 3 μL droplet of milli-q water was placed on the surface of the membrane. The contact angle was calculated from a digital image by SCA software included in the apparatus. The measurements were repeated three times on different spots of surfaces, and an average value was calculated.

Moreover, the overall membrane porosity (ε), defined as the volume of the pores divided by the total volume of the membrane, was calculated using a method based on density measurements. For blank membranes, the overall membrane porosity was determined from bulk and polysulfone densities by using the following equation:

$$\varepsilon = \left(1 - \frac{\rho_m}{\rho_{psf}}\right) 100\% \quad (1)$$

where ρ_m and ρ_{psf} (1.24 g/cm^3) correspond to membrane and polysulfone density respectively. For the membranes with activated carbon the equation is slightly different:

$$\varepsilon = \left(1 - \frac{\rho_m}{\rho_{psf+ac}}\right) 100\% \quad (2)$$

where ρ_m is a membrane density and ρ_{psf+ac} is a weighted average of the material density which is 95 % ρ_{psf} and 5 % ρ_{ac} ($\rho_{psf+ac} = 1.198 \text{ g/cm}^3$, considering $\rho_{ac} = 0.4 \text{ g/cm}^3$).

III.2.4. CO₂ capture studies

The resulting membranes were used in CO₂ absorption experiments conducted in a gas-liquid membrane contactor. 100 ml of a 0.64 M KOH solution was employed as a liquid absorbent at the bottom side of a flat sheet membrane in cross-flow module (**Fig. III. 2**). The liquid flow rate was tested within a range of 35 – 438 ml/min. The experiments were run for 1 h under continuous magnetic stirring. The absorbent was in contact with air through holes on the top side of the module. The initial and final samples were collected and examined for CO₂ content. All of the experiments were carried out in ambient conditions and each one was repeated three times.

With the purpose of determination of the absorbed CO₂ amount, a carbon dioxide ion selective electrode (Thermo Scientific connected with Thermo Scientific Orion Dual Star pH/ISE Benchtop meter) was used. The diluted sample (1 ml sample + 45 Milli-Q water) was mixed with a CO₂ buffer (5 ml) in order to adjust the pH to the electrode working pH, which is the range of 4.8-5.2. The meter was set to auto read mode and a stable value of CO₂ concentration was recorded. The results were used for calculating the CO₂ flux J [mol/m²*s] in the membrane contactor by using the equation:

$$J_{CO_2} = \frac{Q_i * M_{CO_2}}{A} * 1000$$

where Q_i is the absorbents flow rate [m³/s], M_{CO_2} is the CO₂ concentration in the absorbent [mol/L] obtained from titration and A is the area of the flat sheet membrane [m²].

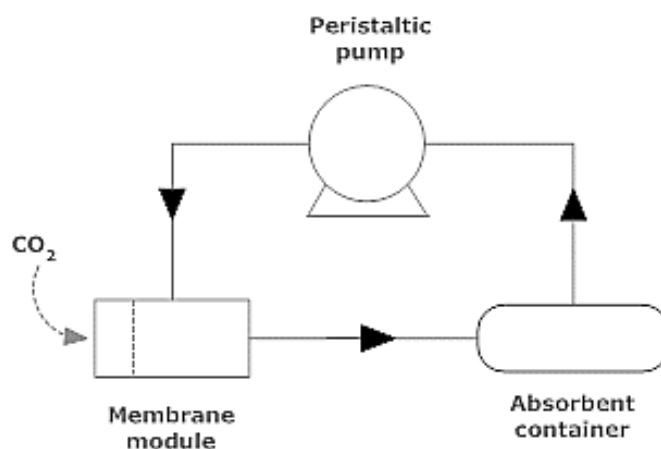


Figure III. 2. System for CO₂ absorption with dynamic module scheme.

III. Polysulfone membrane contactors modified with activated carbon

III.2.5. Statistical analysis

The statistical analysis was performed by Microsoft Excel by using the ANOVA tool for comparison of variables between groups with significance level α of 0.05. All the results are averaged values coming from measurements of at least 3 independent experiments. The errors provided, together with all the numerical results, are corresponding to standard deviation.

III.3. Results and discussion

III.3.1. Membrane characteristics

The influence of activated carbon on the polymeric membrane was analyzed in terms of internal and external morphology, elemental composition and hydrophobicity.

Table III. 2. Characteristics of the resulting carbon modified polysulfone membranes.

Membrane	Thickness [μm]	Assymetry [%]	Porosity (ϵ) [%]	Mean pore diameter [μm]	Average microvoids size [μm^2]	Contact angle [$^\circ$]
M200	105 \pm 1	6	72.87	5.5 \pm 0.3	501 \pm 185	79 \pm 2
M250	128 \pm 2	4	77.42	5.5 \pm 0.2	780 \pm 408	85 \pm 7
MAC100	60 \pm 3	11	77.06	3.2 \pm 0.4	42 \pm 16	64 \pm 4
MAC200	139 \pm 4	3	78.44	13.0 \pm 0.3	883 \pm 472	67 \pm 3
MAC250	152 \pm 3	14	76.36	20.8 \pm 0.6	879 \pm 455	86 \pm 8

Table III. 2 provides membranes characteristics data. Membranes vary in thickness as a results of different casting knife used. Moreover we can see that incorporation of carbon into the membrane bulk results in increase of the membrane thickness when comparing M200 with MAC200 or M250 with MAC250. The membranes are hydrophilic and the porosity does not vary significantly, nevertheless the pores size is larger in thicker membranes. As macrovoids have different dimensions within a single

Ambient carbon dioxide capture and conversion via membranes

membrane cross section, the corresponding standard deviation values are very high (up to 52%).

Cross section micrographs of the surface modified membranes were obtained by SEM. Polysulfone membranes prepared by immersion precipitation process, with NMP as solvent, usually possess finger-like macrovoids elongated in sponge-like bulk. The micrographs confirm the formation of the typical morphology (**Fig. III. 3a**). Moreover, they confirm the creation of a carbon-nafion layer on the top of surface modified membranes (**Fig. III. 3b**) which is not penetrating to the inside (**Fig. III. 3c**).

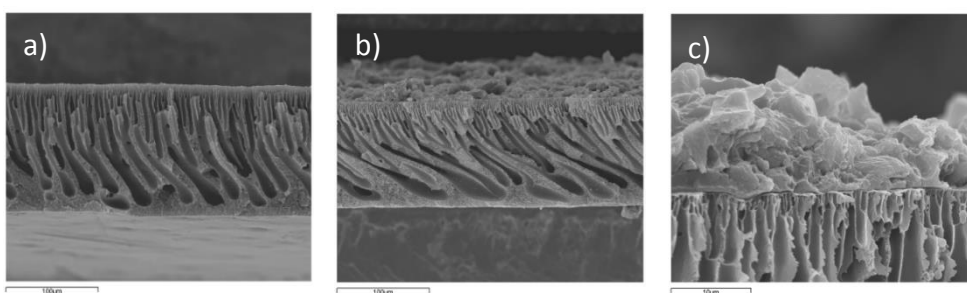


Figure III. 3. SEM representative cross section micrographs: a) M200 - blank membrane, b) 200_LAC_1 - membrane after modification, c) M200_LAC_1 - zoom of the top part of the modified membrane

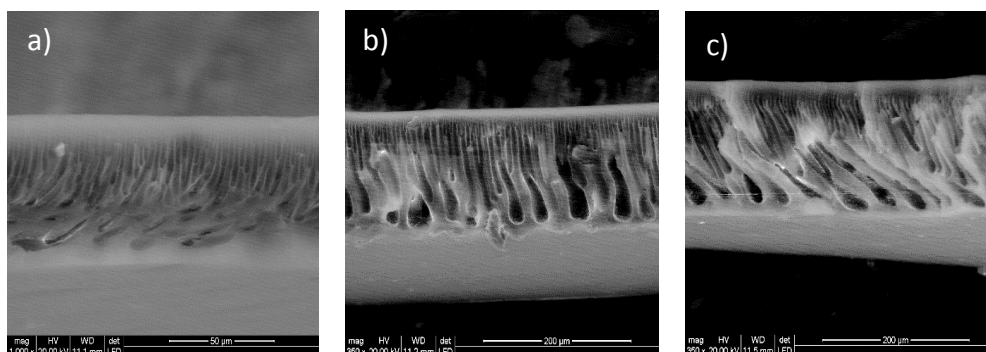


Figure III. 4. ESEM cross section micrographs of membranes containing 5% AC: a) MAC100, b) MAC200, c) MAC250.

The ESEM cross section micrographs of membranes containing CA in the bulk are shown in **Fig. III. 4**. It is possible to see that the incorporation of little amount of carbon does not change the internal morphology of membranes as they maintained the typical finger-like macrovoids.

III. Polysulfone membrane contactors modified with activated carbon

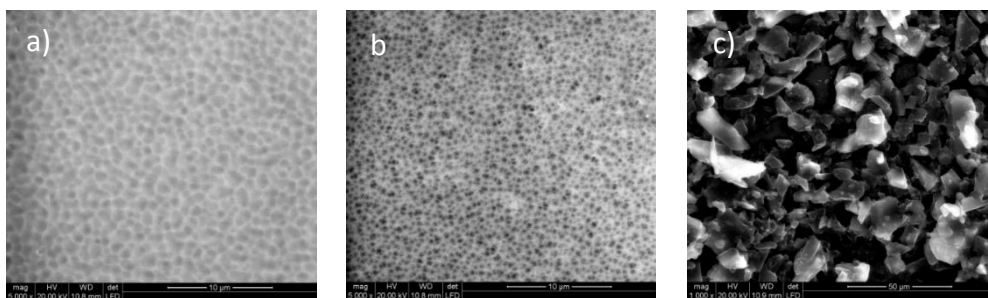


Figure III. 5. ESEM representative surfaces micrographs of membrane M200: a) bottom, b) top before modification, c) top after modification - M200_LAC_1.

In case of surface modification, the bottom sides do not differ as they have not been modified. They have wrinkled surfaces with spherical depressions (**Fig. III. 5a**). The top surface before modification has a porous structure (**Fig. III. 5b**) whereas after modification we can observe carbon agglomerations (**Fig. III. 5c**).

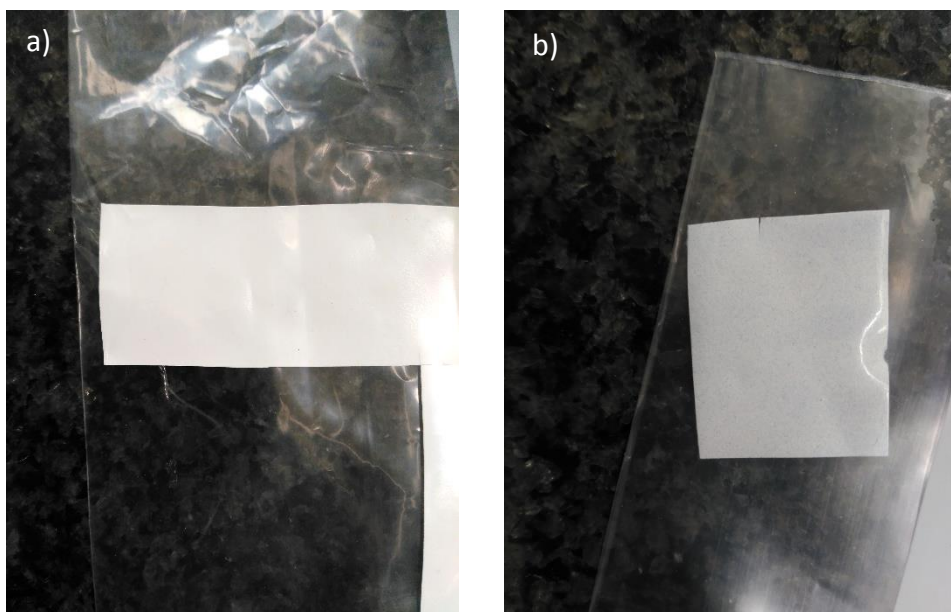


Figure III. 6. Pristine (a) and carbon-modified (b) membrane photo.

Ambient carbon dioxide capture and conversion via membranes

The bulk modified membranes were visibly darker (**Fig. III. 6**) as the blank polysulfone membrane is white while activated carbon is black. The top surface structure remained unchanged (**Fig. III. 7b**), whereas the bottom one small pores appeared (**Fig. III. 7a**). Similar effects were discovered by Spahis et al. [13] in the preparation of polymethyl methacrylate of methyl incorporating different amounts of AC (2, 4, 6, 8 and 10 wt% of the polymer mass) into the matrix. The study revealed that AC can enhance considerably the porosity of the membrane. The presence of pores increases the contact surface area, which is a favourable feature in membrane contactor operations. Nevertheless, if their size is too large they might cause an increase in wetting.

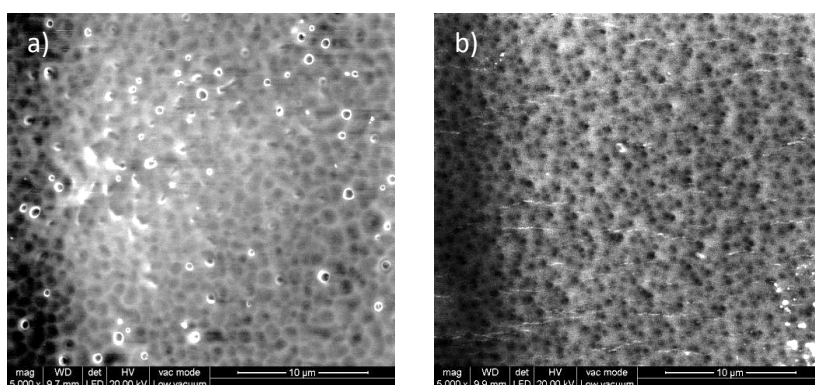


Figure III. 7. ESEM micrographs of surfaces of MAC200: a) bottom, b) top.

Microanalysis by EDX provides the composition of the membranes surfaces (**Table III. 3**). The difference in amount of C between the blank and membranes with carbon incorporated in the bulk is not significant ($p=0.16$). According to the statistical analysis, the difference is lower than 5%. The theoretical final amount of the polymer is 95% and 5% of AC: the results indicate that some carbon is dispersed within the membrane and incorporated by the polymer.

In case of surface modification, the results proved that the bottom surfaces of modified membranes are made up only of polysulfone as their elemental content is pretty much the same as the one of blank membranes. On the other hand, the difference in content between the top surfaces of samples before and after coating is significant ($p=0.029$). Phosphorus found in the top layer is probably coming from an impurity of the starting materials.

III. Polysulfone membrane contactors modified with activated carbon

Table III.3. Elemental analysis of carbon modified membranes surfaces by ESEM.

Membrane	Surface	The elements [wt.%]				
		C	O	F	P	S
M200	Top	73.37	17.68	-	-	8.96
	Bottom	73.65	18.67	-	-	7.68
M200_LAC_1	Top	47.72	12.99	35.71	1.69	1.89
	Bottom	73.06	19.12	-	-	7.82
M200_LAC_2	Top	57.97	13.66	24.12	1.21	3.04
	Bottom	73.57	18.62	-	-	7.81
M250	Top	71.85	17.51	-	-	9.66
	Bottom	72.81	18.32	-	-	8.87
M250_LAC_1	Top	52.2	13.54	30.78	1.79	1.69
	Bottom	73.43	18.19	-	-	8.38
M250_LAC_2	Top	58.13	14.08	22.88	1.03	3.88
	Bottom	73.77	17.41	-	-	8.82
MAC100	Top	74.62	16.54	-	-	8.82
	Bottom	74.81	17.19	-	-	7.99
MAC200	Top	74.14	16.49	-	-	9.36
	Bottom	74.92	17.26	-	-	7.81
MAC250	Top	74.43	16.41	-	-	9.15
	Bottom	74.12	18.40	-	-	7.48

Table III. 4. Carbon layer characteristics.

Membrane	Carbon layer thickness [μm (%)]	Carbon layer weight [mg (%)]	Surface contact angle [$^{\circ}$]
M200	-	-	69 ± 1
M200_LAC_1	21.7 (17.1)	9.1 (13.0)	131 ± 2
M200_LAC_2	16.7 (13.7)	3.6 (5.8)	124.9 ± 0.9
M250	-	-	68 ± 2
M250_LAC_1	31.7 (19.8)	7.5 (9.0)	125 ± 2
M250_LAC_2	21.7 (14.5)	2.0 (3.0)	126 ± 4

In addition, measurements of the layer thickness and its weight were performed for direct quantification (**Table III. 4**). The obtained values

Ambient carbon dioxide capture and conversion via membranes

indicate variations between 3.0 – 13.0 % of total weight, while layer thickness is in between 16.7 – 31.7 μm , which is not more than 20% of total thickness.

Furthermore, the analysis of layer hydrophobicity was also performed. The contact angle measurements show an increase of membrane hydrophobicity caused by the presence of activated carbon. Carbon hydrophobicity made the layer contact angle to approximately double after modification: the surfaces are transformed from hydrophilic to hydrophobic (**Table III. 4**).

III.3.2. CO₂ absorption studies

The CO₂ absorption properties of AC modified membranes were tested and compared with the results obtained for blank membranes (the CO₂ flux values of blank membranes were imported from the [Chapter 1](#) for comparison purposes). **Fig. III. 8** shows the CO₂ absorption flux for all obtained membranes as a function of the absorbent flow rate.

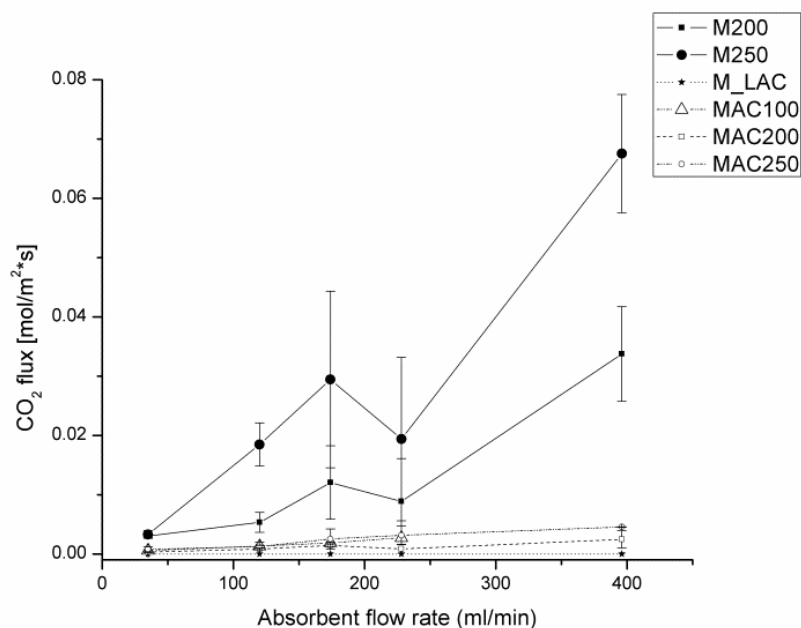


Figure III. 8. CO₂ absorption flux as a function of absorbent flow rate for pristine and carbon modified polysulfone membranes.

III. Polysulfone membrane contactors modified with activated carbon

It can be observed that incorporation of AC in the membrane bulk or on the membrane top surface do not improve the carbon dioxide sorption abilities. All the membranes with a carbon layer on top, independently of the AC layer composition or size, result in flux blockage. The SEM cross section micrographs show how the carbon layer did not penetrate into the membrane pores, what is more the additional layer might contribute to the membrane mass transfer resistance. Also, membranes with carbon in the bulk gave very small CO₂ flux values.

The CO₂ flux values of the modified membranes are presented in **Fig. III. 9** for a clearer view of the results. The results for MAC100 in the highest absorbent flow rate are not available because the thin membrane could not stand the cell pressure and broke.

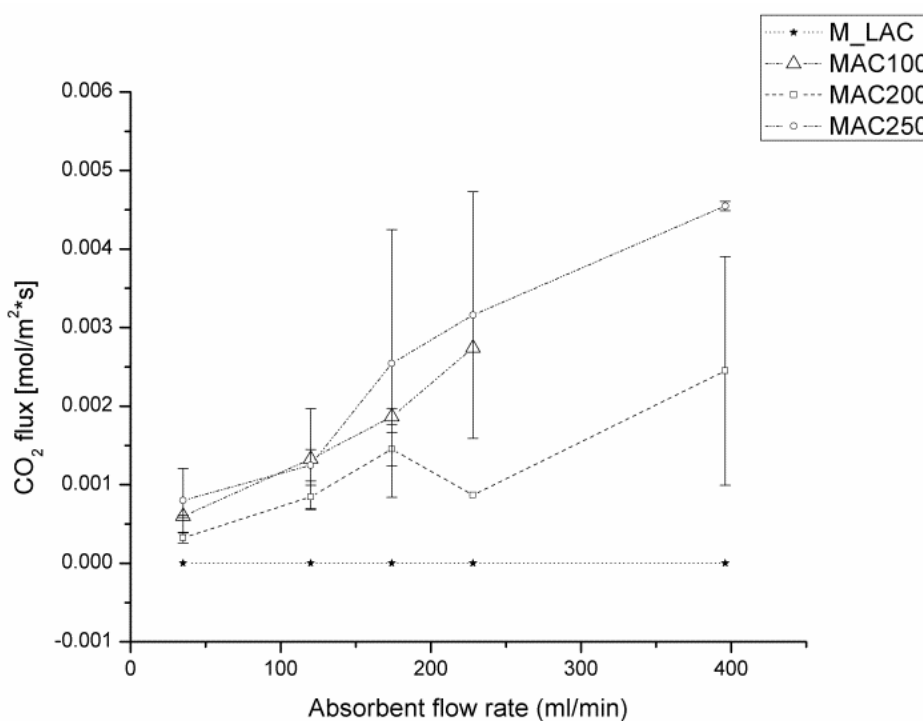


Figure III. 9. CO₂ absorption flux as a function of absorbent flow rates for carbon modified membranes.

In previous studies it was stated that the absorbent flow speed has a positive influence on the CO₂ flux, which is confirmed by the obtained results. Also, as seen for blank membranes, a thicker membrane (MAC250) gives better results than a thinner one (MAC200). However, statistical analysis gave a $p = 0.13$, meaning that the difference is not significant in

that case. Yet, the CO₂ capture rate is not improved, and there could be two possible reasons for this: 1) the pores created on the bottom surface of the membrane might get partially wetted and decrease the contact surface area; 2) the affinity of the carbon to adsorb CO₂ is too strong and there is no active passage of the gas to the absorbent solution. The second explanation is less likely, as judging from the elemental analysis the carbon particles were incorporated into the polymer, thus the access to the active site was small.

III.4. Conclusions

The incorporation of AC into the polymeric bulk caused increase of the membrane thickness and contribute to pores formation on the bottom surface of the membrane. The hydrophilicity was not improved. Even though the obtained membranes were visibly darker than blank membranes, elemental analysis did not detect increased amount of C atoms in the structure. The gas absorption test results shows no improvement of the membrane performance. It is possible that AC was incorporated by the polymer, quenching the possible positive influence of AC on the membrane properties. Another possible explanation is the membrane wetting caused by entrance of the absorptive liquid through the mentioned newly-formed pores on the bottom surface.

Modification of the polysulfone surface by coating with active carbon layer was successfully performed. The cross section images of the modified membranes showed that the layer did not penetrate into the membrane. All of the examined modified surfaces showed a much higher contact angle values than ones of their blank counterparts. The introduction of AC by ink spraying might result in blockage of the surface membrane pores and thus CO₂ cannot pass, as proven by CO₂ capture experiments. The additional layer increased membrane mass transfer resistance which decreases its effectiveness as a membrane contactor.

References

- [1] L.C. Bo Guo, Kechang Xie, *Adsorption of Carbon Dioxide on Activated Carbon*, Journal of Natural Gas Chemistry, 2006, **15**: p 223-229.
- [2] C.-H.H. Cheng-Hsiu Yu, Chung-Sung Tan, *A Review of CO₂ Capture by Absorption and Adsorption*, Aerosol and Air Quality Research, 2012, **12**: p 745-769.

III. Polysulfone membrane contactors modified with activated carbon

- [3] A.A.G. Soodabeh Khalili, Mohsen Jahanshahi, *Carbon dioxide captured by multiwalled carbon nanotube and activated charcoal: a comparative study*, Chemical Industry & Chemical Engineering Quarterly, 2013, **19**: p 153–164.
- [4] .K.K. Brett P. Spigarelli, *Opportunities and challenges in carbon dioxide capture*, Jurnal of CO₂ utilization, 2013, **1**: p 69-87.
- [5] B.B. P.Rajiv, M. Naveen Kumar, P.Vanathi, *Synthesis and characterization of biogenic iron oxide nanoparticles using green chemistry approach and evaluating their biological activities*, Biocatalysis and Agricultural Biotechnology, 2017, **12**: p 45-49.
- [6] S.Y. Nor Adilla Rashidi, *Potential of palm kernel shell as activated carbon precursors through single stage activation technique for carbon dioxide adsorption*, Journal of Cleaner Production, 2017, **168**: p 474 - 486.
- [7] F.F. C. Torras , J. Paltakari , R. Garcia-Valls, *Performance, morphology and tensile characterization of activated carbon composite membranes for the synthesis of enzyme membrane reactors*, Journal of Membrane Science, 2006, **282**: p 149–161.
- [8] J.-C.C. Li-Luen Hwang, Ming-Yen Wey, *The properties and filtration efficiency of activated carbon polymer composite membranes for the removal of humic acid*, Desalination, 2013, **313**: p 166 -175.
- [9] J.M. Marcia Ansona, Eduardo Garis, Nelio Ochoaa, Cecilia Pagliero, *ABS copolymer-activated carbon mixed matrix membranes for CO₂/CH₄ separation*, Journal of Membrane Science, 2004, **243**: p 19-28.
- [10] E.A.C. M. Prasanna, T.-H. Lim, I.-H. Oh, *Effects of MEA fabrication method on durability of polymer electrolyte membrane fuel cells*, Electrochimical Acta, 2008, **53**: p 5434–5441.
- [11] C.-Y.L. Chia-Chi Sung, Colin C.J. Cheng, *Performance improvement by a glue-functioned Nafion layer coating on gas diffusion electrodes in PEM fuel cells*, International Jurnal of hydrogen energy, 2014, **39**.
- [12] R.G.-V. Carles Torras, *Quantification of membrane morphology by interpretation of scanning electron microscopy images*, Journal of Membrane Science, 2004, **233**: p 119-127.

Ambient carbon dioxide capture and conversion via membranes

[13] M.D. Nawel Spahis, Hacene Mahmoudi, *Synthesis and Characterization of Polymeric/Activated Carbon Membranes*, *Procedia Engineering*, 2012, **33**: p 47-51.

III. Polysulfone membrane contactors modified with activated carbon

IV. BIOMIMETIC POLIMERIC MEMBRANES

*Part of the studies has been published in the proceedings of The 7th Advanced Functional Materials and Devices conference (AFMD 2017) in Functional Materials Letters: Adrianna Nogalska, Mario Ammendola, Carla A. M. Portugal, Bartosz Tylkowski, Joao G. Crespo, Ricard Garcia – Valls, *Polysulfone biomimetic membrane for CO₂ capture*, Functional Materials Letters 2018.

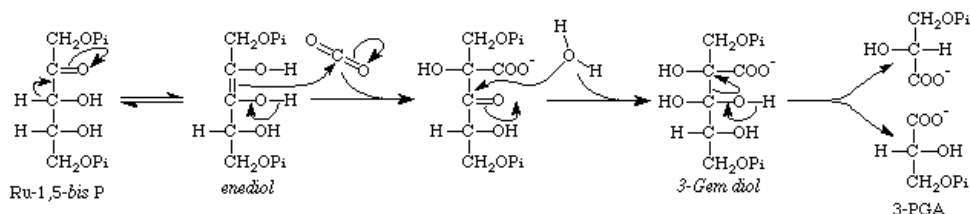
IV. Biomimetic polymeric membranes

The aim of the study described in Chapter IV is to combine a polymeric membrane with one of the enzymes involved in carbon fixation: RuBisCo or CA. Two approaches were studied: physical attachment by adsorption and chemical attachment by covalent binding to amine terminated magnetic nanoparticles dispersed within the membrane. The enzyme structural alterations, activity and CO₂ sorption abilities were determined. In order to evaluate the real influence of covalent binding on the immobilization, the adsorption studies were performed on both blank and nanocomposite membranes.

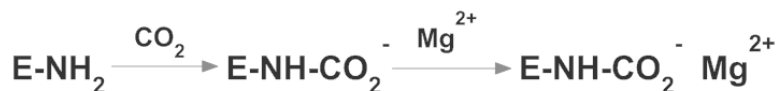
Ambient carbon dioxide capture and conversion via membranes

IV.1. Introduction

The CO₂ capture process has been refined though millions of years by photosynthetic organisms. The carbon dioxide fixation phenomenon is the first step of the Calvin cycle, in which CO₂ is converted together with water to energy-rich molecules. The enzyme involved in this first step of the process is the ribulose-1,5-biphosphate carboxylase/oxygenase (RuBisCo), which is the most abundant enzyme on Earth. In chemical terms, RuBisCo catalyses the carboxylation of ribulose-1,5-bisphosphate (**Scheme 1**), where 3-PGA is being formed. In macroscale a CO₂ unit is firstly covalently linked to the epsilon amino group (-NH₂) of a lysine residue (lysine-COO⁻; carbamate) (**Scheme 2**) of a large subunit of the protein [1]. A big part of the enzymes involved in the Calvin cycle is sensitive to the proton concentration of the chloroplast stromal compartment. In the case of RuBisCo, the optimum pH for its activity is 7.8 and the proton level control is coupled to magnesium interaction with carbamates. In other words, magnesium stabilizes carbamate formation and thus activates RuBisCo.



Scheme 1. Reaction of carboxylation of RuBP catalysed by RuBisCo.

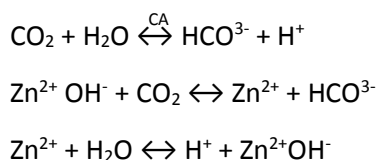


Scheme 2. Carbamate formation stabilized by magnesium ion during the CO₂ fixation on RuBisCo.

As RuBisCo is both a carboxylase and an oxygenase, there will be a competition between CO₂ fixation and O₂ fixation. Which reaction will occur, mainly depends on the compound concentration in the vicinity of the enzyme. Some plants, in order to overcome the problem, developed a inorganic carbon concentration mechanism (CCM) which is shifting RuBisCo

IV. Biomimetic polymeric membranes

selectivity towards CO₂ fixation [2]. One of the solutions implemented by plants is the active CO₂ transfer mechanism relying on the presence of carbonic anhydrase (CA). Carbonic anhydrases are Zn-metalloenzymes that catalyse the reversible hydration of carbon dioxide into bicarbonate. The reaction involves a two-step mechanism (**Scheme 3**). The first step is the nucleophilic attack of a zinc-bound hydroxide ion on CO₂. The second step is the regeneration of the active site by ionization of the zinc-bound water molecule and removal of a proton from the active site.



Scheme 3. CO₂ hydration reaction by CA.

The introduction of an enzyme into a membrane containing system by immobilization results in improved resistance to environmental changes and storage stability. There are several methods for introducing an enzyme into the polymeric membrane: bind the enzyme covalently, physically adsorbed it or entrap in the membrane pores [3]. The presence of binding sites on the membranes is a prerequisite. The covalent binding is based on the chemical attachment to functional groups, which are already present or are introduced on the membrane surface. The most commonly used functional groups are: epoxy-, carboxyl- or, mostly used, amino-. Glutaraldehyde coupling method is most commonly used to immobilize enzyme on the amino-functionalized support matrix based on Schiff base reaction [4]. In general, covalent binding leads to strong and stable enzyme support attachment but at the same time may also reduce enzyme activity due to changes in the enzyme's native structure. The physical attachment is based on hydrophobic, hydrophilic or electrostatic interactions occur between an enzyme and a membrane. Adsorption is one of the most simple and common mechanisms. The method is easier in terms of preparation of support and enzyme prior to binding, however, the risks of enzyme leaching from the support are higher due to weaker enzyme-support interactions.

In order to follow the eventual structural changes, researchers most commonly perform fluorescence studies. The study of protein behaviour in immobilization experiments requires a labelling process. Tryptophan, which is in both CA and RuBisCo structures, is a source of intrinsic protein

Ambient carbon dioxide capture and conversion via membranes

fluorescence, thus there is no need for the labelling. The indol group of tryptophan is considered the main source of UV absorbance at ~280 nm and emission at ~350 nm in proteins. It is highly sensitive to the local environment. Changes of fluorescence emission may be related to structural changes of the protein: a decrease in fluorescence emission may occur as a consequence of the proximity of quenchers, such as disulfide and hydrogen bonds, and the metallic active centers of the enzymes (e.g. heme group) [5].

Fluorescence anisotropy is based on the principle of photoselective excitation of fluorophores by polarized light, resulting in polarized emissions. The polarized emission is influenced by a number of processes, including motions that occur within the lifetime of the excited fluorophore (rotational diffusion). Fluorescence anisotropy provides information on proteins such as its shape, size and flexibility, protein-protein associations, fluidity of the membrane, bindings and conformational dynamics [5].

IV.2. Experimental

IV.2.1. Materials

The reagents were purchased from Sigma Aldrich (where not specified) and used without purification. Polymers used for membrane preparation were: PVA (Mowiol) of Mw 145,000 and Polysulfone (pellets) of Mw 35,000 purchased and the solvent: N-Methyl-2-pyrrolidone (NMP, ACS). Nanoparticles were made of Iron (II) chloride tetra-hydrate puriss. p.a. , $\geq 99.0\%$ (R.T.) and Iron (III) chloride hexa-hydrate, ACS reagent, 97% in ammonia solution - NH₄OH puriss. p.a., reag. ISO, reag. Ph. Eur., ~25 NH₃ basis. The functionalization of ferrite particles with amine groups was done by (3-Aminopropyl)triethoxysilane 99%. Phosphate saline buffer was prepared by dissolving a proper amount of tablets (PBS, tablet). During the enzymes immobilization were used: Ammonium sulfate (Reag.Ph.Eur) Panreac; Glutaraldehyde 25%; Triton - x - 100 Fluka; NaBH₄, purum p.a. $\geq 96\%$ (gas – volumetric). The carbonate - bicarbonate buffer was made of Sodium bicarbonate, ACS reagent, $\geq 99.7\%$ and Sodium carbonate, anhydrous, ACS. The enzymes: Carbonic anhydrase Lyophilized powder, $\geq 3,000$ W-A units/mg protein and D-Ribulose 1,5-Diphosphate Carboxylase from spinach, partially purified powder 0.01-0.1 unit/mg solid.

IV. Biomimetic polymeric membranes

IV.2.2. Synthesis and functionalization of magnetic nanoparticles (MNPs)

Magnetic nanoparticles of magnetite (Fe_3O_4) were synthesized by coprecipitation of iron salts in alkaline medium [6]. 50 mL of an aqueous solution containing 0.36 M FeCl_2 and 0.72 M FeCl_3 was added at 5.0 ml/min into 450 ml of a 1 M NH_4OH aqueous solution under continuous mechanic stirring at room temperature. The obtained black precipitate was separated from the liquid phase by centrifugation, then washed three times with ultrapure water (MilliQ) and twice with phosphate buffered saline (PBS, 100 mM sodium phosphate, 150 mM NaCl, pH 7.4). N_2 gas was continuously bubbled into all solutions during the process. The resulting magnetic nanoparticles contain $-\text{OH}$ groups on their surface, which were further converted to $-\text{NH}_2$ with APTS as follows: MNPs (300 mg, dry weight) were incubated with 30 ml of 2% (v/v) APTS at 70°C under orbital shaking (200 rpm). After 24 h, they were washed three times with PBS and maintained in the same buffer at 4°C before use.

IV.2.3. Characterization of MNPs

The ferrite nanoparticles were characterized via bright field transmission electron microscopy (TEM) analysis using a FEI Tecnai G12 Spirit Twin, equipped with a LaB6 source and a FEI Eagle 4k CCD camera (Eindhoven, Netherlands). Acceleration voltage was set at 120 kV. Before the analysis, the nanoparticles were dispersed in ethanol by sonication with a Sonics Vibracell VCX500 apparatus (Newtown, CT, USA) for 10 min, with 25% amplitude. After sonication, the dispersed nanoparticles were poured onto carbon coated TEM copper grids. The obtained micrographs were analyzed with Image J in order to obtain the size distribution.

The structural characterization of the nanoparticles was performed via wide angle X-ray diffraction (WAXD) using a Siemens EM – 10110BU model D5000 powder diffractometer, irradiated with a Ni-filtered Cu K-radiation (wavelength 1.5418 Å).

Energy Dispersive X-ray (EDX) analysis was performed on nanoparticles using a scanning electron microscope (SEM) FEI Quanta 200 FEG equipped with an Oxford Inca Energy System 250 and an Inca-X-actLN2-free analytical silicon drift detector (Abingdon, UK). The EDX analysis was performed in high vacuum mode at 20-30 kV acceleration voltage. Average results and standard deviation values are based on three consecutive measurements on different areas of each sample.

IV.2.4. Membrane preparation

Polysulfone membrane

Polysulfone membranes were made via phase inversion method. The polymeric solution used for the fabrication consisted of 20 % wt. polysulfone for blank membranes (PSF) and 19% wt. for membranes with nanoparticles (PSF_MNP), dissolved in 1-Methyl-2-pyrrolidone for 48 h under stirring. The nanoparticles were added to the homogeneous solution in a concentration of 1 wt% and the solution was sonicated for 1 h before membrane preparation. The resulting solutions were cast on a glass support using a casting knife of 250 μm thickness and immediately immersed into water, where the membranes precipitate. The prepared flat-sheet membranes were dried at ambient conditions.

PVA membrane

PVA (8%) was dissolved in H_2O at 80°C (PVA). The corresponding amount of nanoparticles was dispersed in water by sonication and the two solutions were merged (PVA_MNP). The obtained solution was sonicated for 2h, then mixed with 3% of cross-linking glutaraldehyde (GDA) followed by 3% of HCl (initiator) and cast in a petri dish. The membrane jellified and naturally detached from the petri dish.

IV.2.5. Enzyme immobilization

The immobilization experiments were performed in a closed flask placed on the orbital shaker. Firstly, the enzyme (CA or RuBisCo) aqueous solutions in range of concentrations 10 mg/L, 100 mg/L and 1 g/L were prepared adding Triton x 100 (0.017 wt. %) and stirring. Then the corresponding membrane was suspended in the solution: blank polymeric membrane for adsorption (A_PSF or A_PVA) or membrane with nanoparticles for adsorption (A_PSF_MNP or A_PVA_MNP) and covalent binding (CB_PSF_MNP or CB_PVA_MNP). Subsequently the ammonium sulphate 0.32 g was added. After 5 min, a 10 ml of a 25% glutaraldehyde solution was added to the solution of experiment for covalent binding. Finally, the membrane was left stirring in the broth for 48 hours. After this time the membranes was washed in PBS three times. In order to evaluate the influence of Triton on the adsorption on the immobilization efficiency, additional experiments without it were performed.

The covalent binding experiment required an additional step for reducing Schiff bases from unreacted enzymes and glutaraldehydes. For this

IV. Biomimetic polymeric membranes

reason, the membrane was treated with a sodium borohydride solution prepared from a basic (pH=10) carbonate-bicarbonate buffer. In order to prepare 250 ml of carbonate-bicarbonate buffer, a solution of 0.2M anhydrous sodium carbonate and a solution of 0.2M sodium bicarbonate were mixed in ratio of respectively 4.5 ml: 57.5 ml. MilliQ water was used to bring the volume to 250 ml and the pH was controlled to 10. To 200 ml of buffer with membrane (3), 0.0122 g NaBH₄ is quickly weighed and added while continuing stirring. The stirring was continued for two hours after which the membrane is removed from the NaBH₄ solution and washed firstly with 2 M NaCl in PBS and then with 1% (v/v) Triton X-100 in PBS.

IV.2.6. Characterization of the enzyme and the membrane

The membrane morphology was analysed from ESEM micrographs (FEI Quanta 600). Membranes were fractured in liquid nitrogen and fixed to the support suitable for cross-section analysis. The obtained images were analysed with Image J for determining membrane thickness and macrovoids size and with Ifme for asymmetry and mean pores size.

The hydrophobicity was analyzed by contact angle measurements using Dataphysics OCA 15EC. A 3 µL droplet of Milli-q water was placed on the bottom surface of the membrane and contact angle was calculated from a digital image by SCA software included in the apparatus. The measurements were repeated at least three times on different zones of the surfaces and an average value was taken.

The overall membrane porosity (ϵ), defined as the volume of pores divided by the total volume of the membrane, was measured using a method based on density measurements. It was determined from the bulk and the polysulfone density using the following equation:

$$\epsilon = \left(1 - \frac{\rho_m}{\rho_{psf}}\right) 100\% \quad (1)$$

where ρ_m and ρ_{psf} correspond to membrane and polysulfone density respectively.

Determination of the immobilized amount of the enzyme by inductively coupled plasma spectroanalysis (ICP)

The Inductively Coupled Plasma-Atomic Emission Spectrometer (ICP, Horiba Jobin-Yvon) allowed the determination of the immobilized amount

Ambient carbon dioxide capture and conversion via membranes

of the enzyme on the membrane by analysis of the remaining amount in the experimental solution. The concentration of Zn^{2+} ions which directly corresponds to CA (1:1), was performed using emission line acquired at 213.856 nm. Whereas RuBisCo concentration was determined according to the Mg^{2+} concentration estimation by measurements at 279.553 nm; 4 Mg ions correspond to 1 RuBisCo unit.

Carbonic anhydrase activity assay

The assay consists on measuring of the time needed for the pH of a 0.02 M Tris-HCl buffer to drop from 8.3 to 6.3 at 3° C in presence of carbonic anhydrase and sparkling water. The water was used as a reliable source of CO_2 because it has a specific concentration of CO_2 (the saturation one). Cold Tris-HCl buffer is placed in a beaker and a pH meter equipped with thermometer is dipped in the solution while stirring. Then, CA solution is added followed by sparkling water and the time needed for the pH to drop is measured. The enzyme active units in the experimental solution and on the membrane were calculated based on the calibration curve obtained by using CA solutions of known concentration.

Monitoring of structural changes induced by immobilization via fluorescence spectroscopy and anisotropy

Fluorescence was acquired by SPEX 212 I Fluorolog Spectrofluorimeter equipped with emission and excitation polarizers. The emission spectra in range of λ_{em} 300-550 nm were recorded at an excitation wavelength λ_{ex} of 290 nm with an increment step of 1 nm and integration time of 0.1 s. The spectra of the enzyme in the experimental solution and on the membrane were recorded.

Anisotropy was calculated according to the ratio of fluorescence intensities collected at different combinations of the excitation and emission polarizers positions as a result of equation (2). IVV is the fluorescence intensity collected with both polarizers at the vertical position, IVH the fluorescence intensity acquired with the excitation polarizer in the vertical and the emission polarizer in the horizontal position, IHH the fluorescence intensity acquired with both polarizers at the horizontal position and IHV the fluorescence intensity acquired with the excitation polarizer horizontally and the emission polarizer vertically oriented. G is a parameter that takes into account the sensitivity of the detection system for vertically and horizontally polarized lights.

IV. Biomimetic polymeric membranes

$$r = \frac{I_{vv} - I_{VH} * G}{I_{vv} + 2 * I_{VH} * G} \quad (2)$$

$$G = \frac{I_{HV}}{I_{HH}} \quad (3)$$

Emission spectra of the enzyme on membrane were obtained by normalization followed by subtraction of the untreated membrane spectra from the spectra of CA-containing membrane. Described data formatting allowed analysis of displacement of the tryptophan peak.

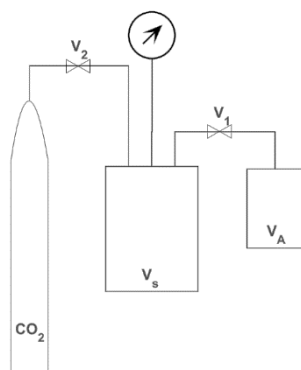


Figure IV. 1. Schematic representation of the system for CO₂ solubility studies of biomimetic membranes.

Membrane sorption studies – CO₂ solubility

The storage chamber (V_s) and the absorption chamber (V_A), were connected by a valve (**Fig. IV. 1**). Both volumes were decreased (up to 57 % of storage volume and 85 % of adsorption one) by adding steel spheres in order to adjust the conditions to used membrane types. The membrane was placed in the chamber V_A. The system was purged with CO₂ in order to remove air. Afterwards the about to be mentioned procedure was followed: the valve connecting both chambers (V₁) was closed and V_s was filled with the gas until a pressure of 7-8 mbar was reached; after reaching pressure stabilization (30 min), valve V₁ was opened and the gas spread to both chambers; the gas was absorbed by the membrane causing a decrease in pressure. The pressure was monitored by a high accuracy pressure gauge for 20 h.

To calculate the amount of CO₂ absorbed by the membrane, n_{CO_2} [mol], the following relation was used:

$$n_{CO_2} = \frac{p^0 \cdot V_S - p \cdot (V_S + V_A - V_M)}{RT} \quad (4)$$

Ambient carbon dioxide capture and conversion via membranes

where p_0 (Pa) is the pressure test used to fill the storage volume, V_s [m^3], p [Pa] is the monitored pressure, V_A [m^3] is the adsorption chamber volume, V_M [m^3] is the membrane volume, R (8.314 J/K·mol) is the gas constant and T (296.15 K) is the temperature.

The solubility coefficient S_{CO_2} , expressed in [m^3 (STP)/ m^3 polymer·atm] units, was calculated through:

$$S_{CO_2} = \frac{V_{CO_2m}(STP)}{V_m \cdot p_{established}} \quad (5)$$

where V_{CO_2m} (STP)[m^3] is the volume of CO_2 corresponding to n_{CO_2} at STP conditions (1 atm, 273.15K), and $p_{established}$ [atm] is the pressure measured at equilibrium conditions.

Membrane contactors CO_2 sorption abilities estimation

The obtained modified membranes were applied in the cross-flow module as contactors between the air and the absorption solution. The absorption experiments were performed during 1 h. The effect of the liquid flow rate was tested within a range of 35–438 ml/min for different enzymes attached by covalent binding to polysulfone membranes. Carbon dioxide ion selective electrode was used to determine the total CO_2 concentration in collected samples. The results enable to calculate CO_2 flux [$mol/m^2 \cdot s$] in the membrane contactor following this equation:

$$J_{CO_2} = \frac{Q_i \cdot M_{CO_2}}{A} \cdot 1000 \quad (6)$$

where Q_i is the absorbent flow rate [m^3/s], M_{CO_2} is CO_2 concentration in the absorbent [mol/L] obtained from the measurements and A is the area of the flat sheet membrane [m^2].

IV.3. Results and discussion

IV.3.1. Nanoparticles and membranes physico-chemical characterization

IV. Biomimetic polymeric membranes

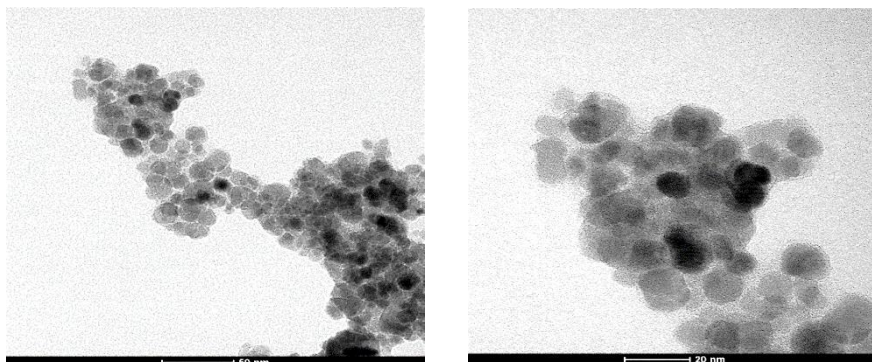


Figure IV. 2. TEM images of $Fe_2O_3-NH_2$ nanoparticles at different magnifications. Nanoparticles characteristics

The nanoparticles physical aspect was analysed by TEM. The analysis shows that they possess circular shape. Moreover, the size distribution was determined from the second image (**Fig. IV. 2**) on 31 nanoparticles showing a broad distribution (of ~ 10 nm) in dimension. The mean size calculated on the collected data is 11.15 ± 2.77 nm (**Fig. IV. 3**).

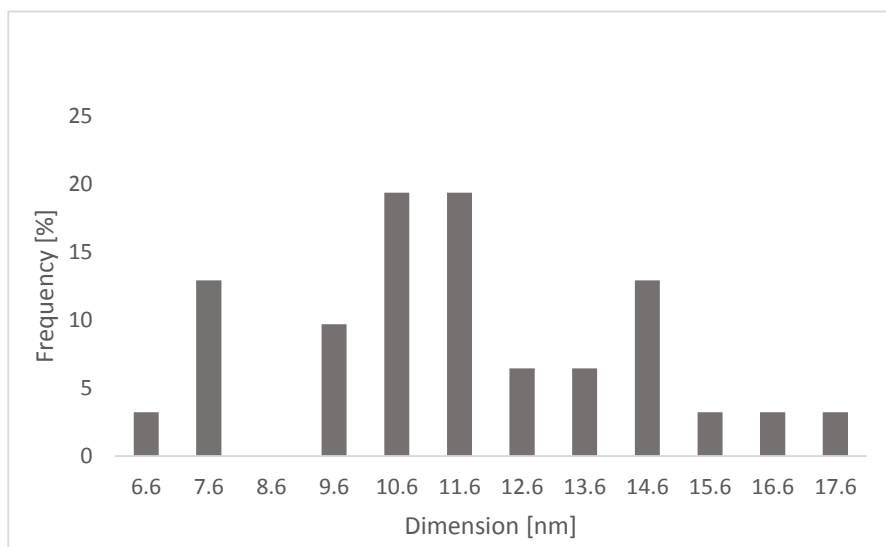


Figure IV. 3. $Fe_2O_3-NH_2$ nanoparticles size distribution.

WAXD spectra confirm the formation of Fe_2O_3 nanoparticles with a cubic structure (**Fig. IV. 4**). In particular, diffraction peaks at $2\theta = 30.1, 35.1, 43.4, 54.6, 57.1$ and 63.7 which represent the Bragg reflections from the (220), (311), (400), (422), (511) and (440) planes, are present in the

Ambient carbon dioxide capture and conversion via membranes

diffraction patterns of both spectra [7]. The obtained peaks and their relative intensities are in both cases in agreement with literature data [7].

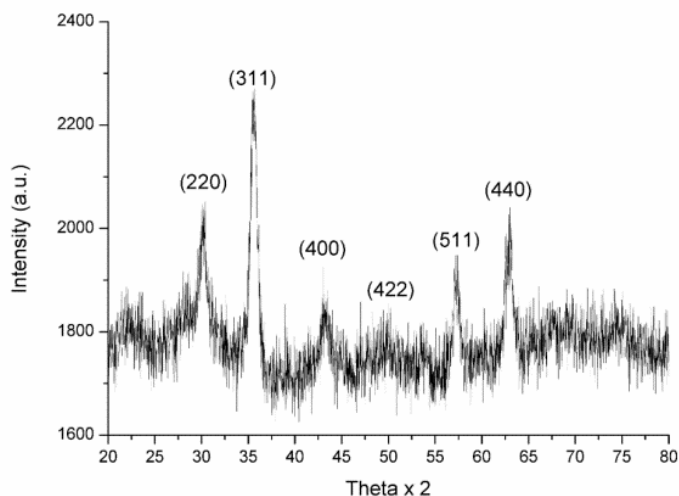


Figure IV. 4. X-ray spectrum of the $\text{Fe}_2\text{O}_3\text{-NH}_2$ nanoparticles.

The amount of the main elements obtained based on the EDX measurements are: Fe 38.9 % and O 61.1%, showing a good agreement with the expected stoichiometry.

Membrane characterization

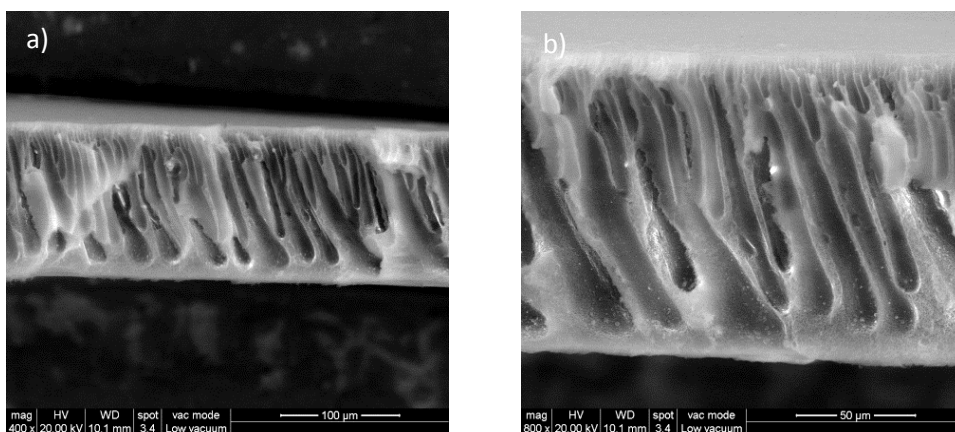


Figure IV. 5. SEM micrographs of biomimetic polysulfone membranes containing: a) CA, b) RuBisCo.

IV. Biomimetic polymeric membranes

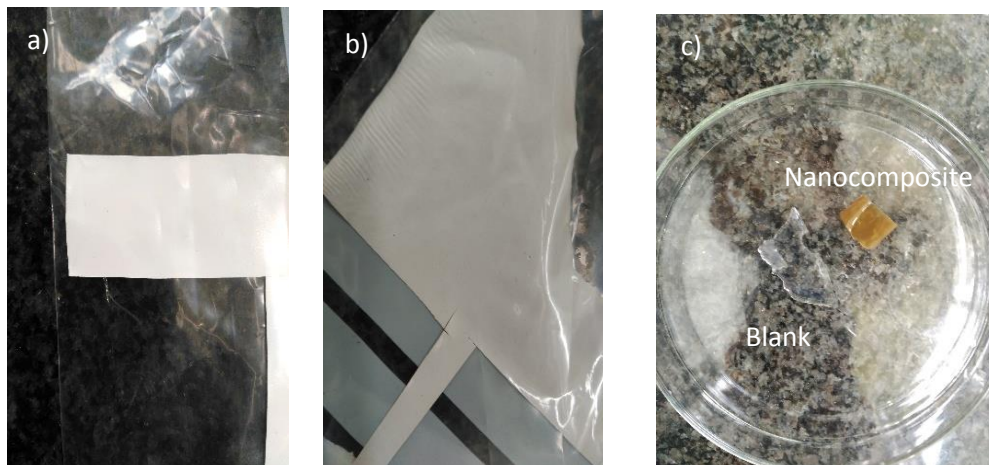


Figure IV. 6. Membranes photos: a) polysulfone pristine, b) polysulfone nanocomposite, c) PVA pristine and nanocomposite.

The previously studied polysulfone based membrane with incorporated nanoparticles or activated carbon in the bulk revealed no influence of the modification on the membrane structure with low amount of additives. Cross section images (**Fig. IV. 5**) together with their analysis by Ifme and ImageJ confirmed that here is no change in polysulfone membrane morphology caused by enzyme incorporation (**Table IV. 1**). Moreover we observed an increase of the membrane hydrophobicity, which is in agreement with previous studies. However immobilizing enzymes decreased it again.

During PVA membranes examination no pores were detected. The high hydrophilic character of those membranes caused difficulties during the physical characterization. As an ESEM analysis requires dry samples and PVA-based membranes lose elasticity when dried and get easily broken, the cross sectional images were not grabbed. In this case the thickness was obtained by micrometric measurements giving $235 \pm 3 \mu\text{m}$ for the blank membrane and $182 \pm 5 \mu\text{m}$ for the nanocomposite-incorporating one. The membranes were obtained by jellification in Petri dish without control of its thickness, thus it cannot be assumed that the change in thickness was caused by the introduction of nanoparticles. Besides, during the contact angle measurements the blank membrane was instantaneously adsorbing water, thus the value was considered to be 0° . On the other hand the moist nanocomposite-incorporating membrane has a contact angle of 0° , but when dried the contact angle increased up to 28° .

Ambient carbon dioxide capture and conversion via membranes

Table IV. 1. Characteristics of the resulting biomimetic membranes.

Membrane	Thickness [μm]	Asymmetry [%]	Porosity (ε) [%]	Mean pore diameter [μm]	Mean macrovoids size [μm^2]	Contact angle [°]
PSF	99.0 \pm 0.4	11	72.9	40 \pm 7	600 \pm 100	63 \pm 3
PSF_MNP	92.5 \pm 0.3	10	69.8	31 \pm 6	700 \pm 200	83 \pm 5
PSF_MNP_RuBisCo	100 \pm 1	7	70.1	35 \pm 6	600 \pm 100	78 \pm 3
PSF_MNP_CA	97 \pm 3	13	67.2	25 \pm 4	800 \pm 200	76 \pm 3

IV. Biomimetic polymeric membranes

IV.3.2. Protein evaluation in terms of structural changes and CO₂ sorption capacity induced by the immobilization on :

IV.3.2.1. Polysulfone based membrane

The modified membranes are named accordingly to the immobilization method (A-for physical adsorption and CB- for covalent binding) and the membrane used as support (PSF- blank membrane, PSF_MNP- nanocomposite).

Determination of the immobilized amount of the enzyme by inductively coupled plasma spectroanalysis (ICP)

Immobilization efficiency was estimated by ICP studies, as the detergent and cross linking agent were interfering during the standard Bradford assay with use of UV-Vis.

Table IV. 2. CA immobilization efficiency on polysulfone based membranes (n.d. – not detected).

	Experiment	Immobilized amount [mg]	Experiment efficiency %	Concentration on membrane [mg/cm ²]
10 mg /L	A_PSF_CA	0.291	32.35	0.00026
	A_PSF_MNP_CA	n.d.	n.d.	n.d.
	CB_PSF_MNP_CA	0.106	8.85	0.00009
100 mg/L	A_PSF_CA	0.114	5.17	0.01182
	A_PSF_MNP_CA	1.632	70.95	0.21115
	CB_PSF_MNP_CA	1.412	64.16	0.1784
1 g/L	A_PSF_CA	0.500	20.00	0.00088
	A_PSF_MNP_CA	0.750	32.61	0.00199
	CB_PSF_MNP_CA	0.394	17.91	0.00116

Ambient carbon dioxide capture and conversion via membranes

From the CA immobilization efficiency analysis we can see that the enzyme is being attached with a higher efficiency to the membrane containing magnetic nanoparticles, except when the lowest concentration was used (10 mg/L) (**Table IV. 2**). Nevertheless the introduction of a cross linker in order to initiate the covalent bond formation does not improve the immobilization.

The maximum immobilization efficiency was reached for the 100 mg/L solution. When increasing the concentration on one hand a higher concentration of the enzyme on the membrane can be achieved but at the same time a high concentration can cause the agglomeration of the enzyme in the solution reducing the accessibility due to steric hindrance, decreasing the experiment efficiency. Moreover, a higher concentration might require longer time of reaction. As the best results were achieved with a 100 mg/L concentration, this condition was adopted for immobilization of RuBisCo.

Unfortunately, when the immobilization of RuBisCo was tried following the method explained above (**IV.2.4.**), which includes Triton-x-100, no attachment was achieved. The use of detergent may prevent the enzyme immobilization on its active centre and promote the enzyme orientation in the support, whereas in case of RuBisCo the solubilisation operated by triton prevents the contact with the membrane and the enzyme remained in solution. As the experiments for covalent binding require the presence of surfactant (once you add glutaraldehyde the enzyme might create aggregates) RuBisCo cannot be covalently attached with the studied method, but only physically attached.

Table IV. 3. Comparison of CA and RuBisCo immobilization efficiencies in absence of Triton – X-100 on polysulfone based membranes (n.d. – not detected).

	Experiment	Immobilized amount [mg]	Experiment efficiency %	Concentration on membrane [mg/cm ²]
CA	A_PSF	n.d.	n.d.	n.d.
	A_PSF_MNP	0.232	12.20	0.030
RuBisCo	A_PSF	0.142	7.46	0.014
	A_PSF_MNP	0.130	6.86	0.017

IV. Biomimetic polymeric membranes

Hence, experiments were performed in absence of the detergent (**Table IV. 3**), showing that the efficiency of RuBisCo attachment is similar to both studied membranes – plain polysulfone and nanocomposite- suggesting that nanoparticles are not involved in the physical attachment. On the other hand, CA was not physically attached to the polymer but by the -NH₂ terminated magnetic nanoparticles.

Table IV. 4. Influence of Triton – X- 100 on CA immobilization efficiency on polysulfone based membranes (n.d. – not detected).

Experiment		Immobilized amount [mg]	experiment efficiency %	Concentration on membrane [mg/cm ²]
A_PSF_CA	With triton	0.11	5.17	0.011
	No triton	n.d.	n.d.	n.d.
A_PSF_MNP_CA	With triton	1.63	70.95	0.211
	No triton	0.232	12.20	0.030

The results of ICP analysis on CA 100 mg/L experiments with and without use of triton are gathered in **Table IV. 4** for comparison. It is possible to see how triton is improving the enzyme attachment in case of CA and the influence is more marked in case of the nanoparticles-containing membrane. The solubilized enzyme was attached to the hydrophilic membrane and -NH₂ terminated nanoparticles.

This phenomenon might be explained by the different interactions between enzyme, detergent and membrane. Considering that triton possess hydrophilic and hydrophobic parts, while solubilizing an enzyme the corresponding end will interact with it. CA is hydrophilic, thus the hydrophilic head of the detergent will face the enzyme, while the hydrophobic tale will react with the membrane. Contact angle measurements showed that the membrane after introduction of nanoparticles becomes more hydrophobic, hence it can be postulated that the nanoparticles should be hydrophobic. RuBisCo is a hydrophobic enzyme, for this reason an inverted orientation of triton would in principle hamper the enzyme approach to the membrane.

Ambient carbon dioxide capture and conversion via membranes

Carbonic anhydrase activity assay

Table IV. 5. Activity test results of CA immobilized on polysulfone based membranes in range of concentrations and with use of different techniques (n.d. – not detected; n.a. - not analysed).

	Experiment	Active amount [mg]	Active concentration [$\mu\text{g}/\text{cm}^2$]	Active percentage %
10 mg /L	A_PSF_CA	0.0014	1.204	0.464
	A_PSF_MNP_CA	n.a.	n.a	n.a.
	CB_PSF_MNP_CA	0.007	6.225	6.65
100 mg/L	A_PSF_CA	0.014	21.188	12.28
	A_PSF_MNP_CA	n.a.	n.a.	n.a.
	CB_PSF_MNP_CA	0.009	9.623	0.638
1 g/L	A_PSF	0.013	23.435	2.67
	A_PSF_MNP_CA	0.007	18.708	0.94
	CB_PSF_MNP_CA	n.d.	n.d.	n.d.

The measurements of the activity of the enzyme were performed using the modified membranes. Very little enzyme activities were detected (**Table IV. 5.**). Moreover in some cases the enzyme-attached membranes were reacting much slower with CO₂ than untreated membranes. The calibration curve was obtained based on CA aqueous solutions of known concentration, so the blank membrane influence was not taken into consideration. Therefore obtained activity results might not be reliable.

IV. Biomimetic polymeric membranes

Membrane sorption studies – CO₂ solubility

CO₂ solubility of blank polysulfone membrane and the membrane with 1 % of MNP was not detected. That means that applied experimental conditions allowed to obtain the CO₂ solubility values correlated strictly to the enzyme. The obtained results were normalized to 1 mg of attached enzyme in order to disclose the real difference in CO₂ solubility according to which attached enzymes and attachment techniques were employed.

The CO₂ sorption experiments results (**Table IV. 6**) are in agreement with the ICP results, suggesting that higher amount of the enzyme on membrane results in better sorption abilities.

Attached RuBisCo has the analogous activity for both membranes, which enforces the assumption that the enzyme is just attached to the polysulfone and not to nanoparticles. Comparing those results to the CA attached to polysulfone (A_PSF_CA with triton) it can be noticed how it has a much worst CO₂ solubility performance.

Although the use of triton is meant for improving the attachment of CA it is also influencing the enzyme CO₂ solubility rate. As it is improving the attachment to nanoparticles the interactions might be stronger than ones with the blank polysulfone membrane. In this case the enzyme arrangement would influence the access to the active site.

Ambient carbon dioxide capture and conversion via membranes

Table IV. 6. CO₂ solubility in the biomimetic polysulfone based membranes.

Experiment	CA 10 mg/L		CA 100 mg/L		CA 100 mg/L (no triton)		RuBisCo 100 mg/L (no triton)	
	A_PSF	A_PSF_MNP	A_PSF	A_PSF_MNP	A_PSF	A_PSF_MNP	A_PSF	A_PSF_MNP
n _{CO2} [μmol]	2.272	70.309	148.476	181.860	27.256	61.860	57.956	51.900
S [m3 STP/m3 atm]	0.53	21.44	35.05	38.72	21.34	27.65	34.31	31.07
Normalized n: μmol CO ₂ / mg CA	7.81	n.d.	1349.78	111.57	n.d.	266.64	408.14	399.23

IV. Biomimetic polymeric membranes

Monitoring of structural changes induced by immobilization via fluorescence spectroscopy and anisotropy

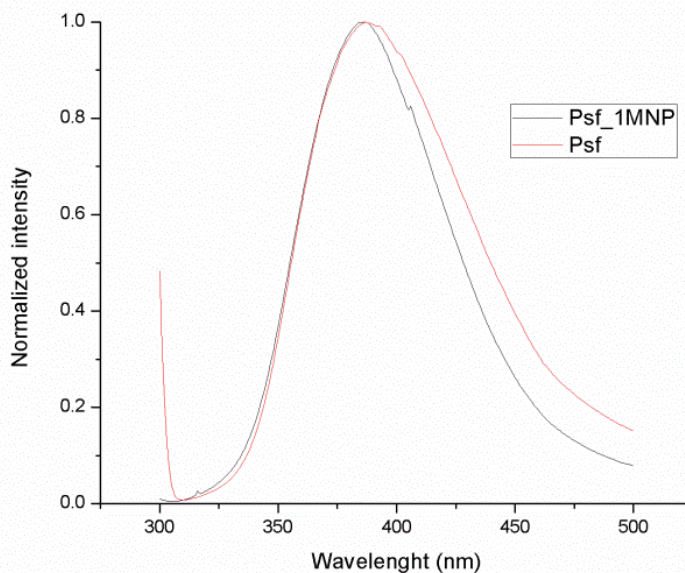


Figure IV. 7. Fluorescence spectra of polysulfone-based membranes.

Polysulfone is emitting light very strongly at a wavelength of 391 nm as it is containing benzene in the structure as well as multiple double bonds [8]. After the incorporation of ferrite nanoparticles, the peak width is lowered down by the quenching of the metal ions (**Fig. IV. 7**).

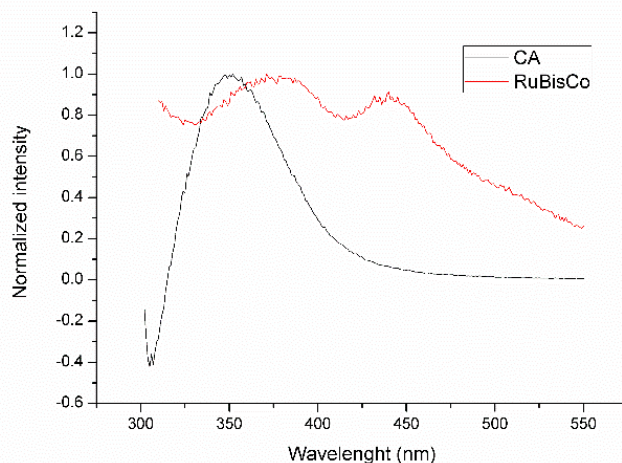


Figure IV. 8. Fluorescence emission spectra of CA and RuBisCo.

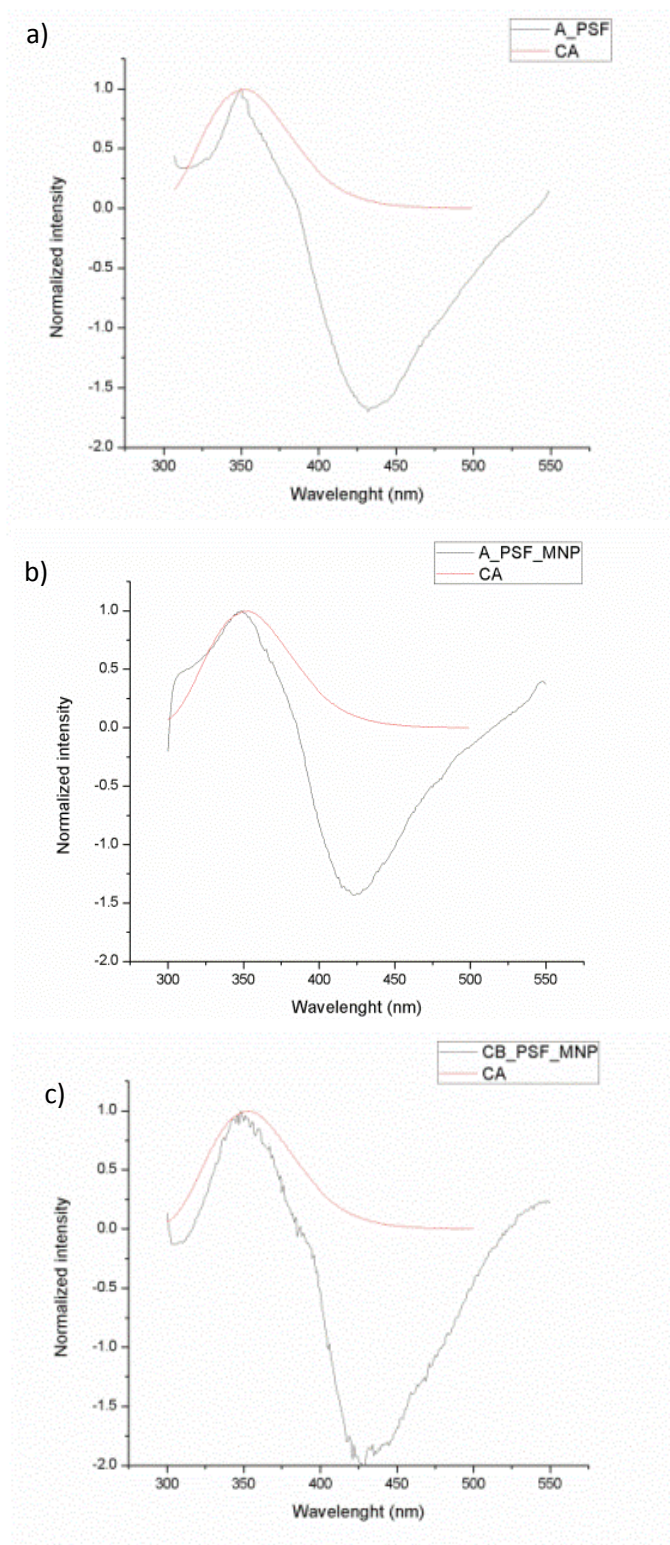
Ambient carbon dioxide capture and conversion via membranes

Fig. IV. 8 shows normalized emission spectra of Carbonic Anhydrase and RuBisCo. The maximum emission for CA is at 350 nm which corresponds to tryptophan; RuBisCo has 2 emission bands with lower relevance at 380 nm and 440 nm. RuBisCo is a very large molecule containing different fluorophores and Mg²⁺ which causes the quenching of the tryptophan signal. The obtained spectrum is a fingerprint of the protein and it depends on the peptide sequence [9]. The two peaks in RuBisCo spectra arise from different fluorophores different to tryptophan. So we can analyse the changes in the structures of such fluorophores but not of tryptophan. Displacement of the bands in the emission spectra of the modified membranes can be connected to a structural change of the enzyme caused by the immobilization process. Therefore, all changes in fluorescence parameters would be the result of the structural modifications that take place within the immobilization process.

Fig. IV. 9 represents the spectra of CA in solution and on the membrane. The peak at around 350 nm comes from CA and it is not changing position with the immobilization, suggesting that there was no change in the enzyme conformation caused by the immobilization process, independently on the approach used. There is also a visible negative peak, a decrease in the membrane emission intensity which is a result of the enzyme attachment.

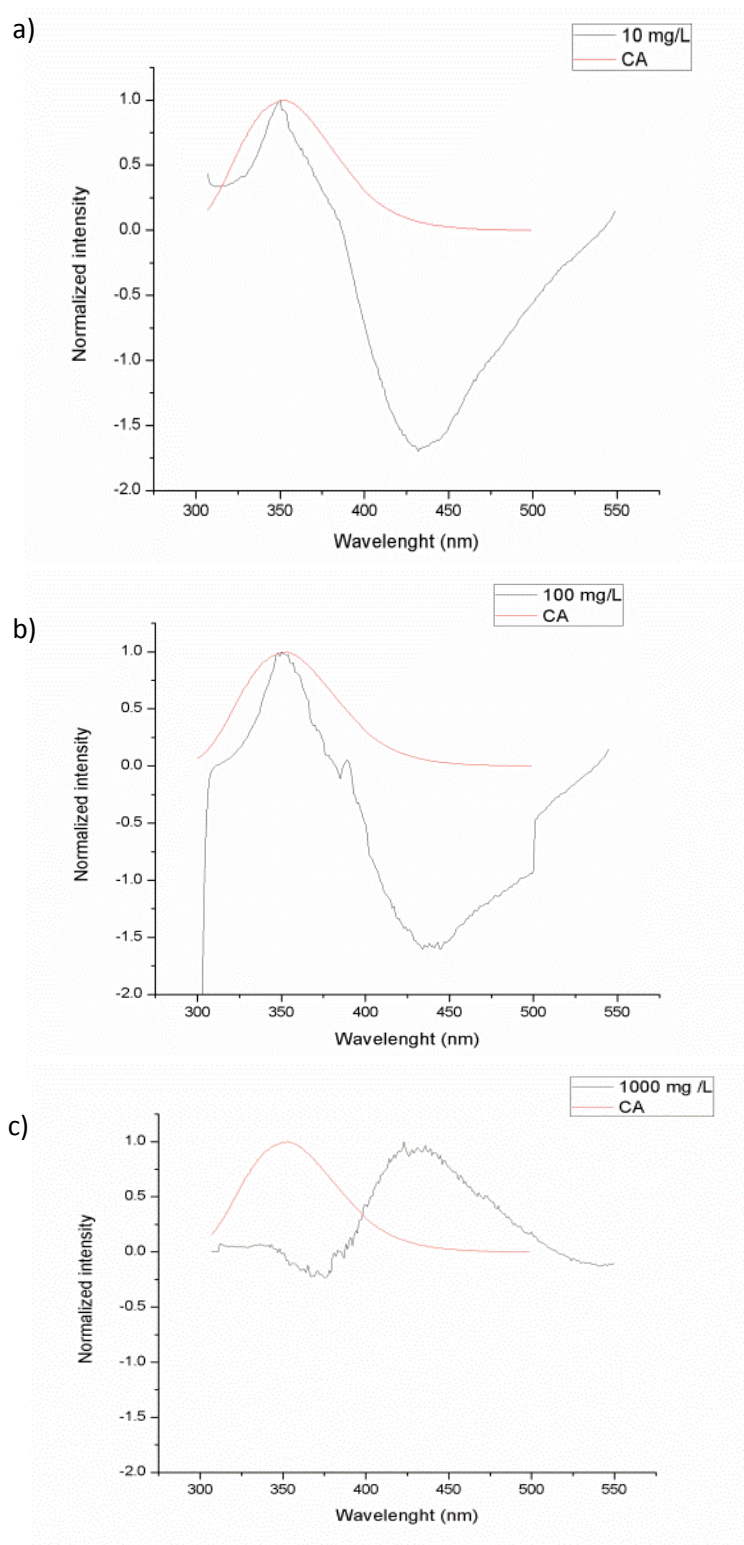
IV. Biomimetic polymeric membranes

Figure IV. 9. Fluorescence spectra of CA in solution and attached to the polysulfone membrane by 3 different approaches: a) A_PSF, b) A_PSF_MNP, c) CB_PSF_MNP.



Ambient carbon dioxide capture and conversion via membranes

Figure IV. 10. Fluorescence spectra of CA in solution and on a membrane at different concentrations: a) 10 mg/L, b) 100 mg/L, c) 1 g/L.



IV. Biomimetic polymeric membranes

By increasing the enzyme concentration in the experimental solution, enzyme concentration on the membrane also increased. Up to 100 mg/L (**Fig. IV. 10**), fluorescence spectra are substantially similar, indicating that there are no remarkable changes of the enzyme structures after being attached to the membrane; but when the concentration is higher (1g/L), the membrane emission increased so much that the peak of CA is no longer detectable.

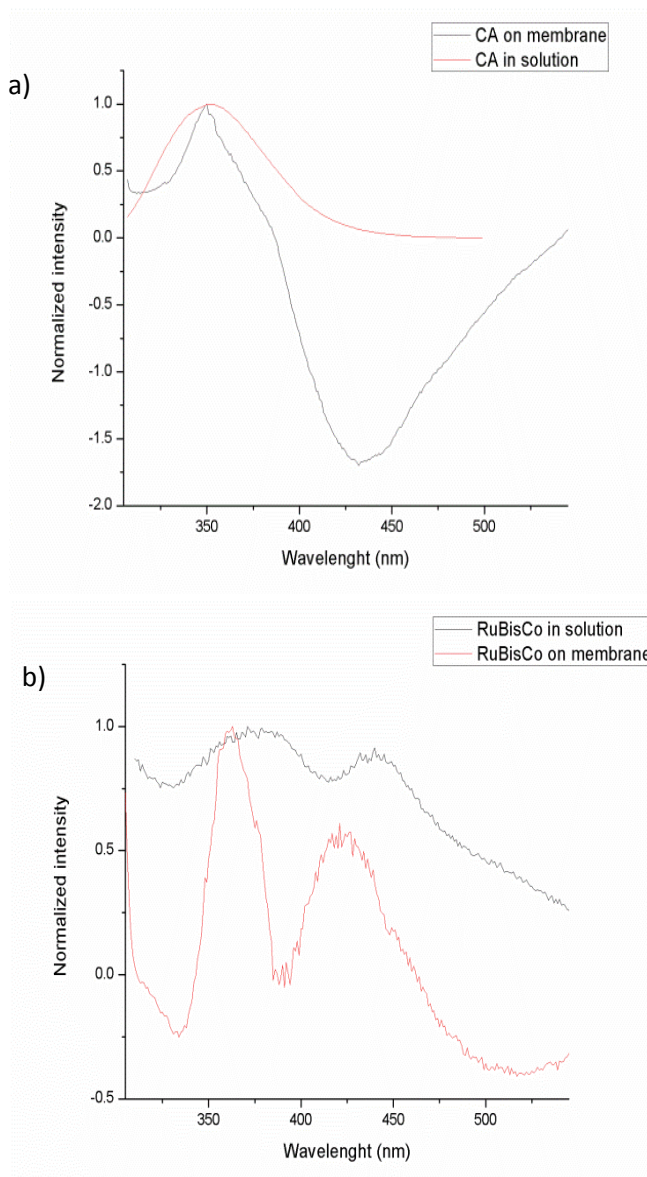


Figure IV. 11. Fluorescence spectra of the enzymes in solution and on polysulfone membrane: a) CA, b) RuBisCo.

Ambient carbon dioxide capture and conversion via membranes

As previously mentioned, there is no marked displacement of maximum emission of tryptophan in CA after being attached to the membrane, while the maximum emission peaks of RuBisCo are being blue-shifted (**Fig. IV. 11**). The fluorophores corresponding to those peaks have not been determined. Nevertheless we can see that the RuBisCo has changed its structure. Assuming that the same forces are driving the fluorophores and tryptophan, the shift would suggest enzyme folding. The fluorophore is entering to the hydrophobic core of the protein and exposing the hydrophilic part. Confirming that the attached by the hydrophilic polysulfone was favourable.

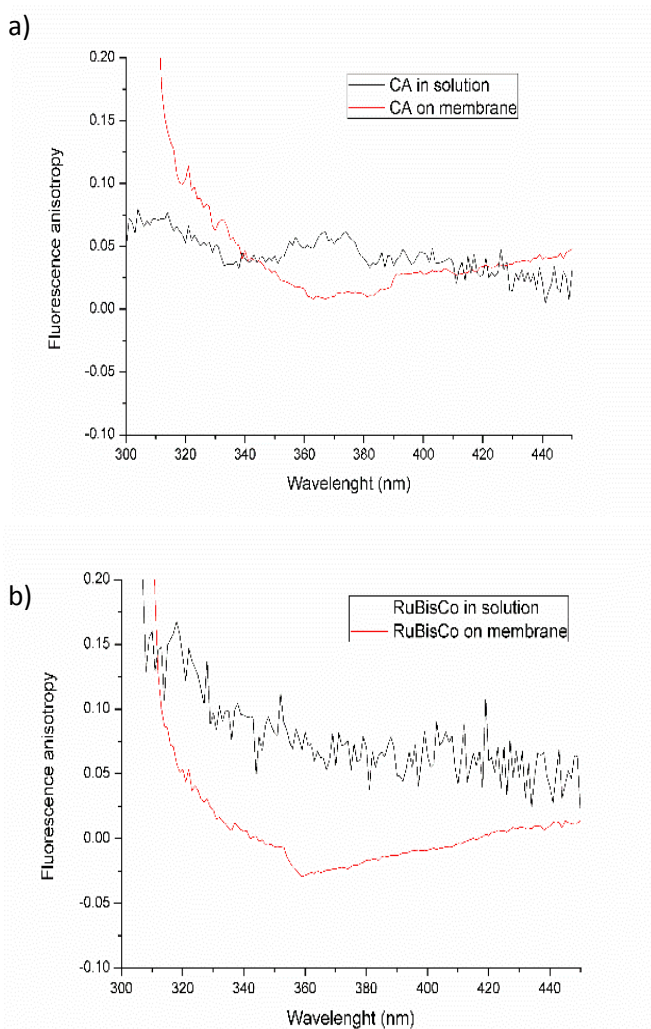


Figure IV. 12. Fluorescence anisotropy spectra of the enzymes in solution and on polysulfone membrane: a) CA, b) RuBisCo.

IV. Biomimetic polymeric membranes

Further anisotropy studies (**Fig. IV. 12**) also did not reveal any significant changes of the CA conformation in experimental solution nor on the membrane in all studied cases. On the other hand, RuBisCo slightly decreased the anisotropy of the membrane from 0.008 to -0.006, which suggests an increase of protein mobility.

Membrane contactors CO₂ sorption abilities estimation

There is a visible improvement of the CO₂ absorption rate with the increase of absorbent flow rate (**Fig. IV. 13**). It is a well-known tendency which had been proved before for the polysulfone membranes and deeply described in Chapter I. The same applies to the introduction of the nanoparticles - it results in a decrease of the CO₂ flux into the system. This is most probably due to blocking of pores and decrease of the mass transfer.

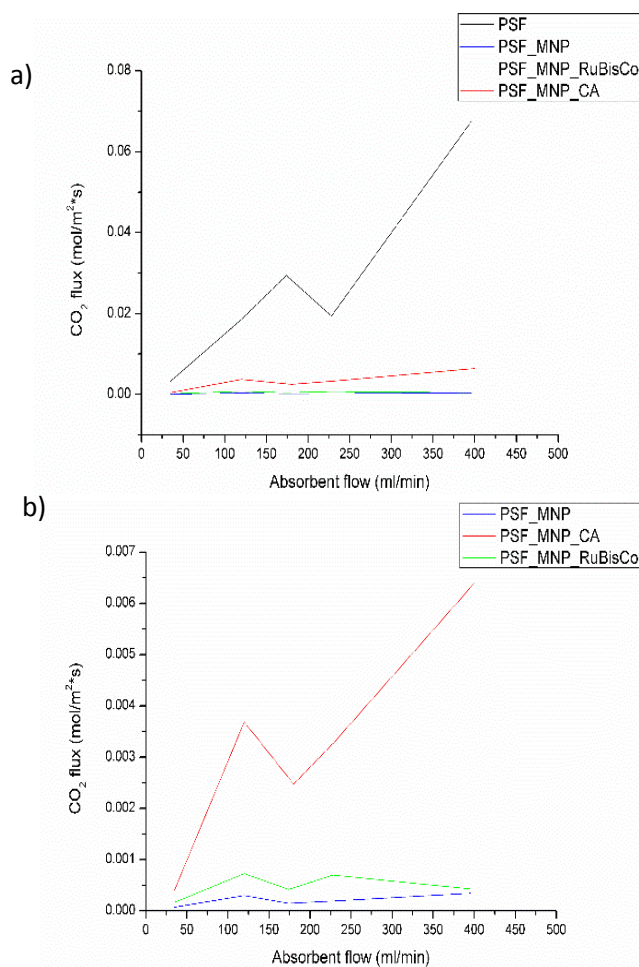


Figure IV. 13. Influence of enzyme immobilization on the membrane contactor CO₂ capture abilities: a) all studied membranes, b) zoom for modified membranes.

Ambient carbon dioxide capture and conversion via membranes

Nevertheless the introduction of the enzyme to the membrane containing nanoparticles showed the increase in its CO₂ sorption abilities ($p = 0.0042$), with CA exhibiting a stronger effect than RuBisCo. As CA needs water to work properly, the aqueous absorbent solution is favourable environment allowing the active passage. On the other hand, RuBisCo ($p = 0.0417$) captures CO₂, but there is no observable active mass transfer.

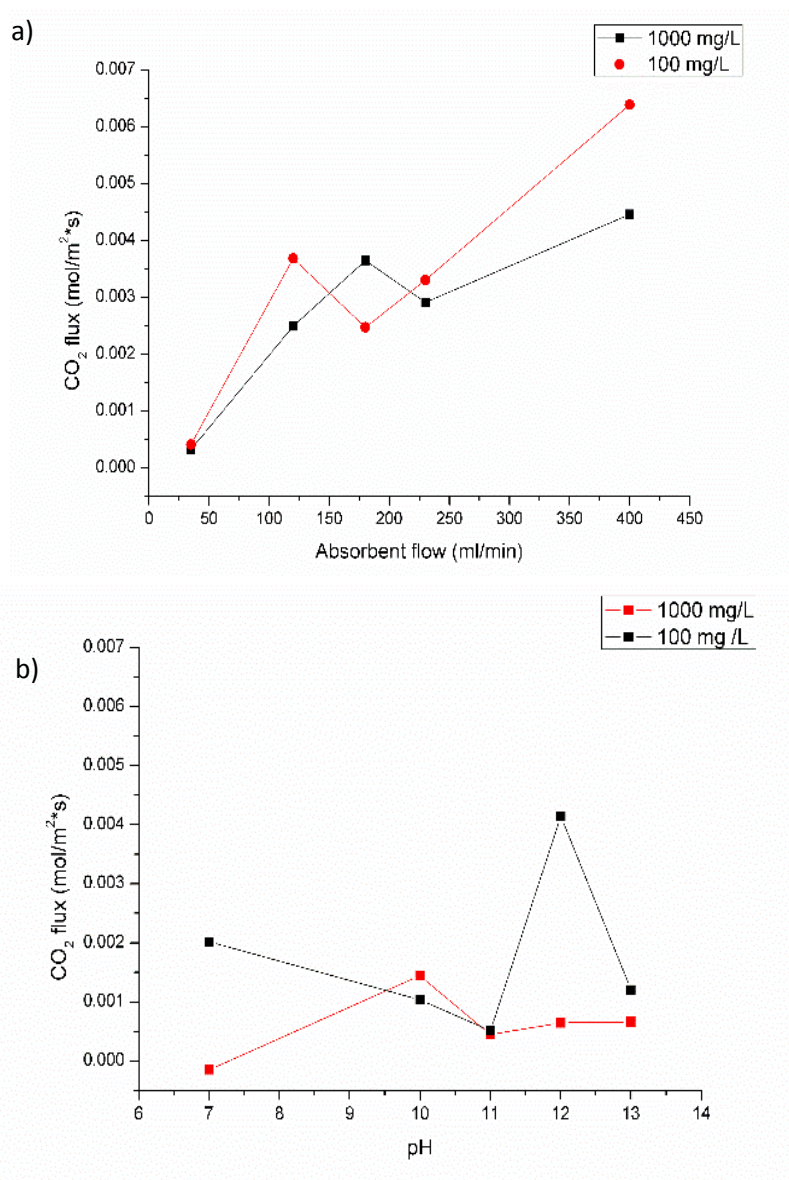


Figure IV. 14. CO₂ flux into polysulfone membrane containing CA: a) as a function of absorbent flow rate at pH 13.3, b) as a function of pH at 230 ml/min flow rate.

IV. Biomimetic polymeric membranes

Afterwards, the influence of the absorbent solution pH and CA concentration on the membranes performance was studied closer (**Fig. IV. 14**). The increase of the CA concentration on the membrane slightly improved the sorption abilities in range of the absorbent flow and in different pH but the change was not significant (respective p values: 0.6954 and 0.1267). According to the statistical analysis there was neither important influence of the pH on the CO₂ capture rate in the membrane containing CA (p = 0.6787).

IV.3.2.2. PVA based membranes

As the use of polysulfone based membranes for the enzymes immobilization was not productive in terms of attachment efficiency and structural changes analysis due to high membrane fluorescence intensity, use of another polymeric membrane was advisable: PVA membranes were tested. PVA (**Fig. IV. 15**) is transparent, thus the problem in the fluorescence analysis should disappear. Furthermore, it is highly hydrophilic, which should help with CA immobilization and activity.

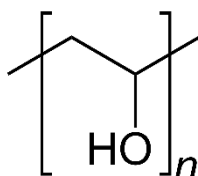


Figure IV. 15. PVA structure.

The modified membranes are named accordingly to the immobilization method (A-for physical adsorption and CB- for covalent binding) and the membrane used as support (PVA- blank membrane, PVA_MNP- PVA membrane with magnetic nanoparticles).

Determination of the immobilized amount of the enzyme by inductively coupled plasma spectroanalysis (ICP)

ICP results suggest that RuBisCo is being attached with a higher efficiency than Carbonic Anhydrase to PVA based membranes (**Table IV. 7**). The enzyme loading decrease is as follows: A_PVA > A_PVA_MNP > CB_PVA_MNP. The tendency is less marked with the increase of enzyme concentration. All of the studies were performed using triton-x-100, as the PVA membranes are highly hydrophilic. Hence, we can conclude that the enzyme was being attached mainly by the polymer.

Ambient carbon dioxide capture and conversion via membranes

Table IV. 7. *Enzymes immobilization efficiency on PVA-based membranes with enzymes concentration of 100 mg/L.*

Experiment		Immobilized amount [mg]	Experiment efficiency [%]	Concentration on membrane [mg/cm ²]
CA	A_PVA	0.115	5.480	0.0127
	A_PVA_MNP	0.115	5.473	0.0174
	CB_PVA_MNP	0.425	21.248	0.0505
RuBisCo	A_PVA	0.909	33.662	0.104
	A_PVA_MNP	0.513	26.984	0.0931
	CB_PVA_MNP	0.334	15.195	0.0490

Table IV. 8. *Enzymes immobilization efficiency on PVA-based membranes with enzymes concentration of 1 g/L.*

Experiment		Immobilized amount [mg]	Experiment efficiency [%]	Concentration on membrane [mg/cm ²]
CA	A_PVA	1.877	10.916	0.219
	A_PVA_MNP	4.681	27.055	0.727
	CB_PVA_MNP	0.186	1.052	0.028
RuBisCo	A_PVA	5.803	58.619	1.140
	A_PVA_MNP	4.842	64.565	0.972
	CB_PVA_MNP	4.432	38.204	0.898

Furthermore, as predicted, increase of enzyme concentration (**Table IV. 8**) in the experimental solution results in increased immobilization

IV. Biomimetic polymeric membranes

efficiency and the enzyme loading on the membrane, except for covalently-immobilized CA. CA immobilization by physical adsorption reveals that the enzyme can be attached by both – polymer and nanoparticles. Whereas during the covalent bonding it can be seen clearly that only MNP are taking part in the immobilization suggesting the successful creation of the new bond.

Carbonic anhydrase activity assay

The activity assay was performed on experimental solutions as well as on the membranes. Due to the low concentration of the enzyme on the membrane, the obtained values were out of the calibration curve range and were negative, thus these results are not given in the tables. Moreover, the activity assay performed on the solutions containing the remaining CA shows a very poor CO₂ hydration performance: the obtained values are very small – laying within the error – or even negative. Hence, the attachment to the membranes is decreasing CA activity.

The activity assay gives information about the active amount of the CA in the experimental solution and how this amount changes after being in contact with the membrane. In the final experimental solution some remaining CA is present. Negative values indicate that the activity is higher after immobilization, while positive ones indicate stable or decreased activity, because of attachment or changes in the structure caused by the interactions with the membrane or the solution components. It is expected that the enzyme on the membrane undergo a similar activation or deactivation as the enzyme in the experimental solution.

Table IV. 9. CA activity test results from the experimental solutions from the preparation of PVA-based biomimetic membranes (initial concentration of CA: 100 mg/L) (n.d. – not detected).

Solution sample		Time [s]	Active amount [mg]	Active percentage [%]	Difference in activity [%]
A_PVA	initial	53	0.941	44.84	- 47.00
	final	69	0.418	21.07	
A_PVA_MNP	initial	74	0.279	13.28	315.47
	final	56	0.832	41.89	
CB_PVA_MNP	initial	90	n.d.	n.d.	-
	final	93	n.d.	n.d.	

Ambient carbon dioxide capture and conversion via membranes

Table IV. 10. CA activity test results from the experimental solutions from the preparation of PVA-based biomimetic membranes (initial concentration of CA: 1 g/L) (n.d. – not detected).

Solution sample		Time [s]	Active amount [mg]	Active percentage [%]	Difference in activity [%]
A_PVA	initial	79	0.299	1.74	- 75.09
	final	81	0.200	1.31	
A_PVA_MNP	initial	82	0.151	0.87	- 50.48
	final	84	0.057	0.44	
CB_PVA_MNP	initial	95	n.d.	n.d.	-
	final	108	n.d.	n.d.	

The calibration curve has a logarithmic trend of the activity during time in [s], following the equation $y = -19.83 \ln(x) + 88.141$, with a fit of $R^2 = 0.8971$. Negative values of active CA amount in solution means that the measurements were out of calibration curve; this type of results were obtained for samples from covalent binding experiments (**Table IV. 9**), even in initial solutions, suggesting that glutaraldehyde might cause deactivation of the enzyme in solution. Furthermore, there was a very low activity of CA in the initial samples. CA is more active in the solution of lower concentration. Moreover, an increase of the activity in the final sample was observed only in A_PVA_MNP.

With 1 g/L enzyme concentration (**Table IV. 10**), the percentage of active CA units is around 1 % and drops by 25 – 50% after immobilization experiments. The very low activity might be caused by agglomerations or structural changes.

Membrane sorption studies – CO₂ solubility

CO₂ solubility values in PVA membranes are visibly smaller as compared to the polysulfone membranes. Also, even unmodified membranes exhibit some sorption abilities, whose values do not significantly differ from the ones for modified membranes (**Table IV. 11**). The CO₂ sorption values are likely coming only from the membranes themselves and not from the attached enzyme. Therefore, enzyme immobilization did not improve the CO₂ sorption of the PVA membrane, independently on the enzyme used – CA or RuBisCo - or its concentration on the membrane. The reason might lie in the very low activity of the enzyme and comparatively high membrane efficiency.

IV. Biomimetic polymeric membranes

Table IV. 11. CO₂ solubility in the PVA -based biomimetic membranes.

Membrane	PVA	PVA_ MNP	CA 100 mg/L	RuBISco 100 mg/L	CA 1000 mg/L	RuBISco 1000 mg/L	CA 1000 mg/L	RuBISco 1000 mg/L
			A_PVA_MNP	A_PVA_MNP	A_PVA_MNP	A_PVA_MNP	CB_PVA_MNP	CB_PVA_MNP
n_{CO_2} [μmol]	62.66	59.70	54.57	49.04	61.22	55.18	50.08	65.10
S [m^3 STP/ m^3 atm]	3.83	7.08	5.55	5.86	5.57	7.21	5.90	8.59

Ambient carbon dioxide capture and conversion via membranes

Monitoring of structural changes induced by immobilization via fluorescence spectroscopy and anisotropy

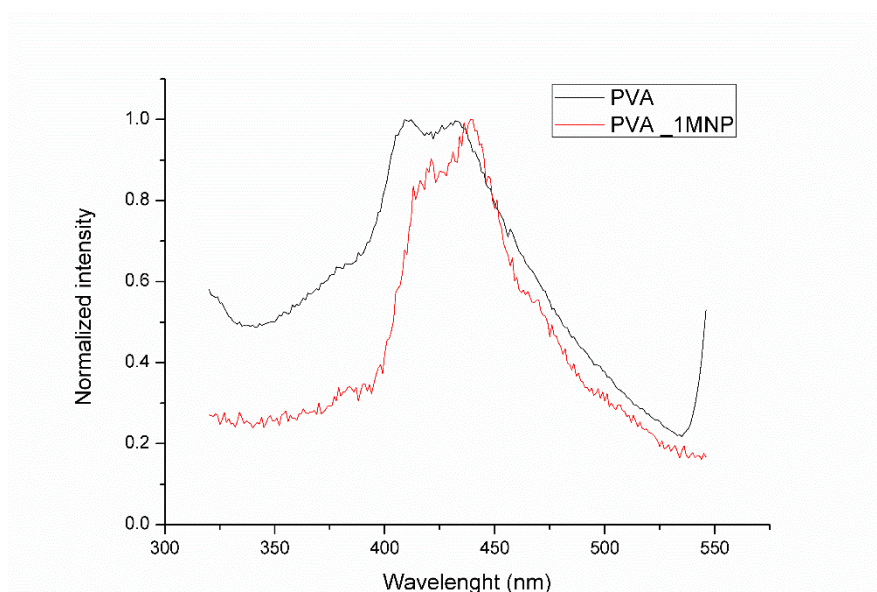


Figure IV. 16. Fluorescence emission spectra of PVA - based membranes.

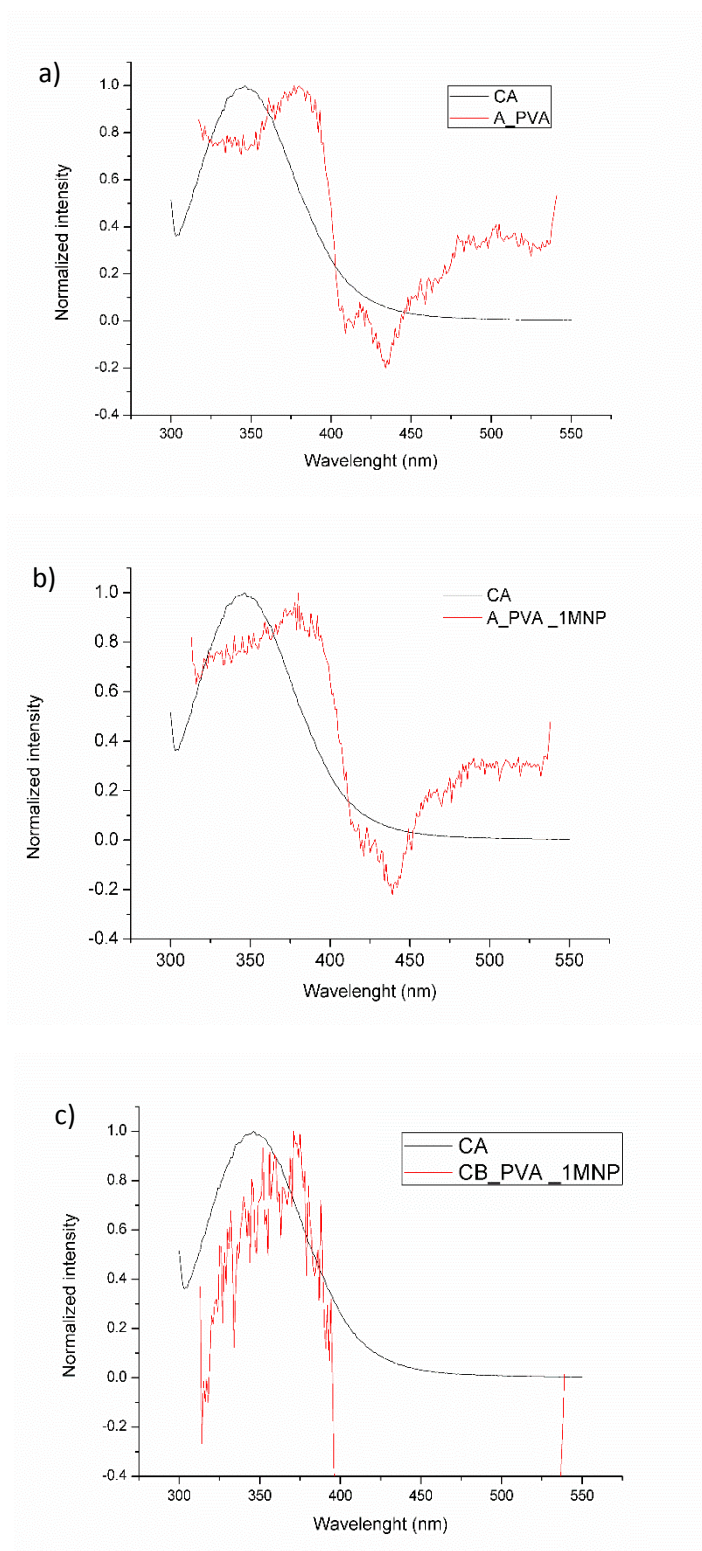
Fig. IV. 16 shows the normalized emission spectra of the membranes before immobilization experiments. There is a high impact of the introduced nanoparticles on the maximum emission wavelength position. The blank PVA membrane has two main peaks at 410 nm and 430 nm. Also, it can be observed the quenching effect of MNP, as previously stated for the polysulfone-based membranes.

Table IV. 12. CA-modified PVA membranes fluorescence measurements results.

	Membrane	Max peak λ_{em} [nm]	Anisotropy, r , at max peak	CA concentration on membrane [mg/cm ²]
100 mg/L	A_PVA	383	0.059	0.013
	A_PVA_MNP	383	0.543	0.017
	CB_PVA_MNP	373	0.625	0.051
1000 mg/L	A_PVA	373	0.008	0.219
	A_PVA_MNP	384	0.436	0.727
	CB_PVA_MNP	395	0.073	0.028

IV. Biomimetic polymeric membranes

Figure IV. 17. Fluorescence emission spectra of CA in solution and on PVA-based membranes: a) A_PVA, b) A_PVA_1MNP, c) CB_PVA_1MNP with insert zoom.



Ambient carbon dioxide capture and conversion via membranes

Spectra in **Fig. IV. 17** represent the changes in CA emission caused by the 3 different immobilization techniques. In almost all cases we observed a red shift, suggesting an exposure of tryptophan to the aqueous environment—e.g. due to molecular unfolding. The data obtained for all of the analysed membranes are summarized in **Table IV. 12**. The displacement of an emission maximum in covalently-bonded CA might be caused not only by the creation of new bonds with the nanoparticles but also by interaction with glutaraldehyde. Unfortunately, the liquid samples containing glutaraldehyde were not provided because of the intensive noise obtained during the analysis. It can be noticed a very intensive negative peak in spectra of the membrane with covalently bonded CA, meaning that the membrane emission decreased after immobilization due to the enzyme coverage. Indeed, according to ICP, this membrane has the highest CA concentration as compared to the other ones.

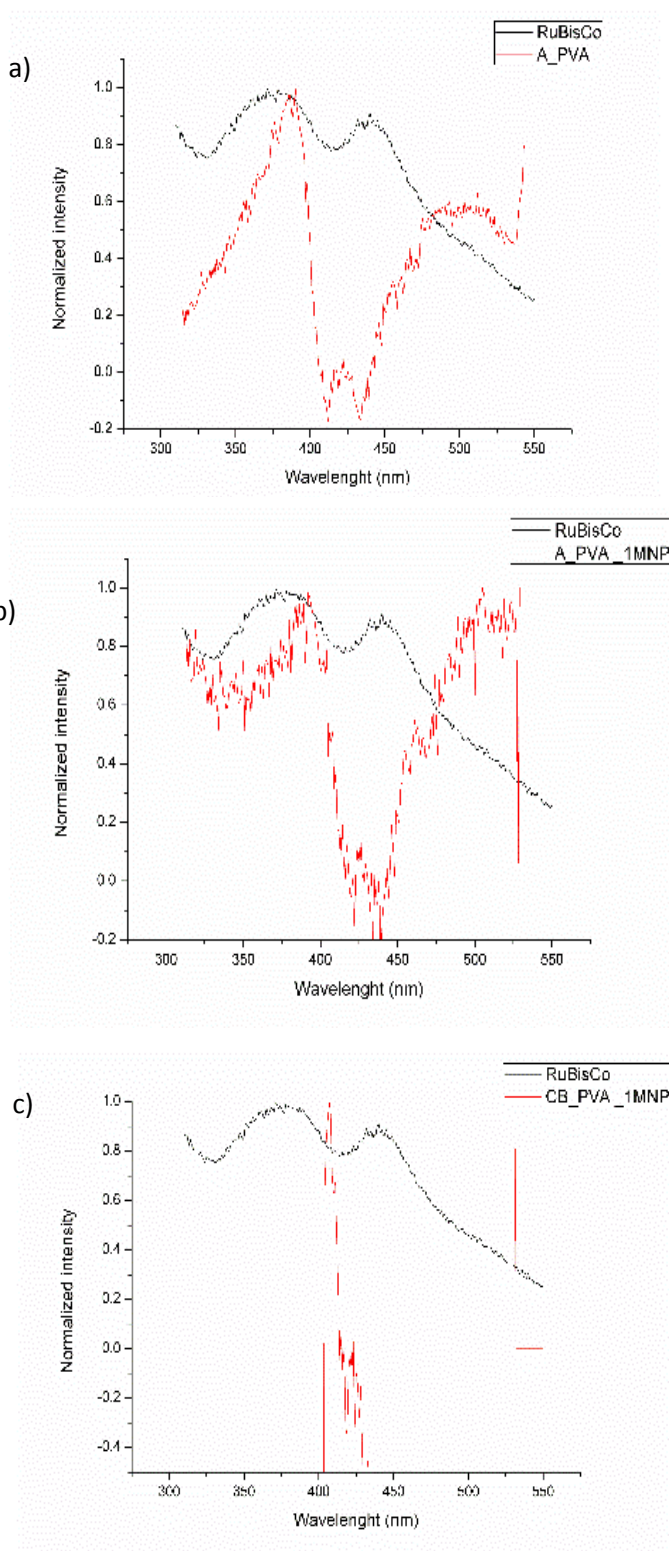
Anisotropy of the CA on the membrane was obtained by subtracting the initial spectra of the corresponding PVA membrane to the final one. The numerical data collected at maximum peak wavelength for each experiment is listed in the **Table VI. 12**. The anisotropy of the CA in solution in 350 nm was 0.044 and it did not change after immobilization experiments. The adsorption to blank PVA membrane doesn't change the enzyme mobility, while adsorption to the membrane containing 1 % of the MNP results in decrease of the mobility by aggregation or structural packing. In case of covalent binding it can be seen that is the higher the concentration of CA on the membrane the less mobile the enzyme becomes, even though it is getting more unfolded.

Table IV. 13. *RuBisCo-modified PVA membranes fluorescence measurements results.*

	Membrane	Max peak λ_{em} [nm]	Anisotropy, r , at max peak	RuBisCo concentration on membrane [mg/cm ²]
100 mg/L	A_PVA	391	0.136	0.104
	A_PVA_MNP	393	0.567	0.093
	CB_PVA_MNP	408	0.169	0.049
1 g/L	A_PVA	390	0.073	1.140
	A_PVA_MNP	n.d.	0.515 (380 nm)	0.972
	CB_PVA_MNP	395	0.074	0.898

IV. Biomimetic polymeric membranes

Figure IV. 18. Fluorescence emission spectra of RuBisCo in solution and attached by different techniques to PVA-based membranes: a) A_PVA, b) A_PVA_1MNP, c) CB_PVA_1MNP with insert zoom.



Ambient carbon dioxide capture and conversion via membranes

Judging from the fluorescent analysis RuBisCo undergo the same structural changes as CA after being immobilized to PVA-based membrane (**Table IV. 13**) (**Fig. IV. 18**). We can suspect that the displacement of the maximum peak to higher wavelength is connected to the molecular unfolding.

Taking into consideration that the emission maximum of the fluorophore in the enzyme structure is at 380 nm, it can be postulated that the RuBisCo emission after immobilization undergo a slight red shift. The biggest shift was observed for the membrane with the lowest enzyme concentration on the surface. What is suggesting the unfolded conformation of the enzyme on the membrane, as the steric hindrance was not limiting the observed change. The other peak at 440 was not found in the attached enzyme emission spectra.

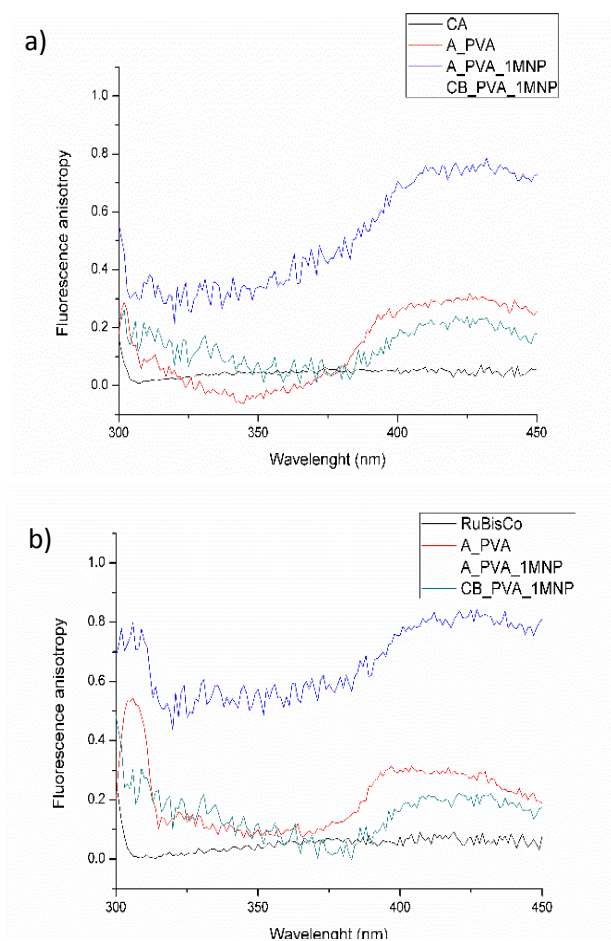


Figure IV. 19. Fluorescence anisotropy spectra of enzymes in solution and on the PVA-based membranes: a) CA, b) RuBisCo.

IV. Biomimetic polymeric membranes

Anisotropy of tryptophan at 380 nm is 0.059 (**Fig. IV. 19**). Comparing this value with the values obtained for the immobilized enzyme we observed a red shift but only in the membranes with low enzyme concentration, which is suggesting decrease of the mobility. It can be concluded that at a low concentration the enzyme is spreading and being attached by a large surface what in consequence is causing is low mobility.

IV.4. Conclusions

Biomimetic membranes, consisting of enzymes attached to a polymer - based membrane, were successfully developed. Incorporation of small amount of magnetic nanoparticles into polymeric membrane bulk result in increase of water contact angle, while the membrane morphology remained unchanged, which is in agreement with previous reports.

It was also observed that RuBisCo immobilization is favourable to more hydrophilic surfaces and the use of triton was not necessary. On the other hand, triton does improve CA immobilization efficiency. The solubilized enzyme was physically attached to the hydrophilic membrane and NH₂- terminated nanoparticles, but there was no evidence of covalent binding.

Although the use of triton improves the attachment of CA, it also influences the enzyme CO₂ solubility rate. As it is improving the attachment to nanoparticles, the interactions might be stronger than ones with the blank polysulfone membrane, and the active site might be not reachable. However fluorescence analyses did not reveal any structural changes in case of CA immobilization, while RuBisCo structure was altered during the process.

PVA membrane was found to be a good support for enzyme immobilization due to its high hydrophilicity. Studies show, that the enzyme immobilization did not improve the CO₂ sorption of the membrane, independently on the enzyme used – CA or RuBisCo - or its concentration. Moreover, both enzymes show signs of a molecular unfolding, which could change the availability of the active center and cause the decrease of activity.

Additional membrane contactor studies were not performed on the PVA membranes due to its characteristic. Nevertheless, polysulfone based

bio-mimetic membranes showed slight increase in the nanocomposite membrane CO₂ absorption, yet the blank membrane still shows the best performance.

References

- [1] Hartman, F.C.H., M.R., Structure, function, regulation, and assembly of D-ribulose-1,5-bisphosphate carboxylase/oxygenase. *Annual Review of Biochemistry*, 1994. **63**: p. 197-234.
- [2] Eduardo Zabaleta, M.V.M., Hans-Peter Braun, A basal carbon concentrating mechanism in plants? *Plant Science*, 2012. **187**: p. 97-104.
- [3] Peter Jochems, Y.S., Ludo Diels, Winnie Dejonghe, Enzyme immobilization on/in polymeric membranes: status, challenges and perspectives in biocatalytic membrane reactors (BMRs) *Green chemistry*, 2011. **13**: p. 1609–1623.
- [4] Sachin A. Sarode, J.M.B.a.J.M.N., An efficient magnetic copper ferrite nanoparticle catalysed ligand and solvent free synthesis of N-aryl amide from aldoximes and iodobenzene. *RSC Advances*, 2015. **5**: p. 105353-105358.
- [5] Valeur, B., *Characteristics of fluorescence emission*, in *Molecular Fluorescence. Principles and Applications*, Germany: Wiley/ VCH, 2002, p. 34-70
- [6] Alvaro Cruz-Izquierdo, E.A.P., Carmen Lopez¹, Juan L. Serra¹, Maria J. Llama, Magnetic Cross-Linked Enzyme Aggregates(mCLEAs) of *Candida antarctica* Lipase: An Efficient and Stable Biocatalyst for Biodiesel Synthesis. 2014. **9**(12): p. 1-22.
- [7] M.M. Rashad, R.M.M., M.A. Ibrahim, L.F.M. Ismail, E.A. Abdel-Aal, Magnetic and catalytic properties of cubic copper ferrite nanopowders synthesized from secondary resources. *Advanced Powder Technology*, 2012. **23**: p. 315-323.
- [8] Hidehito Nakamura, Hisashi Kitamura, Nobuhiro Sato, Masaya Kanayama, Yoshiyuki Shirakawa, Sentaro Takahashi, *Polysulfone as ascintillation material without doped fluorescent molecules*, *Nuclear Instruments and Methods in Physics Research*, 2015. **797**: p 206–209

IV. Biomimetic polymeric membranes

- [9] J.R Albani, *Fluorescence Fingerprints of animal and vegetal species and/or varieties*, in Structure and dynamics of macromolecules: absorption and fluorescence studies, Elsevier, 2004, p 373-386, ISBN: 0-444-51449-X

V. BICARBONATE ELECTO-REDUCTION TO FORMIC ACID

V. Bicarbonate electro – reduction to formic acid

Chapter V describes the preliminary studies on electro - reduction abilities of copper. The working electrode was prepared by electro-polishing followed by annealing and characterized by LSV. The conversion of bicarbonate to formic acid by electro-reduction was achieved in potentiostatic conditions. Obtained products were analyzed by H NMR.

V.1. Introduction

The conversion of bicarbonate to useful hydrocarbons or alcohols is a promising way to reuse the captured carbon dioxide. The most promising method is the electrochemical conversion, which leads to the formation of e.g. formic acid, methane, methanol and other related products [1]. Formic acid is formed in high yields as the reduction potential of the reaction is low. Moreover, formic acid is an interesting product as it can be further used as a fuel in direct formic acid fuel cells. Unfortunately, water reduction is a very competitive reaction during the electro-reduction of carbon dioxide in aqueous electrolytes. In this case the mainly obtained product is hydrogen. A number of metals and metal oxides were studied to be applied in the process, in search of the best faradic efficiency and selectivity [2, 3].

Bismuth is an example of a metal which was reported to be selective in CO₂ conversion to formate. Bertina et al. [4] studied both bismuth and its oxide-derived films. Experiments show that although the oxide was significantly more active, the faradic efficiency did not vary. Fu et al. [5] studied the selectivity of crystalline SnO₂ nanospheres incorporated to a gas diffusion electrode, and found that the catalyst activity depends on the electrolyte conditions. A faradic efficiency of 56% towards formation of formate was achieved by using 0.5 M KHCO₃ as an electrolyte. Moreover, the optimum pH favouring the selectivity is 8.3, which allowed maintaining the oxide stable. Similar results were achieved by Lee and his group using a copper oxide electrode [6]. Generally, Cu based electrodes are very common in electro-reduction processes due to its unique abilities to catalyze the formation of hydrocarbons and alcohols. Li [7] established that a low overpotential for the electro-reduction can be obtained by electrochemical reduction of CuO₂ prior to the CO₂ reduction. In the study, a Cu₂O layer was obtained by annealing of Cu foil on air. As a result, the electrode surface roughness was increased accordingly to the time and temperature of the process.

The following studies aimed to reproduce the work of Li [7] and analyze the copper-based electro-catalyst abilities to reduce bicarbonate.

V.2. Experimental

V.2.1. Materials

Copper foil (99.98% trace metals basis), 0.025 mm thick, used as a working electrode and highly pure KHCO₃ (Bio Ultra 99.5%) with a content of iron lower than 5 mg/Kg used for preparation of the electrolyte were

V. Bicarbonate electro – reduction to formic acid

purchased from Sigma Aldrich. The electro-polishing procedure was performed with phosphoric acid of 85 % wt. from Panreac. The Nafion®117 membrane (Sigma-Aldrich) was washed with solutions of 30% hydrogen peroxide (Sigma-Aldrich) and 95-97% H₂SO₄ (Serviquimia). To prepare standard for ¹H NMR analysis, 99.8% D₂O from Panreac and 99.7% DMSO (Chromasolv Plus) from Sigma Aldrich were used.

V.2.2. Working electrode preparation

The preparation of the copper foil was a sequence of electro-polishing, followed by annealing and finally by reduction of the oxide: the copper foil was electrochemically polished by applying -1.6 V for 6 minutes in H₃PO₄ 85%; then, the foil was washed in distilled water and put in muffle furnace (300 °C, 3h). Finally, the oxidated copper was reduced in 0.5 M KHCO₃ with - 0.9 V until current density was close to 0 and stable.

V.2.3. Electrochemical behavior

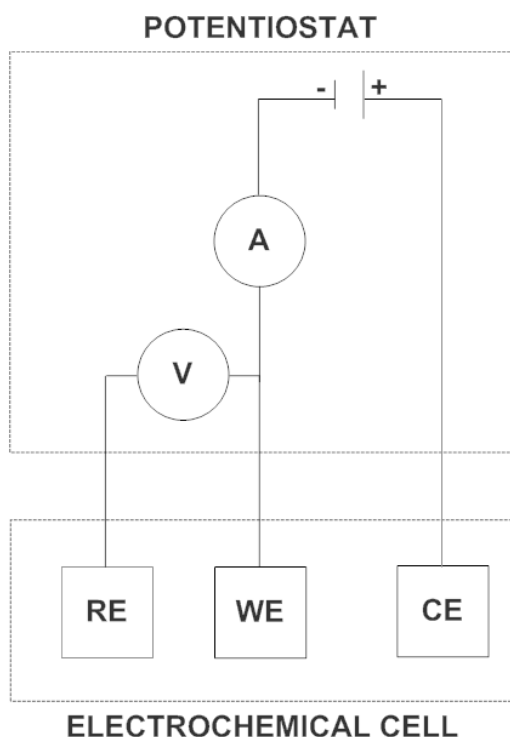


Figure V. 1. Diagram of connections between the potentiostat and electrodes.

Ambient carbon dioxide capture and conversion via membranes

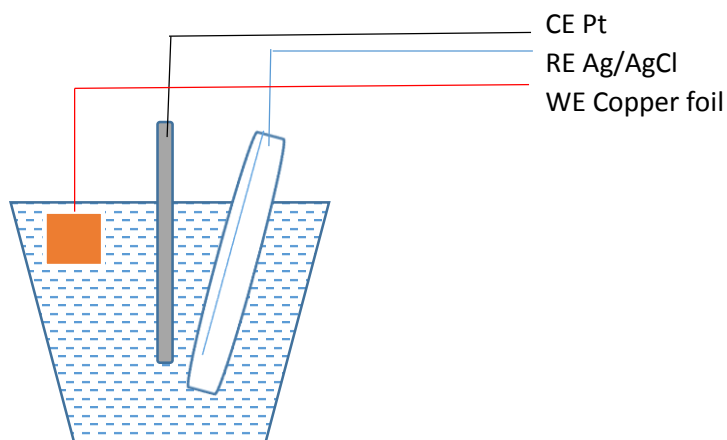


Figure V. 2. Schematic representation of the system for LSV.

The electrochemical behaviour of the electrodes was evaluated using linear sweep voltammetry (LSV) (**Fig. V. 2**) at a scan rate of 50 mV/s. A 0.5 M KHCO_3 aqueous solution was used as an electrolyte in a standard three-electrode electrochemical cell equipped with a Pt as the counter electrode and an Ag/AgCl as the reference one. Portions (about 5 cm^2 geometric area) of the prepared electrodes were cut and used as working electrodes. An AutoLab PGSTAT 302N potentiostat (Metrohm, Autolab B.V.) was used in all the electrochemical experiments. The potentials ranged from -0.5 – -2 V vs. Ag/AgCl (0.21 V).

V.2.4. Electro-reduction experiments

The electrolysis experiments were performed in a Teflon H-cell. A Nafion membrane was used to separate the working and counter electrodes compartments to prevent oxidation of the reduced CO_2 products (**Fig. V. 3**). The membrane was washed by immersion in heated up to 80 °C aqueous solutions in following order: H_2SO_4 , H_2O_2 3%, distilled water for 1 h in each solution. A potential of -1.6 V was applied for 1 h to electrolyte consisting of 0.5 M KHCO_3 . The progress of the experiment was followed through pH measurements. Analysis of the obtained products was performed by ^1H NMR (VARIAN Mercury VX400). DMSO in D_2O was used as internal standard for quantification of obtained products. Catholyte samples of 600 μL were mixed together with 100 μL of standard. In order to obtain the peaks coming from products, the suppression of the water peak by irradiation was required.

V. Bicarbonate electro – reduction to formic acid

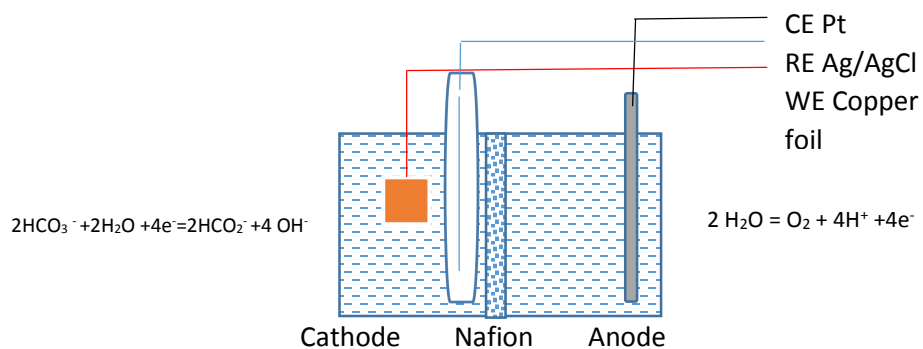


Figure V. 3. Schematic representation of the system for electro-reduction experiments.

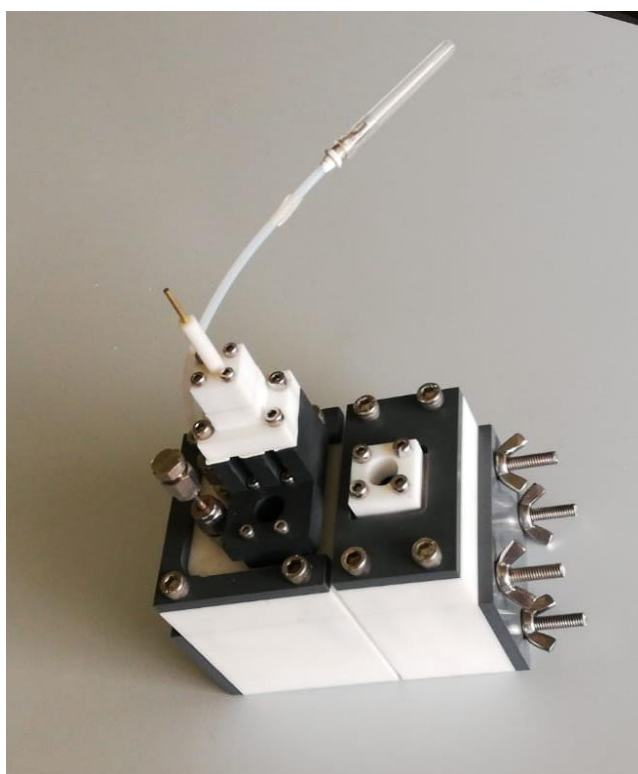


Figure V. 4. Module for electro-reduction studies.

V.3. Results and discussion

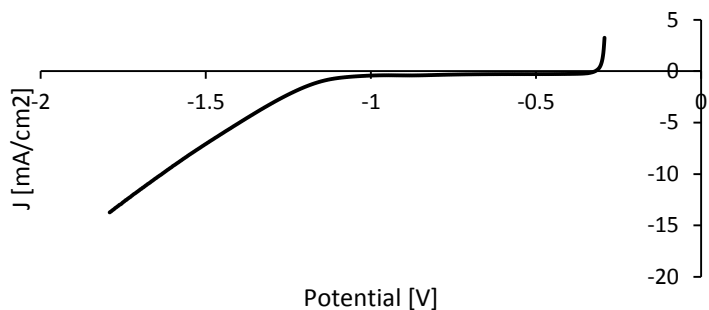


Figure V. 5. LSV spectrum obtained for treated Cu foil in 0.5 M KHCO_3 .

The LSV spectrum (**Fig. V. 5**) was obtained prior to electroreduction experiments in order to choose the proper working electrode potential to be applied. The reduction starts at -1.0 V, while bubbles formation (suggesting H_2 production) started at around -1.7 V, thus a potential of -1.6 V was chosen.

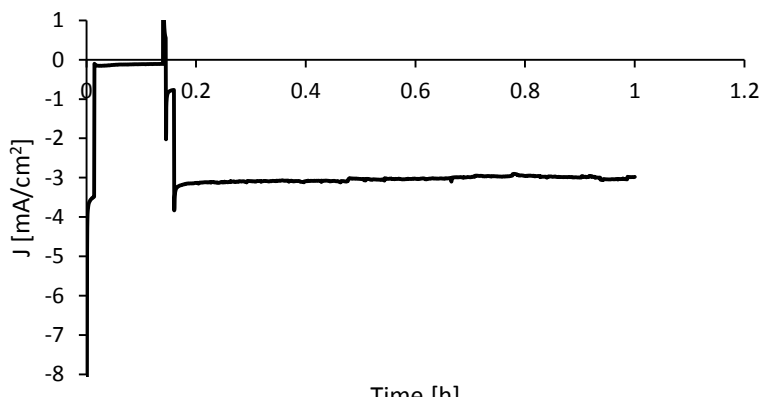


Figure V. 6. Chronoamperogram recorded during the electroreduction experiment

The electro-reduction was stable in terms of current density during the experiment (**Fig. V. 6**). The initial increase of current refers to the reduction of the copper. The pH changed from 8.46 to 7.66 at the anode and 9.01 at the cathode.

V. Bicarbonate electro – reduction to formic acid

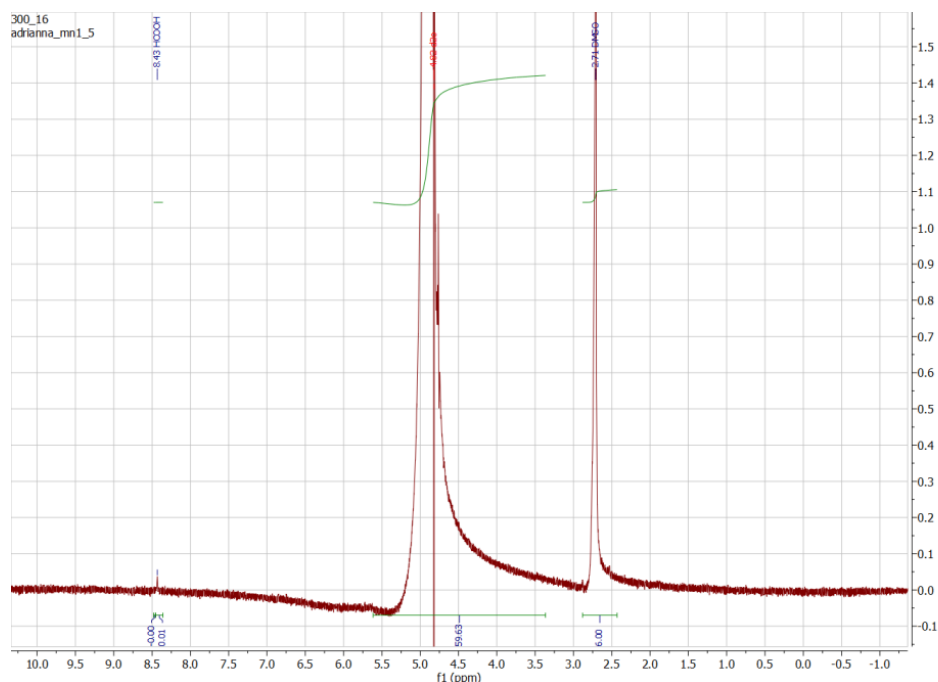


Figure V. 7. *1H NMR spectra of the bicarbonate solution after the electro-reduction experiment.*

NMR analysis (**Fig. V. 7**) showed peaks in 8.43 which corresponds to HCOOH, in 4.82 to water and in 2.71 to DMSO. Unfortunately, the conversion has a very low yield. Within the limits of detection, the amount of formic acid was calculated to be only 30 mM with initial amount of 0.5 M of bicarbonate.

Considering the low yield and change in pH in both compartments we can conclude that the main product of the electro-reduction process was hydrogen. Hydrogen generation is a common competitive reaction at the cathode in electro-reduction systems working in aqueous electrolytes, while at the anode oxygen is generated.

V.4. Conclusions

The conversion of bicarbonate to formic acid by electro-reduction by using modified copper foil was achieved. Unfortunately, low yield of reaction was obtained, suggesting that the main reaction occurring during the experiment was hydrogen generation.

Further modification of the working electrode and method must be tested in order to improve the selectivity of the reaction.

References

- [1] Zhong-Li Wang, Cuiling Li, Yusuke Yamauchi, *Nanostructured nonprecious metal catalysts for electrochemical reduction of carbon dioxide*, *Nano Today*, 2016, **11**: p 373–391.
- [2] Narayanaru Sreekanth, Kanala Lakshminarasimha, *Selective reduction of CO₂ to formate through bicarbonate reduction on metal electrodes: new insights gained from SG/TC mode of SECM†*, *Chemical Communications*, 2014, **50**: p 11143-11146.
- [3] Fan Cai, Dunfeng Gao, Rui Si, Yifan Ye, Ting He, Shu Miao, Guoxiong Wang, Xinhe Bao, *Effect of metal deposition sequence in carbon-supported Pd–Pt catalysts on activity towards CO₂ electroreduction to formate*, *Electrochemistry Communications*, 2017, **76**: p 1–5.
- [4] Erwan Bertin, Sébastien Garbarino, Claudie Roy, Sona Kazemi, Daniel Guay, *Selective electroreduction of CO₂ to formate on Bi and oxide-derived Bi films*, *Journal of CO₂ Utilization*, 2017, **19**: p 276–283.
- [5] Yishu Fu, Yanan Li, Xia Zhang, Yuyu liu, Xiaodong Zhou, Jinli Qiao, *Electrochemical CO₂ reduction to formic acid on crystalline SnO₂ nanosphere catalyst with high selectivity and stability*, *Chinese Journal of Catalysis*, 2016, **37**: p 1081–1088.
- [6] Seunghwa Lee, Sujik Hong, Jaeyoung Lee, *Bulk pH contribution to CO/HCOO⁻ production from CO₂ on oxygen - evacuated Cu₂O electrocatalyst*, *Catalysis Today*, 2017, **288**: p 11-17.
- [7] Christina W. Li, Matthew W. Kanan, *CO₂ Reduction at Low Overpotential on Cu Electrodes Resulting from the Reduction of Thick Cu₂O Films*, *Journal of the American Chemical Society*, 2012, **134**: p 7231–7234.

V. Bicarbonate electro – reduction to formic acid

4. GENERAL CONCLUSIONS

4. General conclusions

Ambient carbon dioxide capture and conversion via membranes

- Inspired by nature, an artificial stomata for CO₂ absorption based on polysulfone membrane contactor was designed and developed. By using the phase inversion precipitation method and applying different membrane preparation parameters (such as different solvents, coagulation bath composition, casting knife thickness), membrane contactors in the 76–176 μm thickness range with different morphologies (from spongy-like to open macrovoids-containing ones) were obtained.
- According to the results, it can be concluded that polysulfone membranes can be used with potassium hydroxide solutions, as the swelling results are very low (close to 0) and the contact angle is high.
- The study indicates that the CO₂ flux increases when increasing the absorbent flow rate over the range of liquid velocities investigated. Moreover, the flux grows with the increase of membrane macrovoids size, due to decrease of the membrane mass transfer resistance. Results obtained during dynamic module operations revealed the superior CO₂ assimilation abilities of the unit (284.2 μmol/m²*s) over a natural leaf (40 μmol/m²*s).
- The experiments with the static operation of the module show inferior CO₂ flux comparing to the dynamic one, still similar to a leaf performance. Furthermore, the lack of energy consumption of the system is compensating its lower performance.
- Incorporation of nanoparticles does not change the membrane internal morphology. However, it increased surface roughness and CO₂ permeability. CuFeO₃ nanoparticles proved to be capable of capturing CO₂, but when introduced to the polymeric membrane and tested in contactor systems they negatively influenced the CO₂ flux, with respect to the blank polysulfone membranes.
- The incorporation of AC into the polymeric bulk caused an increase of the membrane thickness and contributed to pores formation on the bottom surface of the membrane. The hydrophilicity was not improved. The gas absorption test results show no improvement of the membrane performance. Possibly AC was incorporated by the

4. General conclusions

polymer, quenching the possible positive influence of AC on the membrane properties.

- Modification of the polysulfone surface by coating with active carbon layer was accomplished. The cross section images of the modified membranes showed that the layer was not penetrating into the membrane. Unfortunately, the additional layer increased membrane mass transfer resistance, which decreases its effectiveness as a membrane contactor.
- Biomimetic membranes, consisting of enzymes attached to a polymer - based membrane, were successfully developed. It was observed that RuBisCo immobilization is favorable to more hydrophilic surfaces. The solubilized CA was attached to the hydrophilic membrane and NH₂- terminated nanoparticles, but there was no evidence of covalent binding. Fluorescence analyses did not reveal any structural changes in the case of CA immobilization, while the RuBisCo structure was alternated during the process. Nevertheless, polysulfone based bio-mimetic membranes showed slight increase in the nanocomposite membrane CO₂ absorption, yet the blank membrane still shows the best performance at the tested conditions. Durability was not tested.
- The PVA membrane was found to be a good support for enzyme immobilization due to its high hydrophilicity. Studies show, that the enzyme immobilization did not improve the CO₂ sorption of the membrane, independently on the enzyme used – CA or RuBisCo - or its concentration. Moreover, both enzymes show signs of a molecular unfolding, which could change the availability of the active center and cause the decrease of activity.
- Bicarbonate conversion to formic acid was achieved with a Cu based electrocatalyst with low efficiency. Results suggest that the main reaction occurring during the experiments was hydrogen generation and therefore, the system will be improved in next designs.

4. General conclusions

APPENDIX

Appendix

LIST OF FIGURES

Figure 2. 1. Chart of increase of atmospheric CO₂ concentration during years 1958 – 2010.

Figure 2. 2. Schematic representation of gas liquid membrane contactor for CO₂ capture.

Figure 2. 3. Gas - liquid membrane contactors in dry (a) and wet (b) mode. The contact surface area is marked with red color.

Figure 2. 4. Model reaction of surface hydroxyl groups with fluoroalkyl silanes.

Figure 2. 5. Amines used in CO₂ absorption studies.

Figure 2. 6. CO₂ hydrogenation mechanism on a metallic catalyst.

Figure 2. 7. CO₂ hydrogenation mechanism in photocatalytic reduction.

Figure 2. 8. CO₂ electro chemical conversion mechanism.

Figure 2. 9. CO₂/pH equilibrium diagram.

Figure 2. 10. Schematic representation artificial photosynthetic device.

Figure I. 1. Casting Knife Film Applicator.

Figure I. 2. System for CO₂ absorption (a) with dynamic module (b).

Figure I. 3. Gas permeability system on scheme (a) and on photo (b): 1) CO₂ gas bottle, 2) valve, 3) pressure transducer, 4) manometer, 5) steel module containing membrane, 6) gas flow meter.

Figure I. 4. CO₂ solubility system: 1) CO₂ gas bottle, 2) valve, 3) manometer, 4) steel module containing membrane.

Figure I. 5. SEM micrographs of the fabricated flat sheet membranes cross section, respectively pristine membranes: a) M1, b) M2, c) M3, d) M4 and nanocomposite membranes: e) M6, f) M7, g) M8, h) M9.

Figure I. 6. Internal morphology of the pristine membrane M5.

Figure I. 7. Pristine (a) and nanocomposite (b) membrane photo.

Figure I. 8. TEM micrograph of CuFe₂O₄ nanoparticles.

Figure I. 9. XRD analysis of the produced CuFe₂O₄ powder.

Ambient carbon dioxide capture and conversion via membranes

Figure I. 10. AFM 3D micrographs representing bottom surfaces of pristine and nanocomposite membranes: a) M1, b) M2, c) M3, d) M4, e) M6, f) M7, g) M8, h) M9, i) M9.

Figure I. 11. CO₂ mass transfer coefficient of pristine and nanocomposite membranes.

Figure I. 12. Effect of pristine membranes membrane thickness on CO₂ absorption flux.

Figure I. 13. CO₂ absorption flux into pristine membranes as a function of liquid flow rate.

Figure I. 14. Difference in CO₂ absorption abilities of pristine and nanocomposite membrane contactors.

Figure II. 1. Figure II. 1. Static module scheme (a) and photo (b).

Figure II. 2. ESEM micrographs of the blank polysulfone membranes cross section: a) 250, b) 200, c) 100.

Figure II. 3. AFM 3D images of bottom surface of blank polysulfone membranes: a) 100, b) 200, c) 250.

Figure II. 4. CO₂ absorption as a function of RPM by different blank polysulfone membranes in static module.

Figure II. 5. CO₂ absorption flux by membrane 200 in static module as function of pH.

Figure II. 6. CO₂ absorption flux and CO₂ content change by membrane 200 in static module as a function of time.

Figure III. 1. Airbrush used for the membrane surface modification.

Figure III. 2. System for CO₂ absorption with dynamic module scheme.

Figure III. 3. SEM representative cross section micrographs: a) M200 - blank membrane, b) 200_LAC_1 - membrane after modification, c) M200_LAC_1 - zoom of top part of modified membrane.

Figure III. 4. ESEM cross section micrographs of membranes containing 5% AC: a) MAC100, b) MAC200, c) MAC250.

Figure III. 5. ESEM representative surfaces micrographs of membrane M200: a) bottom, b) top before modification, c) top after modification - M200_LAC_1.

Figure III. 6. Pristine (a) and carbon-modified (b) membrane photo.

Figure III. 5. ESEM surfaces micrographs of MAC200: a) bottom, b) top.

Appendix

Figure III. 6. Structures of compounds: a) nafion ($x=6, z=4, y=2$), b) polysulfone.

Figure III. 7. Contribution of components of the carbon-containing layer on the polysulfone membrane surface.

Figure III. 8. CO₂ absorption flux as a function of absorbent flow rates for pristine and carbon modified polysulfone membranes.

Figure III. 9. CO₂ absorption flux as a function of absorbent flow rates for carbon modified membranes.

Figure IV. 1. Schematic representation of the system for CO₂ solubility studies of biomimetic membranes.

Figure IV. 2. TEM images of Fe₂O₃-NH₂ nanoparticles at different magnifications.

Figure IV. 3. Fe₂O₃-NH₂ nanoparticles size distribution.

Figure IV. 4. X-ray spectrum of the Fe₂O₃-NH₂ nanoparticles.

Figure IV. 5. SEM micrographs of biomimetic polysulfone membranes containing: a) CA, b) RuBisCo.

Figure IV. 6. Membranes photos: a) polysulfone pristine, b) polysulfone nanocomposite, c) PVA pristine and nanocomposite.

Figure IV. 7. Fluorescence spectra of polysulfone-based membranes.

Figure IV. 8. Fluorescence emission spectra of CA and RuBisCo.

Figure IV. 9. Fluorescence spectra of CA in solution and attached to the polysulfone membrane by 3 different approaches: a) A_PSF, b) A_PSF_MNP, c) CB_PSF_MNP.

Figure IV. 10. Fluorescence spectra of CA in solution and on a membrane at different concentrations: a) 10 mg/L, b) 100 mg/L, c) 1 g/L.

Figure IV. 11. Fluorescence spectra of the enzymes in solution and on polysulfone membrane: a) CA, b) RuBisCo.

Figure IV. 12. Fluorescence anisotropy spectra of the enzymes in solution and on polysulfone membrane: a) CA, b) RuBisCo.

Figure IV. 13. Influence of enzyme immobilization technique on the membrane contactor CO₂ capture abilities: a) all studied membranes, b) zoom for modified membranes.

Figure IV. 14. CO₂ flux into polysulfone membrane containing CA: a) as a function of absorbent flow rate at pH 13.3, b) as a function of pH at 230 ml/min flow rate.

Ambient carbon dioxide capture and conversion via membranes

Figure IV. 15. PVA structure.

Figure IV. 16. Fluorescence emission spectra of PVA - based membranes.

Figure IV. 17. Fluorescence emission spectra of CA in solution and on PVA-based membranes: a) A_PVA, b) A_PVA_1MNP, c) CB_PVA_1MNP with insert zoom.

Figure IV. 18. Fluorescence emission spectra of RuBisCo in solution and attached by different techniques to PVA-based membranes: a) A_PVA, b) A_PVA_1MNP, c) CB_PVA_1MNP with insert zoom.

Figure IV. 19. Fluorescence anisotropy spectra of enzymes in solution and on the PVA-based membranes: a) CA, b) RuBisCo.

Figure V. 1. Diagram of connections between the potentiostat and electrodes.

Figure V. 2. Schematic representation of the system for LSV.

Figure V. 3. Schematic representation of the system for electro-reduction experiments.

Figure V. 4. Module for electro-reduction studies.

Figure V. 5. LSV spectrum obtained for treated Cu foil in 0.5 M KHCO_3 .

Figure V. 6. Chronoamperogram recorded during the electroreduction experiment.

Figure V. 7. NMR spectra of the electrolyte solution after the electro-reduction experiment.

Appendix

List of Tables

Table I. 1. Polymeric solutions composition and pristine and nanocomposite polysulfone membranes preparation parameters.

Table I. 2. Characteristics of the resulting pristine and nanocomposite polysulfone membranes.

Table I. 3. Composition of the pristine and nanocomposite polysulfone membranes analyzed by EDX.

Table I. 4. Pristine and nanocomposite polysulfone membrane surfaces roughness parameters.

Table I. 5. The contact angle measurements results of pristine and nanocomposite polysulfone membranes surface (where: adv - advancing, rec – receding).

Table I. 6. CO₂ solubility studies results of pristine and nanocomposite polysulfone membranes and nanoparticles.

Table I. 7. The artificial stomata CO₂ assimilation rate in range of 35-400 ml/min liquid flow velocities for pristine and nanocomposite polysulfone membranes.

Table II. 1. Blank polysulfone membrane preparation parameters.

Table II. 2. Characteristics of the resulting blank polysulfone membranes.

Table II. 3. Blank polysulfone membranes surface roughness parameters.

Table II. 4. Swelling test measurements results of blank polysulfone membranes.

Table II. 5. Water and KOH solution contact angle measurements results of blank polysulfone membranes.

Table II. 6. Dynamic contact angle measurements results of blank polysulfone membranes.

Table III. 1. Polymeric solutions composition and carbon modified polysulfone membranes preparation parameters.

Table III. 2. Characteristics of the resulting carbon modified polysulfone membranes.

Table III. 3. Elemental analysis of carbon modified membranes surfaces by ESEM.

Table III. 4. Carbon layer characteristics.

Ambient carbon dioxide capture and conversion via membranes

Table IV. 1. Characteristics of the resulting biomimetic membranes.

Table IV. 2. CA immobilization efficiency on polysulfone based membranes (n.d. – not detected).

Table IV. 3. Comparison of CA and RuBisCo immobilization efficiencies in absence of Triton – X-100 on polysulfone based membranes (n.d. – not detected).

Table IV. 4. Influence of Triton – X- 100 on CA immobilization efficiency on polysulfone based membranes (n.d. – not detected).

Table IV. 5. Activity test results of CA immobilized on polysulfone based membranes in range of concentrations and with use of different techniques (n.d. – not detected; n.a. - not analysed).

Table IV. 6. CO₂ solubility in the biomimetic polysulfone based membranes.

Table IV. 7. Enzymes immobilization efficiency on PVA-based membranes with enzymes concentration of 100 mg/L.

Table IV. 8. Enzymes immobilization efficiency on PVA-based membranes with enzymes concentration of 1 g/L.

Table IV. 9. CA activity test results from the experimental solutions from the preparation of PVA-based biomimetic membranes (initial concentration of CA: 100 mg/L) (n.d. – not detected).

Table IV. 10. CA activity test results from the experimental solutions from the preparation of PVA-based biomimetic membranes (initial concentration of CA: 1 g/L) (n.d. – not detected).

Table IV. 11. CO₂ solubility in the PVA -based biomimetic membranes.

Table IV. 12. CA-modified PVA membranes fluorescence measurements results.

Table IV. 13. RuBisCo-modified PVA membranes fluorescence measurements results.

Appendix

Thesis outcomes

Publications

Authors: Adrianna Nogalska, Mario Ammendola, Bartosz Tylkowski, Veronica Ambrogi, Ricard Garcia-Valls

Title: Ambient CO₂ adsorption via membrane contactors – Value of assimilation from air as nature stomata

Journal: Journal of Membrane Science

Volume: 546

Pages: 41-49

Year: 2018

Authors: Adrianna Nogalska, Adrianna Zukowska, Ricard Garcia-Valls

Title: Atmospheric CO₂ capture for the artificial photosynthetic system

Journal: Science of the Total Environment

Volume: 621

Pages: 186 - 192

Year: 2018

Authors: Adrianna Nogalska, Anna Trojanowska, Ricard Garcia-Valls

Title: Membrane contactors for CO₂ capture processes -critical review

Journal: Physical Sciences Reviews

Volume: 2

Pages: -

Year: 2017

Authors: Adrianna Nogalska, Mario Ammendola, Carla A. M. Portugal, Bartosz Tylkowski, Joao G. Crespo, Ricard Garcia - Valls

Title: Polysulfone biomimetic membrane for CO₂ capture

Journal: Functional Materials Letters

Volume: -

Pages: -

Year: 2018

Book chapter

Authors: A. Nogalska, A. Trojanowska and R. Garcia-Valls

Chapter Title: Membrane contactors for CO₂ capture processes - critical review

Book title: Polymer Engineering

Editorial: B. Tylkowski, K. Wieszczycka, R. Jastrzab

Publisher: Walter de Gruyter GmbH

Year: 2017

ISBN: 978-3-11046828-1

Ambient carbon dioxide capture and conversion via membranes

Patent

Inventors: A. Nogalska, R. Garcia Valls, B. Tylkowski

Title: *Membrana asimétrica de polisulfona secuestrante de CO₂ de la atmósfera, procedimiento para su obtención y sistema de absorción de CO₂ que utiliza dicha membrana*

Reference Number: Spanish Patent Dock# P28664ES00

Date: 21/12/2016

Title-holder entity: Universitat Rovira I Virgili and Centre de Tecnologia Química de Catalunya

Appendix

CURRICULUM VITAE

Adrianna Nogalska was born in 1990 in Czarnkow, Poland. She obtained a Bsc in cosmetic chemistry at Adam Mickiewicz University in Poznan, where she developed a project focused on crystallography. She then pursued a Msc in material chemistry at the same university in 2014, in collaboration with Universitat Rovira I Virgili (URV). Afterwards, Adrianna embarked on her doctoral studies at URV in Meteor group, continuing the project started during her Msc.

Adrianna Nogalska is author of 7 publications, 2 book chapters and holder of a patent. During her doctoral studies she contributed with oral presentations and posters in 4 international congresses. At the “Advances in Energy Systems and Environmental Engineering” congress in 2017 held in Wroclaw she was given the Best paper award by the organisation committee.

Curriculum Vitae

